



**British  
Geological Survey**

NATURAL ENVIRONMENT RESEARCH COUNCIL

# Microbiological effects on transport processes (BioTran) – Data production from column experiments containing Sherwood Sandstone

Radioactive Waste Team

Open Report OR/11/058



BRITISH GEOLOGICAL SURVEY

RADIOACTIVE WASTE TEAM

OPEN REPORT OR/11/058

# Microbiological effects on transport processes (BioTran) – Data production from column experiments containing Sherwood Sandstone (October 2010 - July 2011)

## *Keywords*

Geomicrobiology, Sherwood  
sandstone, biofilms, columns,  
fracture surfaces, .

J M West, K Bateman, P Coombs, H M Harrison, S Holyoake, A E  
Milodowski, J Rushton, G Turner, D Wagner and J Wragg

## *Front cover*

Cover picture details, delete if no  
cover picture.

## *Bibliographical reference*

WEST, JM, BATEMAN, K,  
COOMB, P, HARRISON, HM,  
MILODOWSKI, AE, RUSHTON, J,  
TURNER, G, WAGNER, D AND  
WRAGG, J. 2011. *British  
Geological Survey Open Report*,  
11/058 94pp.

Copyright in materials derived  
from the British Geological  
Survey's work is owned by the  
Natural Environment Research  
Council (NERC) and/or the  
authority that commissioned the  
work. You may not copy or adapt  
this publication without first  
obtaining permission. Contact the  
BGS Intellectual Property Rights  
Section, British Geological  
Survey, Keyworth,  
e-mail [ipr@bgs.ac.uk](mailto:ipr@bgs.ac.uk). You may  
quote extracts of a reasonable  
length without prior permission,  
provided a full acknowledgement  
is given of the source of the  
extract.

Maps and diagrams in this book  
use topography based on  
Ordnance Survey mapping.

## BRITISH GEOLOGICAL SURVEY

The full range of our publications is available from BGS shops at Nottingham, Edinburgh, London and Cardiff (Welsh publications only) see contact details below or shop online at [www.geologyshop.com](http://www.geologyshop.com)

The London Information Office also maintains a reference collection of BGS publications, including maps, for consultation.

We publish an annual catalogue of our maps and other publications; this catalogue is available online or from any of the BGS shops.

*The British Geological Survey carries out the geological survey of Great Britain and Northern Ireland (the latter as an agency service for the government of Northern Ireland), and of the surrounding continental shelf, as well as basic research projects. It also undertakes programmes of technical aid in geology in developing countries.*

*The British Geological Survey is a component body of the Natural Environment Research Council.*

*British Geological Survey offices*

### **BGS Central Enquiries Desk**

Tel 0115 936 3143 Fax 0115 936 3276  
email [enquiries@bgs.ac.uk](mailto:enquiries@bgs.ac.uk)

### **Kingsley Dunham Centre, Keyworth, Nottingham NG12 5GG**

Tel 0115 936 3241 Fax 0115 936 3488  
email [sales@bgs.ac.uk](mailto:sales@bgs.ac.uk)

### **Murchison House, West Mains Road, Edinburgh EH9 3LA**

Tel 0131 667 1000 Fax 0131 668 2683  
email [scotsales@bgs.ac.uk](mailto:scotsales@bgs.ac.uk)

### **Natural History Museum, Cromwell Road, London SW7 5BD**

Tel 020 7589 4090 Fax 020 7584 8270  
Tel 020 7942 5344/45 email [bgs\\_london@bgs.ac.uk](mailto:bgs_london@bgs.ac.uk)

### **Columbus House, Greenmeadow Springs, Tongwynlais, Cardiff CF15 7NE**

Tel 029 2052 1962 Fax 029 2052 1963

### **Maclean Building, Crowmarsh Gifford, Wallingford OX10 8BB**

Tel 01491 838800 Fax 01491 692345

### **Geological Survey of Northern Ireland, Colby House, Stranmillis Court, Belfast BT9 5BF**

Tel 028 9038 8462 Fax 028 9038 8461

[www.bgs.ac.uk/gsni/](http://www.bgs.ac.uk/gsni/)

### *Parent Body*

### **Natural Environment Research Council, Polaris House, North Star Avenue, Swindon SN2 1EU**

Tel 01793 411500 Fax 01793 411501  
[www.nerc.ac.uk](http://www.nerc.ac.uk)

Website [www.bgs.ac.uk](http://www.bgs.ac.uk)

Shop online at [www.geologyshop.com](http://www.geologyshop.com)

# Foreword

This report is the published product of a study by the British Geological Survey (BGS) for the BGS BioTran project.

# Acknowledgements

We acknowledge the BGS for funding the BioTran project. We thank Mr Neil Stacey (BGS Core Store) for Sherwood Sandstone core preparation and BGS Analytical Chemistry Sections for their able assistance. Thanks also to Simon Gregory for his thorough review.

# Contents

<b>Foreword</b> .....	<b>i</b>
<b>Acknowledgements</b> .....	<b>i</b>
<b>Contents</b> .....	<b>i</b>
<b>Summary</b> .....	<b>vi</b>
<b>1 Introduction</b> .....	<b>1</b>
<b>2 Laboratory techniques</b> .....	<b>1</b>
2.1 Experimental overview .....	1
2.2 Flow-through column methodology .....	2
2.3 Preparation of fluids .....	4
2.4 Selection and preparation of intact core material .....	4
2.5 Bacterial culture.....	5
2.6 Decommissioning of experiments .....	6
<b>3 Analytical techniques</b> .....	<b>8</b>
3.1 Chemical analyses .....	8
3.2 Microbiological analyses .....	8
3.3 Characterisation of solid materials .....	8
<b>4 Results</b> .....	<b>21</b>
4.2 Microbiology .....	21
4.3 Fluid Chemistry .....	24
4.4 Physical measurement results .....	31
4.5 Mineralogical and petrographical characteristics of the sandstone starting materials ..	37
4.6 Mineralogical and ESEM Analysis of the post-experimental materials.....	55
<b>5 Discussion</b> .....	<b>65</b>
<b>6 Conclusions</b> .....	<b>67</b>
<b>Appendix 1 X-ray diffraction traces</b> .....	<b>69</b>

<b>Appendix 2</b>	<b>Mercury injection core porosimetry data .....</b>	<b>75</b>
<b>Appendix 3</b>	<b>Fluid Chemistry Data (Control Core) .....</b>	<b>77</b>
<b>Appendix 4</b>	<b>Fluid Chemistry Data (Biotic Core).....</b>	<b>80</b>
<b>References .....</b>		<b>83</b>

## FIGURES

Figure 1 Schematic of column design .....	3
Figure 2 Schematic of pressure vessel with column containing rock core .....	3
Figure 3 Work flow diagram for image processing of EDXA element maps for mineralogical modal analysis .....	12
Figure 4 Diagram showing the locations of samples taken from the post experimental biotic core	17
Figure 5 P/T phase diagram for water in the region relevant to ESEM operation. $T_w$ is the triple point. Source data for the sublimation and melting curves has been derived from Wagner <i>et al.</i> , (1994), and for the boiling / saturation curve is International Association for the Properties of Water and Steam (IAPWS) formulation for industrial use, 1997. Humidity curves have been calculated and superimposed on the gas portion of the diagram. ....	19
Figure 6 P/T phase diagram for water and a 0.25M NaCl aqueous solution in the region relevant to ESEM operation .....	20
Figure 7 Shows the difference in collection syringe volumes from the biotic and control core experiments (determined by weight of liquid collected, assuming $1 \text{ g ml}^{-1}$ ) from the start of the experiment .....	26
Figure 8 Concentrations of Na (grey circles) and Cl (black circles) in $\text{mg l}^{-1}$ plotted against time from start of pressure logging phase of the biotic experiment in hours .....	26
Figure 9 Plot of Na against Cl from start of logging phase in hours for the biotic core (grey circles) and the control core (black circles).....	26
Figure 10 NPOC in $\text{mg l}^{-1}$ for the biotic core (grey circles) and the control core (black circles) plotted against time from start of pressure logging phase .....	27
Figure 11 Plot of pH against time from start of logging phase in hours for the biotic core (grey circles) and the control core (black circles).....	27
Figure 12 Plot of Ca against time from start of logging phase in hours for the biotic core (grey circles) and the control core (black circles).....	28
Figure 13 Plot of Ba against time from start of logging phase in hours for the biotic core (grey circles) and the control core (black circles).....	28
Figure 14 Plot of Al against time from start of logging phase in hours for the biotic core (grey circles) and the control core (black circles).....	29
Figure 15 Plot of K against time from start of logging phase in hours for the biotic core (grey circles) and the control core (black circles).....	29
Figure 16 Plot of Mo against time from start of logging phase in hours for the biotic core (grey circles) and the control core (black circles).....	30
Figure 17 Plot of W against time from start of logging phase in hours for the biotic core (grey circles) and the control core (black circles).....	30

Figure 18 Plot of Ni against time from start of logging phase in hours for the biotic core (grey circles) and the control core (black circles).....	31
Figure 19 Plot of Zn against time from start of logging phase in hours for the biotic core (grey circles) and the control core (black circles).....	31
Figure 20 Biotic experiment: injection pressure and mean bacterial counts (open circles) plotted against pressure logging time in hours. Bacterial count in pump inflow fluid and remaining in pump at the end of the experiment is also given. <i>P. aeruginosa</i> injected at 169 h .....	33
Figure 21 Control experiment: injection pressure and mean bacterial counts (circles) plotted against pressure logging time in hours. Results also shown following injection with killed <i>P. aeruginosa</i> and associated biofilm (injected at 4484 h) in pump in-flow fluid .....	34
Figure 22 Comparison of injection pressure results in biotic (in grey) and control (in black) experiments plotted against pressure logging time (to 4484 h when dead organism were injected into the control experiment).....	35

## PLATES

Plate 1 Photograph of assembled apparatus showing pressure vessel and syringe pump.....	4
Plate 2 Removal of column assembly from pressure vessel (Biotic experiment).....	6
Plate 3 Biotic column after removal from pressure vessel.....	6
Plate 4 Control column after removal from pressure vessel. Arrow indicates direction of fluid flow during the experiment.....	7
Plate 5 Both columns after removal of end pieces just prior to mineralogical analyses.....	7
Plate 6 Biotic sample, showing the post experimental core after some samples have been taken, with distance-from-inlet cm markings on the outer surface of the PTFE sleeve. Note the inner surface of the outlet frit shows only minor corrosion spotting.....	15
Plate 7 Showing the inlet face and inner surface of the inlet face frit. There has been significant localised corrosion of the frit. Some of the corrosion products have transferred onto the inlet face.....	16
Plate 8 Control sample marked up with cm points along its length to assist in locating sample point distances from the inlet face .....	17
Plate 10 BSEM image of sandstone showing moderately compacted detrital fabric of quartz and K-feldspar grains, but with locally “oversized” pores indicative of secondary porosity formed by the dissolution of detrital framework grains. Patchy calcite cement appears partially corroded. Gamston borehole, sample MPLP106 .....	39
Plate 11 BSEM image of sandstone showing a thin “pellicle of illitic-smectitic-chloritic clay outlining an “oversized” secondary pore indicative formed by the dissolution of a detrital framework grain. Brittle deformation and crushing of a K-feldspar by compaction can also be seen. The clay coating was deposited on the surface of the original detrital grain (now removed by dissolution). Gamston borehole, sample MPLP106 .....	39
Plate 12 BSEM image showing patchy micronodular dolomite cement (dolocrete) with overgrowths of later sub-hedral to euhedral dolomite adjacent to open pores. Authigenic kaolinite can be seen partially filling oversized, secondary pores representing framework grain alteration / dissolution sites. Gamston borehole, sample MPLP106.....	40

Plate 13 SEI image showing detrital quartz grain surfaces coated with a thin pellicle of illitic or illite-smectite clay, with illite-smectite clay also forming a meniscus between grains at pore throats. Gamston borehole, sample MPLP106 .....	40
Plate 14 BSEM image showing authigenic kaolinite filling oversized, secondary pore space, representing a framework grain alteration / dissolution site. Remnants of corroded detrital K-feldspar are enclosed within the kaolinite. Gamston borehole, sample MPLP106 .....	41
Plate 15 SEI image showing showing vermicular or book-like crystals of authigenic kaolinite in secondary framework grain dissolution pore space. Wispy, flakey authigenic illite-smectite clay is also present, lining the pore space. Gamston borehole, sample MPLP106 .....	41
Plate 16 Transmitted light scanned image of thin section of sandstone, showing finely-laminated fabric, with thin, dark, ferruginous clay laminae (arrowed). Blue dye resin impregnation reveals relatively uniform distribution of intergranular porosity within cleaner sandstone laminae, with lower porosity within the finer darker laminae. Sample MPLP510, Cleethorpes No.1 geothermal borehole .....	46
Plate 17 Transmitted photomicrograph (plane polarised light) of thin section of sandstone, showing detail of finely-laminated sandstone fabric. The blue dye resin impregnation shows that intergranular porosity is significantly greater in the coarser, cleaner laminae and lower in the thin, dark, ferruginous clay-rich laminae. Many of the intergranular pores in the cleaner sandstone laminae are oversized, indicating that they are secondary and result from framework grain dissolution. Sample MPLP510, Cleethorpes No.1 geothermal borehole ...	47
Plate 18 Transmitted photomicrograph (plane polarised light) of thin section of sandstone, showing sandstone open, well-connected intergranular pore fabric, with moderately well-compacted sand grains, interspersed with “domains” with large oversized pores, indicative of major framework grain dissolution. Sample MPLP510, Cleethorpes No.1 geothermal borehole .....	47
Plate 19 Transmitted photomicrograph (plane polarised light) of thin section of sandstone, showing sandstone open, well-connected intergranular pore fabric, with moderately well-compacted sand grains, interspersed with “domains” with large oversized pores, indicative of major framework grain dissolution. The finer-grained ferruginous lamina running through the middle of the field of view shows very tight packing with the development of mainly long, concavo-convex, and triple-point grain contacts indicative of significant burial compaction. Sample MPLP510, Cleethorpes No.1 geothermal borehole .....	48
Plate 20 BSEM photomicrograph with EDXA-modal mineral distribution map overlay. The colours correspond to different phases: grey – quartz, black – porosity, white – K feldspar (and trace albite), laminated grey/white are lithic clasts, blue-represents dolomite cement and green – scattered clay minerals (both illitic clay and mica within lithic clasts). Sample MPLP510, Cleethorpes No.1 geothermal borehole.....	49
Plate 21 SEM photomicrograph (SEI) showing euhedral authigenic K-feldspar and quartz overgrowth cements locking the grain framework together. The overgrowth surfaces are generally very smooth and clean. Sample MPLP510, Cleethorpes No.1 geothermal borehole	49
Plate 22 SEM photomicrograph (SEI) showing detrital clay coatings on detrital grains, with authigenic illite-smectite forming wispy protrusions from some coatings. Sample MPLP510, Cleethorpes No.1 geothermal borehole .....	50
Plate 23 Transmitted light scanned image of thin section of sandstone, showing only traces of a discontinuous finely-laminated bedding fabric, with thin, dark, ferruginous clay laminae (arrowed). Blue dye resin impregnation reveals relatively uniform distribution of intergranular porosity. Sample MPLP511, Cleethorpes No.1 geothermal borehole .....	50

Plate 24 Transmitted photomicrograph (plane polarised light) of thin section of sandstone, showing sandstone open, very porous well-connected intergranular pore fabric, with moderately well-compacted sand grains, interspersed with “domains” with large oversized pores, indicative of major framework grain dissolution. Sample MPLP511, Cleethorpes No.1 geothermal borehole .....	51
Plate 25 BSEM photomicrograph with EDXA-modal mineral distribution map overlay. The colours correspond to different phases: grey – quartz, black – porosity, white – K feldspar (and trace albite), laminated grey/white are lithic clasts, blue-represents dolomite cement and green – scattered clay minerals (both illitic clay and mica within lithic clasts). Sample MPLP511, Cleethorpes No.1 geothermal borehole.....	51
Plate 26 Transmitted photomicrograph (plane polarised light) of thin section of sandstone, showing well-developed euhedral quartz overgrowths (clear) on detrital quartz grains. Sample MPLP511, Cleethorpes No.1 geothermal borehole.....	52
Plate 27 SEM photomicrograph (SEI) showing the typical morphology of authigenic wispy illite-smectite clay that locally abundantly developed and associated with the dissolution of unstable detrital minerals. Sample MPLP511, Cleethorpes No.1 geothermal borehole .....	52
Plate 28 SEI photomicrograph of dead <i>P. aeruginosa</i> sample (under ESEM). A: Precipitated crystals, two elongate in form, emergent from an amorphous mass of biogenic material, most likely biofilm residue, which is unevenly spread across the striations of the sample holder’s milled surface. B: At 85% theoretical water vapour relative humidity, partial rehydration has occurred, resulting in crystal dissolution and an expansion of the biogenic material .....	56
Plate 29 SEI photomicrograph of the inner face of the inlet frit (under ESEM). This shows the structure of the metallic matrix and pores of the frit .....	57
Plate 30 SEI photomicrograph of the inner face of the inlet frit (under ESEM). The widespread bladed pore-lining bladed deposit is most likely of iron oxide/hydroxide .....	57
Plate 31 SEI photomicrograph of the inner face of the inlet frit (under ESEM). Typical bladed deposit of probable iron oxide/hydroxide on pore walls with scattered angular mineral debris. Fingered amorphous sheet at top right is a probable biofilm residue .....	58
Plate 32 SEI photomicrographs (under ESEM). Samples from the biotic core (A, C, E) and the control core (B, D, F) are shown at different humidities and with different wetting liquids (details on images). All samples are from central portions of the cores except that in C. Liquid is typically imaged as a darker phase coating pore walls, draped between grains and locally filling pores. A shows the highest liquid content, A and C contrast finer and coarser grained sample portions, F is almost completely dry. Arrows in C highlight ridged forms ..	60
Plate 33 SEI photomicrographs of biotic sample from outlet face, prepared with diluted brine, distilled water used as the ESEM wetting liquid. Within a couple of minutes of reducing the humidity to 80%, the sample dried almost completely .....	61
Plate 34 SEI photomicrographs (under ESEM). A: Control sample from the inlet face, showing sparsely scattered pore-lining materials after drying. B: Biotic sample 40 mm in from the end face, showing widespread pore-lining material again in the dry state. In the latter, mineral fines are typically associated with a widespread amorphous film-like deposit.....	62
Plate 35 SEI photomicrographs (under ESEM) of biotic sample, 15 mm in from the inlet face, in a dry condition. This shows an amorphous globular deposit draped across the stepped form of a K-feldspar overgrowth, with associated mineral fines .....	63
Plate 36 SEI photomicrographs (under ESEM) of biotic sample, from 2 mm inside the inlet face, partially dry using brine as the ESEM wetting liquid. Brine remains as a thin film on pore walls, here largely defined by K-feldspar overgrowth, and as thicker pools in pore throats.	

Arrows show two ridges that bridge across the pore margin that are most likely supported by biofilm .....	63
Plate 37 SEI photomicrographs (under ESEM) of biotic sample, 40 mm from inlet face, slightly rehydrated after drying, brine used as the ESEM wetting liquid. Fibrous forms visible within this patch of amorphous pore-lining deposit are incipient halite crystals .....	63
Plate 38 SEI photomicrographs (under ESEM) of biotic sample from outlet face, still wet with a thin film of brine coating pore walls. Indicated fibrous forms emergent from the pore-lining film deposit are most likely illitic clay fibres .....	64
Plate 40 SEI photomicrographs (under ESEM) of biotic sample, at outlet face, distilled-water-wet sample at 100% humidity after a period at 80% humidity. The probable biofilm deposit, including the fibrous portion (unlabelled arrow), showing a fragmented form; this is taken as evidence of beam damage. There are also scattered probable bacterial forms.....	64

## TABLES

Table 1 Summary details of the sandstone core samples .....	5
Table 2 Mean total microbial counts by epifluorescence microscopy of outflow fluids from biotic experiment .....	22
Table 3 Mean total microbial counts by epifluorescence microscopy of outflow fluids from control experiment.....	23
Table 4 Modal mineralogical data for the Sherwood Sandstone Group samples from the Gamston borehole .....	38
Table 5 Quantitative whole-rock XRD analysis from the Gamston borehole sample .....	42
Table 6 Semi-quantitative <2 µm clay mineral XRD analyses from the Gamston borehole .....	43
Table 7 Modal mineralogical data for the Sherwood Sandstone Group samples from the Cleethorpes No.1 borehole .....	45
Table 8 Quantitative whole-rock XRD analysis from the Cleethorpes No.1 borehole samples ...	54
Table 9 Summary of semi-quantitative <2 µm clay mineral XRD analyses from the Cleethorpes No.1 borehole samples .....	54
Table 10 Summary of differences in rock materials from biotic and control experiments.....	59

## Summary

The BioTran project was initiated to examine the effects of microbes on sub-surface transport processes, especially in the context of geological disposal of radioactive waste. Early work focussed on hard rock environments using dioritic material from the Äspö Underground Research Laboratory (URL). In 2008-2009, the scope of Biotran broadened to encompass batch experiments on mudstones, host rocks relevant to radioactive waste management in Japan. The 2009-2010 BioTran work programme used column experiments to investigate the effects of microbes on fractured mudstone. This work was undertaken on behalf of the Japanese Atomic Energy Authority (JAEA) and part-funded by the Ministry of Economy, Trade and Industry of Japan (METI), Japan.

BioTran work in 2010-2011 changed to focus on a different rock type with a more generic application. In the UK, there are uncertainties regarding the host geology for the deep geological

disposal facility (GDF) for low and intermediate level waste (L/ILW). Consequently, some UK microbiological research programmes (e.g. NERC BIGRAD consortium) target, for investigation, a “generic” rock type with a mineralogy that could be considered broadly similar to that of a potential host geology that might be expected in the UK, with an acid/intermediate character containing quartz, feldspars, muscovite/chlorite/illite and iron oxides. In this context, programmes, such as BIGRAD (cf. [www.bigradnerc.com](http://www.bigradnerc.com)) have employed a carbonate, clay, mica (illite)-bearing feldspathic Permo-Triassic sandstone, which is relevant to a number of GDF concepts. The BioTran work has targeted calcite-dolomite-cemented feldspathic sandstone from the Sherwood Sandstone Group for examination, and this report describes pilot studies investigating changes in far-field transport properties that are due to microbial activity within intact core material. The Sherwood Sandstone Group is the UK’s second most important aquifer formation (second only in size to the Chalk), thus representing a major water resource. It is also one of UK’s principal oil and gas reservoirs, and a target formation for natural gas storage. It also contains some of the largest deep saline aquifers that have potential for the geological storage of carbon dioxide (CO<sub>2</sub>), in the southern North Sea and Irish Sea areas offshore of the UK. Consequently, results from this year’s work will also be relevant to this technology.

This pilot study of the Sherwood Sandstone has shown that the common soil organism, *Pseudomonas aeruginosa*, can survive and thrive in pressurised flow through column experiments over a period of 235 days (5642 h) from injection. Numbers of organisms in the biotic experiment appear to stabilise at  $\sim 10^5$  ml<sup>-1</sup> throughout the experiment.

Fluctuations in injection pressure within the cores were detected during the biotic and control column experiments over the experimental period. In the biotic experiment, post inoculation pressure increased with an average injection pressure of 488 kPa compared to 15 kPa in the control experiment. Short but rapid saw-tooth like changes in pressure were only observed under biotic conditions.

Post experimental imaging of the post-experimental rock features showed *P. aeruginosa* derived biofilms significantly covering the pore wall surfaces of the sandstone host. However, there was no evidence of dissolution or alteration effects when compared to the starting materials.

Overall, fluid chemistry results show a steady decline in element concentrations throughout the experiments. There are significant changes in sodium, chloride and Non-Purgeable Organic Carbon (NPOC) concentrations in the biotic column experiments for period between 620 and 2090 h. However, all fluid chemistry changes do not appear to have influenced the physical and microbial results.

These results suggest that, whilst microbial activity does not appear to impact on overall chemistry results, their effects on physical transport properties is profound in terms of fluid flow. This is shown by the quantitative changes in permeability, as demonstrated by increases of the monitored injection pressure in the biotic experiment. Additionally, whilst biofilms form on mineral surfaces which can be imaged, they do not alter the surfaces in any way. Taken together, this would suggest that the production of biofilms is the primary cause of changes in fluid flow which is also observed in studies in other rock types such as mudstones. Microbial activity is likely, therefore, to complicate the physical transport of contaminants in the geological environment. This is likely to be rock type and site/concept specific and the following examples could include:

- Radioactive waste – the effects of microbes on the transport of an alkaline fluid generated from a cementitious repository into the excavation damaged zone and into the host rock;
- Carbon capture and storage - the effects of microbes on the transport of CO<sub>2</sub> and any associated contaminants, such as H<sub>2</sub>S, NO<sub>x</sub> and SO<sub>x</sub>, in saturated water in storage reservoirs.

# 1 Introduction

The BioTran project was initiated to examine the effects of microbes on sub-surface transport processes, especially in the context of geological disposal of radioactive waste. Early work focussed on hard rock environments using dioritic material from the Äspö Underground Research Laboratory (URL). In 2008-2009, the scope of Biotran broadened to encompass batch experiments on mudstones, host rocks relevant to radioactive waste management in Japan. The 2009-2010 BioTran work programme used column experiments to investigate the effects of microbes on fractured mudstone. This work was undertaken on behalf of the Japanese Atomic Energy Authority (JAEA) and part-funded by the Ministry of Economy, Trade and Industry of Japan (METI), Japan and is published elsewhere (Harrison *et al.*, 2010; 2011).

BioTran work in 2010-2011 changed to focus on a different rock type with a more generic application. In the UK, there are uncertainties regarding the host geology for the deep geological disposal facility (GDF) for low and intermediate level waste (L/ILW). Consequently, some UK microbiological research programmes (*e.g.* NERC BIGRAD consortium) target, for investigation, a “generic” rock type with a mineralogy that could be considered broadly similar to that of a potential host geology that might be expected in the UK, with an acid/intermediate character containing quartz, feldspars, muscovite/chlorite/illite and iron oxides. In this context, programmes, such as BIGRAD (cf. [www.bigradnerc.com](http://www.bigradnerc.com)) have employed a carbonate, clay, mica (illite)-bearing feldspathic Permo-Triassic sandstone, which is relevant to a number of GDF concepts. The BioTran work has, targeted calcite-dolomite-cemented feldspathic sandstone from the Sherwood Sandstone Group for examination, and this report describes pilot studies investigating changes in far-field transport properties that are due to microbial activity within intact core material. The Sherwood Sandstone Group is the UK’s second most important aquifer formation (second only in size to the Chalk), thus representing a major water resource. It is also one of UK’s principal oil and gas reservoirs, and a target formation for natural gas storage. In addition it contains the largest deep saline aquifers that have potential for the geological storage of carbon dioxide, in the southern North Sea and Irish Sea areas offshore of the UK. Consequently, results from this year’s work will also be relevant to this technology.

## 2 Laboratory techniques

### 2.1 EXPERIMENTAL OVERVIEW

The aim of this study was to evaluate how biofilms, generated by the soil bacteria *Pseudomonas aeruginosa*, influenced the flow of synthetic saline groundwater through intact Sherwood Sandstone. Two experiments, one biotic and a control, were carried out using a flow-through column operated at a constant flow and under pressurised conditions. Changes in biological and chemical parameters were monitored throughout the experiment together with changes in confining pressure and temperature. The experiments were pilot studies and were carried out using a sandstone sample taken from the Sherwood Sandstone Group from the Cleethorpes borehole (Table 1). A saline groundwater (0.25M as NaCl) was prepared and, for the biotic experiment only, supplemented with sodium acetate (0.25 g l<sup>-1</sup>) to provide a readily available source of organic carbon to sustain bacterial growth. The synthetic groundwater was sterilised by filtration through a Sartorius filter (0.2 µm). The addition of sodium acetate was necessary to promote microbial activity, as this pilot experiment was short-term.

For the biotic experiment, the apparatus was fully assembled and filled with artificial groundwater on 5<sup>th</sup> October 2010 and allowed to stabilise with pressure changes being logged from 5<sup>th</sup> November 2010 and injection with *P. aeruginosa* on 12<sup>th</sup> November 2010, 38 days after apparatus assembly. On the 25<sup>th</sup> February 2011, (143 days after apparatus assembly), the pump

was refilled with groundwater (without additional microorganisms) and pumping continued until the 5<sup>th</sup> July. The pump was stopped and the experiment was decommissioned the next day – a total of 272 days (6528 h) from assembly of the equipment and start of the overall experiment; or 235 days (5642 h) after injection of the organisms.

The control experiment (*i.e.* no injection of microorganisms) started on 5<sup>th</sup> November 2010 with changes in pressure logged from that date. No period of stabilisation was required because the system was unaltered until May 2011. The system was monitored until the 10<sup>th</sup> May 2011, (186 days – 4464 h). A small aliquot approx. 20 ml of the saline groundwater containing organic material (*i.e.* microorganisms killed by overnight exposure to UV light and associated biofilm) was inoculated into the pump on the 11<sup>th</sup> May 2011 and the pump restarted. The ‘control’ core was monitored until the 5<sup>th</sup> July 2011 when the pump was stopped and the experiment was decommissioned on the 6<sup>th</sup> July 2011 – a total of 242 days (5811 h).

## 2.2 FLOW-THROUGH COLUMN METHODOLOGY

The flow-through column experiments were performed using intact Sherwood Sandstone rock core. Core material was positioned vertically in a Teflon sheath with end caps allowing fluid flow through the column, and the assembly placed within a pressure vessel. Schematics of the completed experimental rig with the pressure vessel and rock core assembly are shown in Figure 1 and Figure 2 with a photograph of the assembled apparatus in Plate 1. Once assembled, the pressure vessel was partially filled with deionised water and pressurised to 4000 kPa. The synthetic saline groundwater was used to fill the syringe pump and the flow rate was set at 300  $\mu\text{l h}^{-1}$  ( $\sim 7.2 \text{ ml day}^{-1}$ ). The cores were not pre-saturated with synthetic groundwater prior to the start of the experiment. The first ‘biotic’ column was injected with *P. aeruginosa* after 38 days (approximately 912 h) and the test was terminated after a total of 272 days (6528 h). The second ‘control’ column was not injected with the organisms and the test was run for 186 days (4483 h). At this point, a population of *P. aeruginosa* and associated biofilm that had been killed by overnight exposure to UV light was then injected (4484 h) to ascertain the impact of inert organic material on flow.

Pressure transducers, shown in Figure 1 as PT 1 and PT 2, were used to monitor the pressure changes within the cores while the syringe pumps controlled the flow-rate. The transducer outputs were recorded, along with actual pressure measurements on a calibrated DRUCK DPI 610 pressure calibrator and these data were subsequently used to calibrate the pumps and transducers. Fluid samples were collected by syringe at regular intervals for chemical and biological analyses.

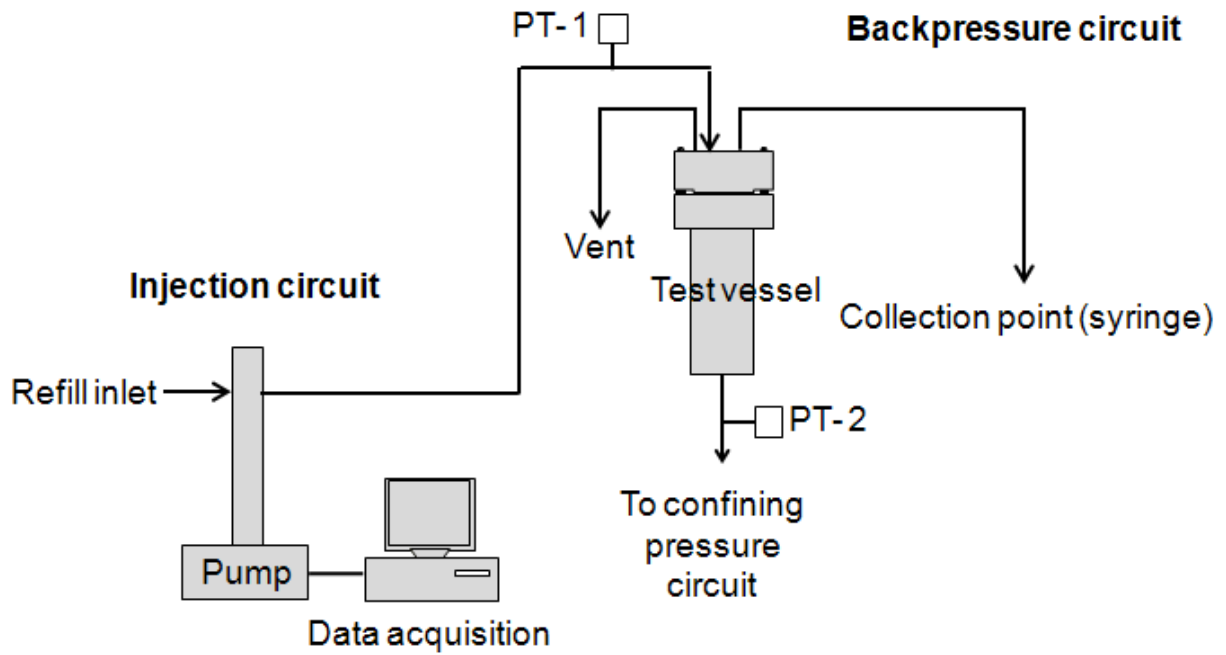


**Figure 1 Schematic of column design**

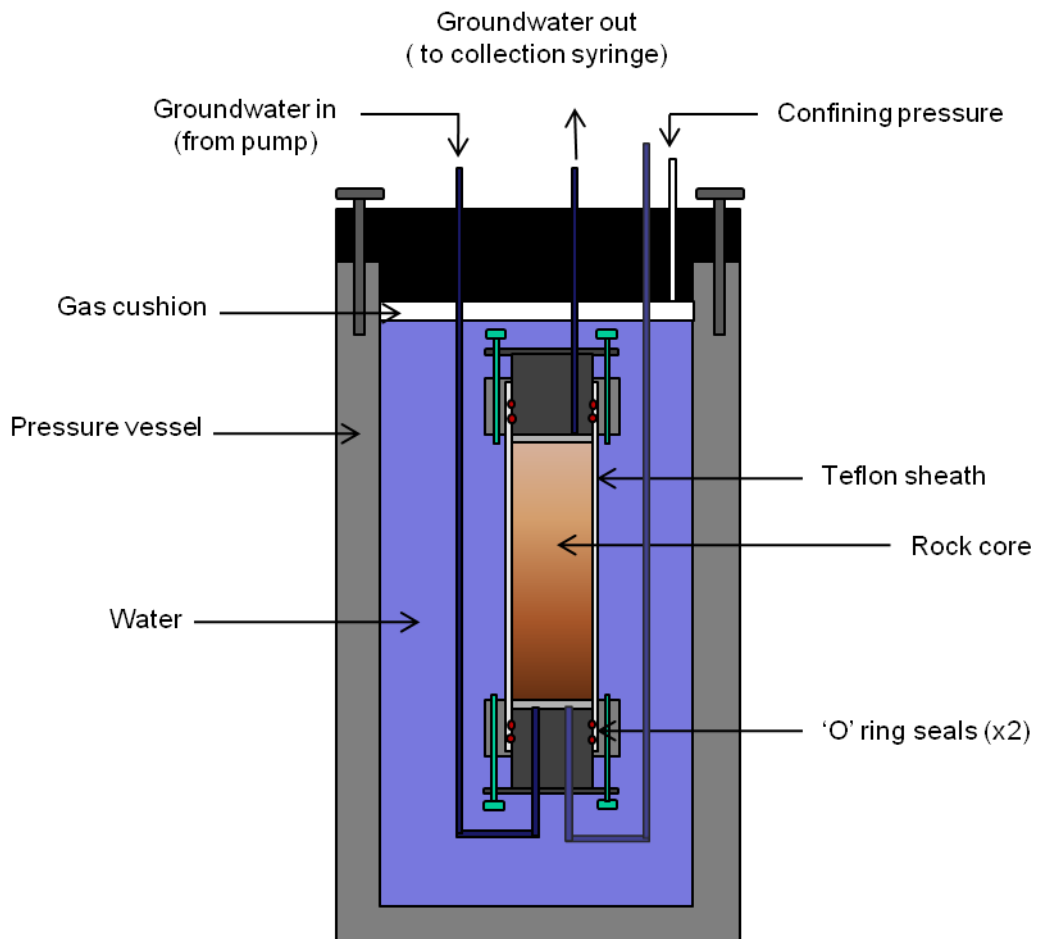


**Figure 2 Schematic of pressure vessel with column containing rock core**



**Plate 1 Photograph of assembled apparatus showing pressure vessel and syringe pump**

### **2.3 PREPARATION OF FLUIDS**

The synthetic groundwater was prepared from Analytical Reagent (AR) grade solid reagents. A saline (0.25M NaCl) solution was prepared by dissolving  $14.6 \text{ g l}^{-1}$  of NaCl in  $18.4 \text{ } \Omega\text{M}$  water. Sodium acetate ( $\text{CH}_3\text{COONa}\cdot 3\text{H}_2\text{O}$ ) was added as  $0.25 \text{ g l}^{-1}$  (TOC =  $22 \text{ mg l}^{-1}$ ). The fluid was then filter sterilised using a  $0.2 \text{ } \mu\text{m}$  filter and refrigerated until assembly of the experiment.

### **2.4 SELECTION AND PREPARATION OF INTACT CORE MATERIAL**

Based on background BGS information on the Sherwood Sandstone Group (Milodowski and Rushton, 2008), cores of Sherwood Sandstone Group and Basal Permian Sandstone Formation material were briefly examined and sampled from the Cleethorpes No.1 Geothermal Borehole and from the Gamston Borehole (BGS Borehole Database Reference SK77NW29). Three samples from Cleethorpes No.1 Geothermal Borehole and 1 sample from the Gamston Borehole (National Geoscience Data Centre, NGDC, Archive Reference No. SSK3828) were taken for petrographical characterisation and evaluation for use in the experiments. The sample details are provided in Table 1.

**Table 1 Summary details of the sandstone core samples**

Borehole	Stratigraphy	Rock Type	Sample Depth (m)	Sample Code
Gamston, Nottinghamshire (SK77NW29)	Sherwood Sandstone Group (Castle Sandstone Formation)	Feldspathic sandstone	198.47 – 198.62	MPLP106
Cleethorpes No. 1 Lincolnshire	Sherwood Sandstone Group (undifferentiated)	Feldspathic sandstone	1312.26-1312.41	MPLP510
Cleethorpes No. 1 Lincolnshire	Sherwood Sandstone Group (undifferentiated)	Feldspathic sandstone	1315.00-1315.13	MPLP511
Cleethorpes No. 1 Lincolnshire	Basal Permian Sandstone	Lithic-feldspathic sandstone	1892.75-1892.90	MPLP512

Following initial assessment of background data, the permeability of the sandstone from the Gamston borehole (MPLP106) was considered to be too high for practical use in the BioTran experiments. The two sandstones from the Sherwood Sandstone Group from the Cleethorpes No.1 borehole were considered to have permeability characteristics that were more appropriate, and were therefore selected for use in the experiments. Three parallel plugs were cut longitudinally from the MPLP510 sample core using a 37 mm (nominal) diameter (ID) diamond-impregnated core barrel, of which one was used for the biotic experiment. Two cores of the 37 mm (nominal) diameter (ID) were cut longitudinally from the MPLP511 sample core, only one of which was suitable for use in the control experiment.

## 2.5 BACTERIAL CULTURE

*Pseudomonas aeruginosa* was selected for its biofilm (exopolysaccharide - EPS) forming properties (Vaughan *et al.*, 2001) and has been used previously in BioTran experiments (Harrison *et al.*, 2009). It categorised as a gram-negative rod, 0.5 to 0.8 µm wide by 1.5 to 3.0 µm in length and is a pathogen of humans. The matrix of the *P. aeruginosa* biofilm is composed of an alginate polymer of mannuronic and glucuronic acids. Its natural habitat is soil but it is also common to water and vegetation. *P. aeruginosa* is primarily aerobic but will grow under anaerobic conditions in the presence of nitrate which it can use as a respiratory electron acceptor; it is also resistant to high concentrations of salts. In this respect, it is a suitable strain for the experiment as synthetic saline groundwater is being utilised.

*P. aeruginosa* (NCIMB 10548) was received in a freeze dried state and resuscitated by adding 0.5 ml of sterile Nutrient broth (OXOID). This suspension was then subcultured onto agar slopes (OXOID CM3) and into a 50 ml flask of sterile nutrient broth. The slopes were refrigerated to maintain a stock culture for future experiments. The flask was placed on an orbital shaker and incubated overnight at 36°C to encourage microbial growth. One ml of the actively growing culture was then further inoculated into 500 ml flasks of sterile nutrient broth to achieve a large volume of bacteria. Within 24 hours, the culture was then transferred to 35 ml sterile tubes and centrifuged at 4600 rpm for 20 minutes. The supernatant was aseptically removed and the volume replaced with sterile artificial saline groundwater. The tubes were remixed and the centrifugation process repeated four times until traces of culture media were 'washed' from the bacteria. Decreasing volumes of synthetic groundwater were added at each stage to concentrate the bacteria. The resulting fluid was then added to approximately 500 ml of synthetic groundwater, this produced sufficient volume to fill the syringe pump. A 1.0 ml sample of each suspended culture was removed by sterile pipette and preserved in glutaraldehyde fixative solution (Jass and Lappin-Scott, 1992) prior to microscopic examination. The total number of bacteria inoculated was then determined by direct counting using epifluorescence microscopy (Hobbie *et al.*, 1977; Jass and Lappin-Scott, 1992).

## 2.6 DECOMMISSIONING OF EXPERIMENTS

Both the biotic and control experiments were terminated on 6<sup>th</sup> July 2011. Plate 2 shows the decommissioning procedure. Plate 3 to Plate 5 show the intact biotic and abiotic (control) columns just prior to opening for mineralogical analyses.



**Plate 2 Removal of column assembly from pressure vessel (Biotic experiment)**



**Plate 3 Biotic column after removal from pressure vessel**

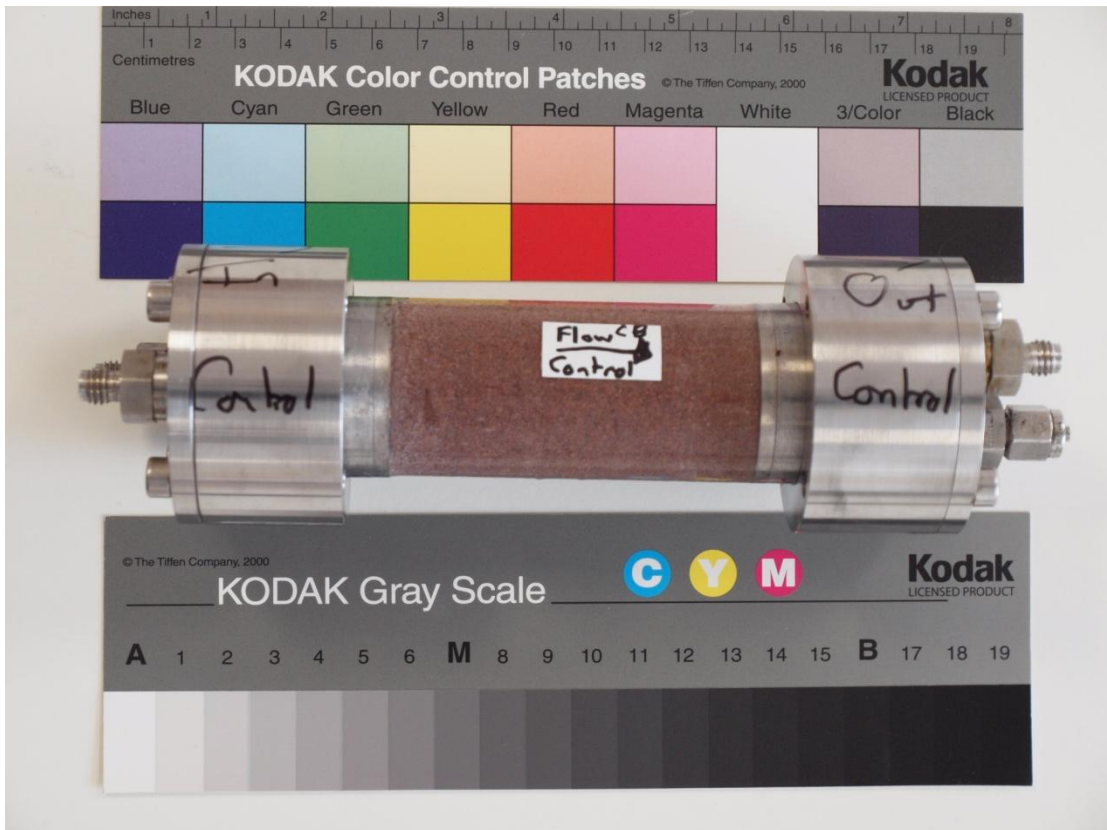


Plate 4 Control column after removal from pressure vessel. Arrow indicates direction of fluid flow during the experiment



Plate 5 Both columns after removal of end pieces just prior to mineralogical analyses

## 3 Analytical techniques

### 3.1 CHEMICAL ANALYSES

A reference sample of the synthetic groundwater used to fill the syringe pump was taken for comparison to the outflow fluids from the biotic and control columns at the start of each experiment (day 0) and at 7 day intervals until the end of the experiments. Chemical analyses included major anions by ion chromatography (IC) and cations by Inductively Coupled Plasma - Mass Spectroscopy, (ICP-MS), as well as redox sensitive species ( $\text{Fe}^{2+}/\text{Fe}^{3+}$ ), pH and selected microbial nutrients (*e.g.* C, P, S and N). Non-Purgeable Organic Carbon (NPOC) was also evaluated which gives an indication of the degradation rate of organic compounds during the experiments.

### 3.2 MICROBIOLOGICAL ANALYSES

A reference sample of the synthetic groundwater used to fill the syringe pump was taken for comparison to the outflow fluids from the biotic and control columns at the start of each test (day 0) and at approximately 7 day (168 h) intervals until the end of the experiments. Microbial biomass was evaluated using epifluorescence microscopy. Epifluorescence microscopy uses a short wavelength transmission source to fluoresce a sample stained with the nucleic acid selective cationic fluorochrome. The fluorescent stain, Acridine Orange [N,N,N',N'-tetramethylacridine 3,6-diamine ( $\text{C}_{17}\text{H}_{19}\text{N}_3$ )], was used to determine total cell counts (Hobbie *et al.*, 1977; Jass and Lappin-Scott, 1992). Acridine Orange is capable of permeating cells and interacting with DNA and RNA by intercalation or electrostatic attractions. When the fluorescent stain interacts with DNA, which is spectrally similar to fluorescein, the excitation maximum is at 502 nm (cyan) and the emission maximum at 525 nm (green), while RNA interactions shift the excitation maximum to 460 nm (blue) and the emission maximum to 650 nm (red). Thus, it is possible to determine if cells are metabolically active as they appear red due to the predominant RNA whereas inactive or slow growing bacterial have mostly DNA and appear green. By examination of 20 randomly selected fields of view, the numbers of bacteria per ml can be counted.

### 3.3 CHARACTERISATION OF SOLID MATERIALS

#### 3.3.1 X-ray diffraction analyses

Quantitative whole-rock mineralogical analysis and qualitative clay mineral analysis of the starting materials were determined by X-ray diffraction (XRD) analysis.

##### 3.3.1.1 SAMPLE PREPARATION

The sample was initially crushed in a pestle and mortar. Approximately 5 g of the crushed material was then subsampled and tema-milled to  $<125 \mu\text{m}$ .

In order to achieve a finer and uniform particle-size for whole-rock XRD analysis, the tema-milled material was wet-micronised under water for 10 minutes and then spray-dried following the method and apparatus described by Hillier (1999). The spray-dried material was then front-loaded into a standard stainless steel sample holder for analysis.

Approximately 10 g of crushed sample was dispersed in deionised water using a reciprocal shaker combined with ultrasound treatment. The suspension was then sieved on  $63 \mu\text{m}$  and the  $<63 \mu\text{m}$  material placed in a measuring cylinder and allowed to stand. In order to prevent flocculation of the clay crystals, 1.0 ml of 0.1M 'Calgon'® (sodium hexametaphosphate, SigmaAldrich (305553)) was added to the suspension. After a time period determined from Stokes' Law, a nominal  $<2 \mu\text{m}$  fraction was removed and dried at  $55^\circ\text{C}$ . 100 mg of the  $<2 \mu\text{m}$  material was then re-suspended in a minimum of distilled water and pipetted onto a ceramic tile

in a vacuum apparatus to produce an oriented mount. The mount was Ca-saturated using 0.1M  $\text{CaCl}_2 \cdot 6\text{H}_2\text{O}$  solution and washed twice to remove excess reagent.

### 3.3.1.2 QUANTITATIVE X-RAY DIFFRACTION

XRD analysis was carried out using a PANalytical X'Pert Pro series diffractometer equipped with a cobalt-target tube, X'Celerator detector and operated at 45kV and 40mA.

The spray-dried sample was scanned from  $4.5\text{-}85^\circ 2\theta$  at  $2.76^\circ 2\theta \text{ min}^{-1}$ . Diffraction data were initially analysed using PANalytical X'Pert Highscore Plus version 2.2a software coupled to the latest version of the International Centre for Diffraction Data (ICDD) database.

Following identification of the mineral species present in the sample, mineral quantification was achieved using the Rietveld refinement technique (*e.g.* Snyder & Bish, 1989) using PANalytical Highscore Plus software. This method avoids the need to produce synthetic mixtures and involves the least squares fitting of measured to calculated XRD profiles using a crystal structure databank. Errors for the quoted mineral concentrations are typically  $\pm 2.5\%$  for concentrations  $>60 \text{ wt}\%$ ,  $\pm 5\%$  for concentrations between 60 and 30 wt%,  $\pm 10\%$  for concentrations between 30 and 10 wt%,  $\pm 20\%$  for concentrations between 10 and 3 wt% and  $\pm 40\%$  for concentrations  $<3 \text{ wt}\%$  (Hillier *et al.*, 2001). Where a phase was detected but its concentration was indicated to be below 0.5%, it is assigned a value of  $<0.5\%$ , since the error associated with quantification at such low levels becomes too large.

The  $<2 \mu\text{m}$  oriented mount was scanned from  $2\text{-}40^\circ 2\theta$  at  $1^\circ 2\theta \text{ min}^{-1}$  after air-drying, after glycol-solvation and after heating to  $550^\circ\text{C}$  for 2 hours.

### 3.3.2 Mercury injection core porosity and permeametry

The porosity and permeability characteristics of the two sandstone samples from the Sherwood Sandstone Group from the Cleethorpes No.1 borehole, that were selected for use in the BioTran experiments, were evaluated in detail using mercury intrusion core porosimetry.

This method employs a Micromeritics AutoPore IV Model 9500 computer controlled scanning mercury intrusion porosimeter. A prepared sample is sealed in a calibrated chamber. Since mercury does not wet most substances and will not spontaneously penetrate pores by capillary action, it must be forced into the pores by the application of external pressure. The required equilibrated pressure is inversely proportional to the size of the pores, only slight pressure being required to intrude mercury into large macropores, whereas much greater pressures are required to force mercury into small pores. Mercury porosimetry analysis is the progressive intrusion of mercury into a porous structure under stringently controlled pressures. From the pressure versus intrusion data, the instrument generates volume and size distributions using the Washburn equation (Abell *et al.*, 1999). Clearly, the more accurate the pressure measurements, the more accurate the resulting pore size data.

Further details on the technical references and research literature for this methodology are available at the equipment manufacturer's website at [www.micromeritics.com](http://www.micromeritics.com).

### 3.3.3 Petrographic characterisation of the starting material

The sandstone starting materials were petrographically characterised by optical thin section petrography and scanning electron microscopy (SEM), using both backscattered scanning electron microscopy (BSEM) and secondary electron imaging (SEI) techniques.

Subsamples of sandstone were prepared as 28 x 48 mm polished thin sections for use by both optical petrography and BSEM. The sandstone subsamples were vacuum-impregnated with epoxy-resin to stabilise the material prior to sectioning. A blue dye was added to the resin to enable the porosity to be readily identified and visualised under the optical petrological microscope.

### 3.3.3.1 OPTICAL PETROGRAPHY

Optical petrographical analysis was carried out using a Zeiss Axioplan II digital petrological photomicroscope fitted with a Zeiss Axiocam MRc5 dedicated digital camera. Images were captured and processed from the photomicroscope using the Zeiss Axiovision software package. Observations were made in transmitted light under both plane-polarised light and under crossed polars, as appropriate.

Low magnification images of whole thin sections were also recorded by digitally scanning of the thin section using an Epsom Perfection 1240U flatbed scanner equipped with a transmitted light (transparency) scanning attachment. Scanned whole-section images were recorded at a resolution of 1200 dpi.

### 3.3.3.2 SCANNING ELECTRON MICROSCOPY

Scanning electron microscopy (SEM) analysis of the starting materials was undertaken using a LEO 435VP variable pressure digital scanning electron microscope fitted with a solid-state 4-element (diode-type) backscattered electron detector, and equipped with an Oxford Instruments INCA Energy 450 energy-dispersive X-ray microanalysis (EDXA) system with a thin window Si-Li X-ray detector capable of detecting elements from boron to uranium. Phase/mineral identification was aided by qualitative observation of the EDXA, which were recorded simultaneously during SEM observation.

#### *Pore morphology characterisation*

Pore morphology and pore surface mineralogy was characterised by secondary electron imaging (SEI) and backscattered electron microscopy (BSEM). Small (*ca.* 10 x 10 x 10 mm) subsamples of core were prepared with freshly-broken surfaces, were prepared and mounted onto 10 mm diameter, pin-type aluminium stubs (Cambridge stubs). Using Leit CCC conducting carbon cement. The stub-mounted samples were then coated with a thin (25nm) layer of carbon, to make the sample surfaces electrically conductive and thereby prevent electrical charging during SEM examination, by evaporation of carbon under vacuum. The sample surfaces were then examined under high vacuum using both SEI mode to observe fine morphological details and in BSEM mode to help differentiate different surface phases, on the basis of their difference in composition and density (which influences the backscattered electron coefficient and thereby image brightness in BSEM *cf.* Goldstein *et al.*, 1981).

#### *Backscattered scanning electron microscopy of polished thin sections*

High-resolution petrographical observations were made of the polished thin sections of sandstone, using BSEM to examine mineralogy and rock fabric in detail. Phase identification was aided by observation of semi-quantitative EDXA spectra that were recorded simultaneously during BSEM observation.

For general petrographical observations, the SEM instrument was operated using a 20 kV electron beam accelerating potential, a beam current between 200-800 pA, and a working distance of 18-20 mm, as required. Phase identification was aided by microchemical information obtained from observation of semi-quantitative EDXA spectra recorded from features of interest. BSEM images for routine observation purposes were recorded digitally via the SEM instrument at a resolution of 1024 x 768 pixels. However, BSEM images that were used for subsequent computerised petrographical image analysis to quantify the porosity characteristics were collected at 1024 x 704 or higher 2048 x 1408 pixel resolutions *via* the Oxford INCA Energy 450 EDXA system.

### 3.3.3.3 MINERALOGICAL MODAL ANALYSIS

Modal mineralogical analyses was performed on the two Sherwood Sandstone Group samples from Cleethorpes No.1 borehole and the single Sherwood Sandstone Group sample from the Gamston borehole.

#### *Image processing and analysis*

Modal mineralogical analysis was carried out by image analysis of digital EDXA elemental X-ray maps recorded from the polished thin sections using the SEM instrument described above. Section areas for EDXA element mapping were selected to be representative of each polished thin section as a whole, on the basis of expert petrographer's judgment, taking into account the variability and heterogeneity observed during optical and BSEM microscopy. Areas for X-ray elemental mapping were imaged by BSEM at a magnification chosen to include approximately 400 image objects (including mineral grains and intergranular pore regions) within each image field of view (Figure 3). For generally homogenous samples, two fields of view (minimum) were recorded. However, where more than one lithology comprised a significant proportion of the thin section at least two images were recorded from each of the lithologies, and the modal mineralogy of each lithology was determined separately.

EDXA element maps were recorded using the 'Mapping' programme "Smart Map" within the Oxford Energy INCA Suite Version 4.08 (2006) software package. EDXA X-ray spectral data were recorded from each pixel the field of view at a resolution of 512 x 512 pixels, using a 20 kV electron beam, 1 nA (1000 pA) beam currents and at a working distance of 19 mm, to give optimum X-ray count rates of between 1200 and 1600 counts per second. X-ray element maps were produced by summation of data recorded from multiple frame scans to produce maps with sufficient X-ray counts per pixel to enable key elements, required for the differentiation of the mineral species present, to be detected above background noise. In general, maps were recorded over a minimum of 20 frame scans were recorded to achieve sufficient analytical sensitivity within a practical time limit of about 1 hour per map area.

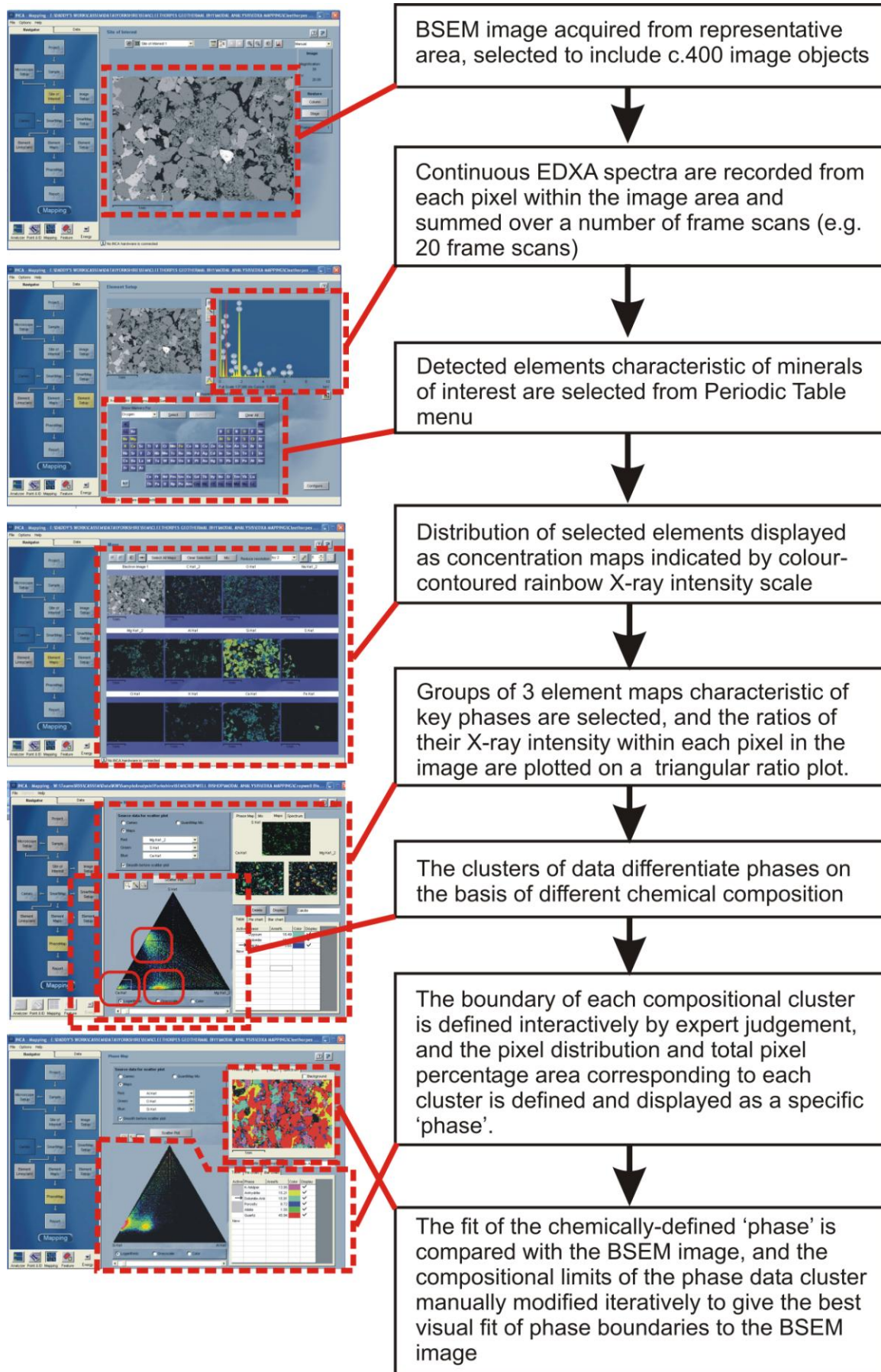


**Figure 3 Work flow diagram for image processing of EDXA element maps for mineralogical modal analysis**

EDXA element maps were processed to differentiate mineral/phase distributions and area percentages using the 'PhaseMap' programme within the Oxford Energy INCA Suite Version 4.15 18d+SP3 (2009) mapping software package (Figure 3). Groups of three elements were selected, as appropriate to define specific minerals or other components phases on the basis of their chemistry. For example, maps of K, Al and Si concentration can be used to differentiate between quartz, K-feldspar and muscovite, on the basis of the difference in the ratios of these elements within these minerals. Similarly, maps for C, O and Si differentiated between most minerals and the epoxy-resin-filled porosity in thin section. The ratio of X-ray count intensities for the characteristic X-ray line (K, L or M line) for each element within each pixel element of the map area was compared and plotted as a triangular ratio plot of the three elements. From this clusters of pixels could be identified with element concentration ratios corresponding to different phases. The compositional boundaries of each cluster of element ratios were defined by expert judgment, and the spatial distribution of pixels within these clusters displayed by the software as a map of that particular phase. The pixel area corresponding specific phase compositions could then be measured and its modal composition calculated in terms of the percentage of the total image area (Figure 3). Three elements were sufficient to define many of the minerals which were significantly different in chemistry. However, in some cases this process had to be repeated using several combinations of three elements to differentiate phases with more subtle differences in chemistry or where X-ray maps had not been acquired with sufficient X-ray counts to reliably detect some key elements (*e.g.* for light elements such as Na and Mg, where the quality of the EDXA data was sometimes noisier and poorer). Where appropriate, some phases were calculated by difference between phase maps produced with different element combinations.

#### *Sources of error and uncertainty*

There are a number of potential sources of error in the determination of the modal mineralogy, including the following:

1. Image resolution and magnification interact to have a potentially significant effect on the resolution of mineral grains, which in turn, influences the mineralogical modal analysis. The EDXA element maps were recorded at a resolution of 512 x 512 pixels per field of view. EDXA data recorded for each pixel represents the average composition within the pixel area. However, the actual area of the petrographic section that each pixel covers is dependent on the magnification of the image. Pixels recorded at a higher magnification sample smaller areas of the thin section, and therefore are more likely to resolve and sample finer grained material as discrete single phases. In contrast, pixels recorded at lower magnification will potentially include several mineral grains where the particle size is close to or finer than the pixel area. For pixels where this is the case, the EDXA data recorded at each pixel will reflect the average of the chemistry of the phases included within the pixel area.
2. Particle size and X-ray generation volume: Errors arise in the definition of the X-ray emission from very fine particles. X-rays may be generated by the electron beam from a region up to several micrometres deep in the sample, depending on mineral density and average atomic number. For fine particles (*ca.* 5 $\mu$ m) X-ray emission may be generated from a region larger than the particle of interest and represent a mixture of phases.
3. Particle edge effects: Pixels at the edges of grains may overlap adjacent minerals. Consequently, pixels around grain margins may report mixed composition of the two adjacent phases.
4. X-ray detection limits for key elements place a major constraint on defining phases. Light elements including O, C, Na and Mg have particularly poor detection limits, and unless a significant number of frame scans are acquired can produce very noisy images. This can affect the discrimination of minerals where these key elements (*e.g.* albite (Na), porosity (C, O in epoxy resin)) are close to detection.

5. Element X-ray line overlaps: Errors can arise where characteristic X-rays from different elements overlap. This may result in a high background and poorer element detection, or erroneous detection of elements (*e.g.* Ba L X-ray lines overlap with Ti K X-ray lines, making it difficult to differentiate between Ti and Ba phases on the basis of these elements alone).

6. Microporosity, pitting and scratching of the section surface and grain pluck sites within the polished section can produce anomalously low concentrations, as a result of the X-ray emission from pixels areas containing voids, returning a composition representing the average between void space and adjacent mineral substrate.

7. Operator definition of phase boundaries of the analysis clusters in compositional element triangular plots can be subjective, particularly if the compositions are gradational. This is very dependent on analyst experience. This was mitigated in this project by (i) experienced expert mineralogist judgement; (ii) visually cross checking the preciseness of the fit between the boundaries of phases defined by X-ray mapping and the BSEM image; and (iii) only accepting measurements giving modal analysis totals between 95 and 105% (before normalisation) — values outside these limits suggest significant missing components or major overlapping of defined phase boundaries.

8. Lithic clasts, chert and polymineralic grains. Conventional modal analysis by point-counting under a binocular microscope will differentiate lithic clasts (rock fragments), chert, polycrystalline quartz and monocrystalline quartz as discrete sedimentological components. This is based on expert judgment and the ability of the mineralogist to differentiate these components on the basis of their optical properties. However, modal analysis by SEM-EDXA phase mapping technique differentiates components on the basis of chemistry. Consequently, polymineralic lithic clasts will tend to be determined as their component minerals rather than as discrete particles, unless there is some distinctive chemical feature of the clast (such as sometimes produced by pervasive alteration). As a result, the modal analyses determined by SEM-EDXA phase mapping underestimate the significance of lithic components normally considered in sandstone classification (*cf.* Pettijohn *et al.*, 1987; Hallsworth and Knox, 1999). Monocrystalline quartz, polycrystalline quartz and chert are all essentially composed of silica (SiO<sub>2</sub>), and are therefore simply grouped together as “quartz”. Similarly, no differentiation can be made between primary sedimentary and secondary or authigenic generations of the same mineral using SEM-EDXA phase mapping.

These errors are difficult to estimate. Previous studies from the Cleethorpes borehole (Milodowski and Rushton, 2008) suggest uncertainties for the principal minerals of the order of ±2-10% for quartz, 10-25% for K-feldspar, dolomite-ankerite and anhydrite, 20-50% for albite and micas, and 10-30% for kaolinite and clay.

### 3.3.4 Petrographic characterisation of the post-experimental material

#### 3.3.4.1 SAMPLING AND SAMPLE PREPARATION

The materials available included:

- Biotic post-experimental core – this sample was stored under refrigerated conditions (<6°C) wrapped in ‘clingfilm’ after removal from the experimental apparatus. The polytetrafluoroethylene (PTFE) sleeve and end frits were left in place to minimise sample disturbance.
- ‘Control’ post-experimental core – as with the biotic sample, this sample was stored under refrigerated conditions (<6.0°C) wrapped in clingfilm after removal from the experimental apparatus. The PTFE sleeve and end frits were left in place.
- A sample of dead *P. aeruginosa* in groundwater – in sealed containers and stored under refrigerated conditions (<6.0°C).

The methods for handling and sampling the post-experimental materials evolved during the analytical process. This resulted from the recognition of unanticipated problems and from the results obtained from early analyses.

### *Biotic Sample*

The biotic sample was sampled and analysed first, to minimise the potential for changes to the distribution of biotic constituents (Plate 6). Initially it was anticipated that retaining the sample under refrigerated conditions and wrapped in 'clingfilm' would be sufficient to maintain the saturated conditions of the sample. It was noted, however, that the first 1-2 cm at each end had visibly reduced saturation levels after only a couple of hours storage under these conditions, probably as a result of evaporation. Consequently after collecting the first few sample portions, the sample was stored immersed in 0.25M NaCl solution (brine), again with the PTFE sleeve and end frits in place (loosely laid in place after sampling of the end faces). Initially this solution was used in a non-sterile state. After approximately 16 hours the original brine was replaced with freshly 0.45 µm filtered 0.25M NaCl brine.

When the inlet end face was first exposed to take samples it was noted that the inner surface of the end frit showed evidence of significant corrosion and that some corrosion products had transferred onto the inlet face (Plate 7). The outlet face end, by contrast only showed evidence for slight corrosion of the inner surface of the frit (Plate 6).

To facilitate accurate sample location, the outer surface of the PTFE sleeve was marked up with cm markers (Plate 6). Samples were taken as rock chips from carefully noted positions along the length of the core. Apart from the first few samples from the inlet face (samples inlet 1, 2 and 3), all chips were kept saturated with brine solution immediately after being taken.

Figure 4 shows the sites where samples were taken from the post-experimental biotic core.



**Plate 6 Biotic sample, showing the post experimental core after some samples have been taken, with distance-from-inlet cm markings on the outer surface of the PTFE sleeve. Note the inner surface of the outlet frit shows only minor corrosion spotting**



**Plate 7 Showing the inlet face and inner surface of the inlet face frit. There has been significant localised corrosion of the frit. Some of the corrosion products have transferred onto the inlet face**

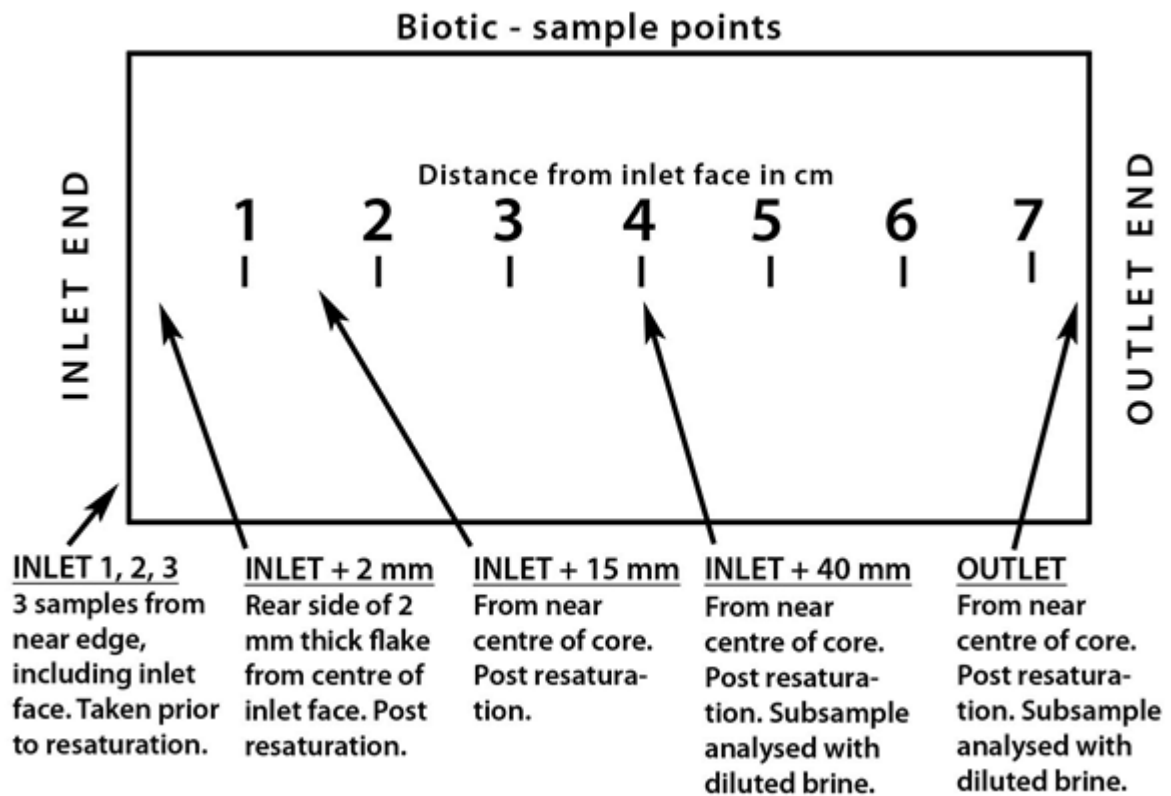


**Figure 4** Diagram showing the locations of samples taken from the post experimental biotic core

*Control sample*

After the experience with the biotic core, the control sample was immersed in sterile (filtered) 0.25M NaCl solution prior to any sampling. As with the biotic sample, the outer surface of the PTFE sleeve was divided into 1.0 cm intervals as a way of accurately locating sample points relative to the inlet face (Plate 8). Due to time pressures, samples were only taken from the inlet end and at a distance of 40 mm from the inlet end face.

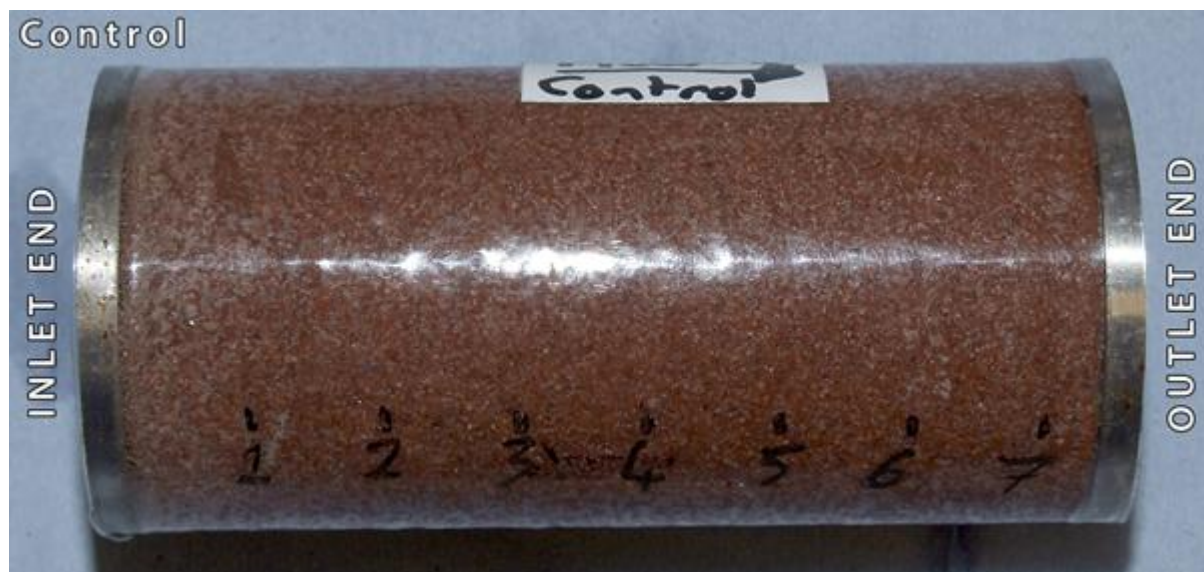


**Plate 8** Control sample marked up with cm points along its length to assist in locating sample point distances from the inlet face

### 3.3.4.2 ENVIRONMENTAL SCANNING ELECTRON MICROSCOPY

Microscopical and petrographic analysis of the experimental materials was performed using an FEI Company QUANTA 600 environmental scanning electron microscope (ESEM) equipped with an Oxford Instruments INCA Energy 450 energy-dispersive X-ray microanalysis (EDXA) system with a large area (50 mm<sup>2</sup>) Peltier-cooled silicon drift detector (SSD) X-ray detector capable of detecting elements from boron to uranium. The EDXA system is used to aid mineral phase identification, on the basis of qualitative micro-chemical observations.

As one of the objectives of the analysis was to observe samples in the wet state with pore fluids in place, the ESEM was used in environmental mode. In this mode the SEM chamber is held at raised pressures relative to normal high vacuum and variable pressure modes (typically in the region of 1-6 Torr). With the combined use of a cooled stage and water vapour atmosphere within the chamber it is possible to keep water in the liquid state at the sample surface. Adjustment of temperature and pressure with reference to a water phase diagram (Figure 5) then allows control of the theoretical sample humidity, with 100% representing the 'dew point' and values <100% resulting in evaporation of the water.

To give good control over the water saturation in the samples, a sample needs to be small so that there is minimal thermal lag, minimal temperature differential between the stage (where sample temperature is measured) and the surface of the sample (where water evaporation/condensation will occur). Additionally, the thermal conductivity between the sample and the cooled stage needs to be good. To fulfil these requirements with rock samples, any sample must be small (mm scale) and should be mounted in a saturated state within a small reservoir of the wetting liquid.

In this study, a variety of approaches were undertaken on the rock samples. As indicated above, the first of the biotic inlet face samples were taken with the sample in a non-saturated state; these were placed in the sample cup with the distilled water as the pool of wetting liquid. Initially, subsequent samples taken from the biotic sample in its re-saturated state used the 0.25M NaCl brine as the wetting liquid in order to maintain the salinity of the system.

A final variation in sample treatment was devised to reduce or eliminate artefacts arising from sodium chloride precipitation during the ESEM analysis whilst minimising the potential damaging effects to the biogenic material of rapid salinity change. This was deemed necessary after ESEM analysis of the first three samples, which were exposed to sharp salinity changes, revealed little identifiable biogenic material. Rock chip subsamples were gradually exposed to saturating brine of reducing salinity. Initially chips were immersed in a 1 in 3 parts dilution of the original 0.25M NaCl brine. Further dilution to a 1 in 10 parts mix (*i.e.* 0.025M NaCl solution) was performed several hours prior to analysis. These chips were then themselves sub-sampled with the final analytical portion being immersed in the sample cup containing a pool of sterile distilled water.

Typical ESEM operating procedures and conditions were as follows:

- The ESEM chamber was set to use an water vapour atmosphere;
- Initial pumping of the sample chamber was performed with the 'purge' setting disabled (purge is an automated ESEM pumping procedure that takes the chamber through a number of cycles with pressure going below and then above a target pressure);
- Target chamber and sample conditions were set up so that the sample would initially remain wet (*i.e.* in the liquid portion, or at the boiling/saturation line; of the pressure-temperature H<sub>2</sub>O phase diagram; Figure 5); typically this was achieved at 2 to 5°C with the chamber pressure between 5-6 Torr;
- Initial beam conditions were 7.5-12.5 kV accelerating voltage at spot size 5;
- Typical optimal working distance was 6-7 mm; and,

- Where a higher accelerating voltage was used initially, it was dropped to 7.5 kV once an optimal working distance had been established in order to reduce the potential for beam damage (this is the damage that can be caused locally through the energy of the electron beam transferring to the sample material).

Through careful control of the temperature of the sample and the pressure of the ESEM chamber it is possible to take samples through deliberate drying and wetting cycles. Drying is achieved by altering the sample conditions such that they are in the gas part of the water phase diagram (Figures 5, 6). This is typically achieved by reducing the sample chamber water vapour pressure at either constant or slightly increasing sample temperature. Humidity values (Figure 5) can be used as an indication of how far from the boiling / saturation line the system is at during a drying cycle and is a guide to the expected drying rates (lower humidity values will result in higher rates of evaporation). Wetting is achieved by reversing the drying process with condensation expected at or near the boiling/saturation line.

Drying episodes allow analysis (composition, morphology) of dry residues in an attempt to identify their origins (mineral, biotic, solution precipitate) and show their distributions.

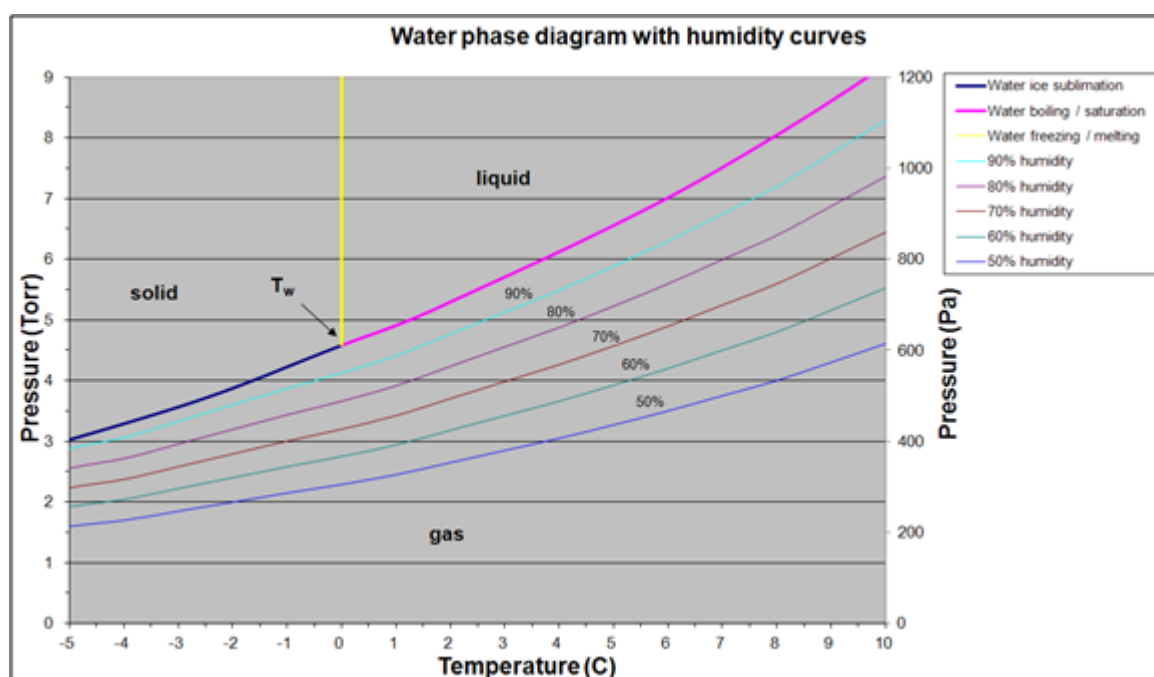


**Figure 5 P/T phase diagram for water in the region relevant to ESEM operation.  $T_w$  is the triple point. Source data for the sublimation and melting curves has been derived from Wagner *et al.*, (1994), and for the boiling / saturation curve is International Association for the Properties of Water and Steam (IAPWS) formulation for industrial use, 1997. Humidity curves have been calculated and superimposed on the gas portion of the diagram.**

*Note on use of 0.25M NaCl brine as a wetting fluid in ESEM mode*

The humidity reference numbers used by the ESEM software utilises data derived from pure water pressure-temperature (P/T) phase data, principally the boiling/saturation line of the phase diagram (Figure 5). The P/T stabilities of solutions diverge from those of pure solvents in a systematic way through changes in their colligative properties that can be derived from Raoult's Law. In any solution of a non-volatile solute in a solvent (such as NaCl in water), the P/T stability field of the liquid solution increases relative to that of the pure solvent through a shift of the boiling line to higher temperatures and of the melting line to lower temperatures (again, relative to those of the pure solvent). This is illustrated in Figure 6 below for pure water and a 0.25M NaCl aqueous solution.

An operational consequence of this increased liquid stability field is that during a drying cycle as described above, a 0.25M NaCl solution will start to evaporate at lower pressures ( $\sim 0.2$  Torr) and/or higher temperatures ( $\sim 0.3$  °C) than would pure water - significantly below the pure water 100% humidity level (*i.e.* under conditions that pure water would already be evaporating). In addition to this, when evaporation starts, its subsequent rate is expected to be slowed (compared to that of pure water) as the concentration of the solution will increase, which will in turn increase the boiling point elevation effect. This feed-back effect will continue until the solution becomes saturated and the solid solute (in this case NaCl) begins to precipitate.

The re-wetting of a dried sample should conform to the pure water P/T phase diagram, with condensation occurring at or near 100% humidity (*i.e.* the boiling/saturation line). For samples dried from a NaCl solution, however, the presence of solid NaCl as a hydrophilic phase on pore walls is likely to induce early condensation (*i.e.* when water humidity is still  $<100\%$ ). Furthermore, as condensation initiates, the solid NaCl will re-dissolved and the expanded liquid stability field of the solution will then become the controlling factor, accelerating the condensation process.

The predicted behaviour described above has to be taken into account when comparing the behaviour of the various samples and their differing wetting liquids. Where samples were analysed wetted with 0.25M NaCl brine the pure water humidity levels are used in the report only as comparative reference points.

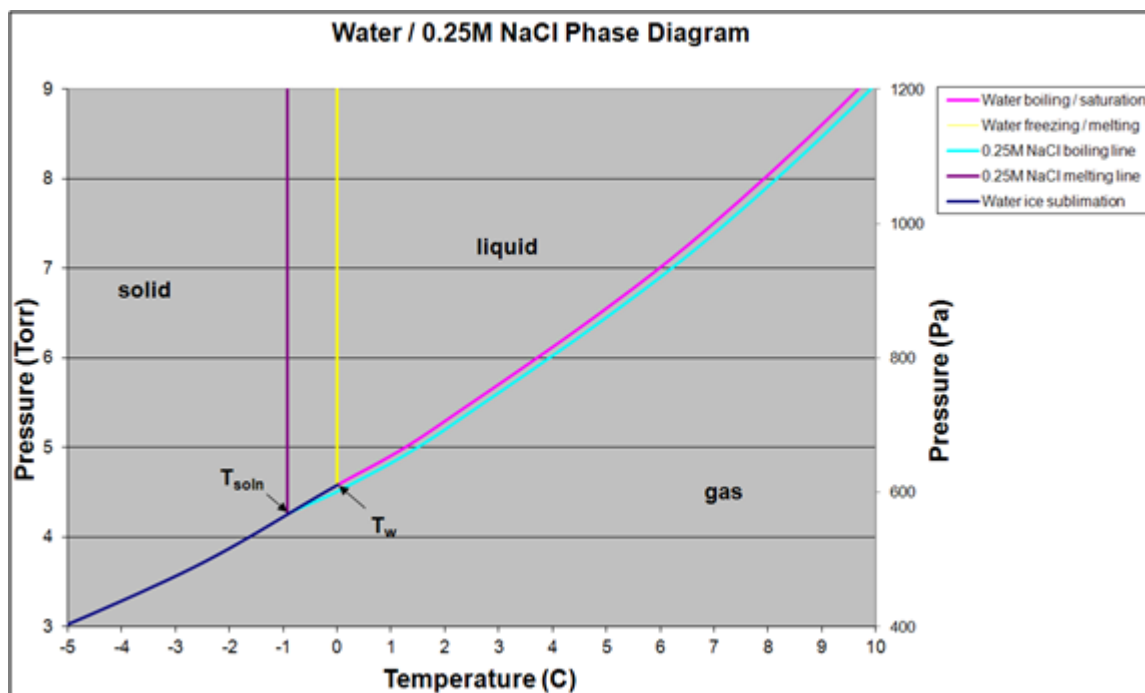


**Figure 6 P/T phase diagram for water and a 0.25M NaCl aqueous solution in the region relevant to ESEM operation<sup>1</sup>**

<sup>1</sup>  $T_w$  and  $T_{soln}$  are the triple points for water and the solution respectively. The 0.25M NaCl solution has an expanded liquid field compared to that of pure water. Once evaporation has occurred, condensation will be as per the water line irrespective of the starting liquid. 0.25M NaCl curves have been calculated by applying equations for raising the boiling point ( $\Delta T_b = i k_b m$ ) and depressing the freezing point ( $\Delta T_f = i k_f m$ ) as derived from Raoult's Law and assuming an ideal solution ( $\Delta T_b$  and  $\Delta T_f$  are the change in boiling and freezing points respectively,  $k_b$  and  $k_f$  are boiling and freezing point constants (for water  $0.512$  °Cmol<sup>-1</sup> and  $1.86$  °Cmol<sup>-1</sup> respectively),  $m$  is the molality of the solute and  $i$  is the number of particles formed by the solute in solution).

## 4 Results

### 4.1.1 Biotic column experiment

Sterile artificial groundwater was pumped through the core assembly for a nominal period (912 h (38 days)) before the *P. aeruginosa* bacteria were injected. The pump was stopped, and the sterile water was replaced with 500 ml of water inoculated with the bacteria. Logging of pressure changes started 169 hours before the bacteria were injected with pumping continuing until the conclusion of the experiment. This study finished after a total of 242 days (5811 h) from the start of logging, 235 days (5642 h) after injection of the organisms, and 272 days (6528 h) after start of the overall experiment.

### 4.1.2 Control column experiment

The control column experiment ran for a total 242 days (5810 h) with no injection of live organisms. Pressure changes were continuously monitored throughout the course of the test. At 187 days (4484 h), dead organisms were added to the fluid to evaluate their impact on transport properties.

## 4.2 MICROBIOLOGY

Mean total microbial counts, obtained by epifluorescence microscopy, for the fluids from the biotic experiment and control (abiotic) experiments are given in Table 2 and Table 3 respectively.

Results from the biotic experiment (Table 2) show that following the injection of *P. aeruginosa* ( $1.21 \times 10^7$  organisms  $\text{ml}^{-1}$  (SE  $1.88 \times 10^6$  organisms  $\text{ml}^{-1}$ )), total numbers in outlet fluid remained at about  $10^5$  organisms  $\text{ml}^{-1}$  (mean) throughout the experiment. Results from the control experiment (Table 3) fluctuated between  $6.02 \times 10^5$  organisms  $\text{ml}^{-1}$  (SE  $3.76 \times 10^4$  organisms  $\text{ml}^{-1}$ ) at the start of the experiment to  $6.04 \times 10^3$  organisms  $\text{ml}^{-1}$  (SE  $1.38 \times 10^3$  organisms  $\text{ml}^{-1}$ ) at 477 hours in the outlet fluid. Interestingly, the total numbers at the completion of the experiment were also about  $10^5$  organisms  $\text{ml}^{-1}$  (mean), the same as for the biotic experiment. This suggests that an indigenous population is present which, again, survives the experimental conditions.

Table 2 Mean total microbial counts by epifluorescence microscopy of outflow fluids from biotic experiment<sup>2</sup>

Time		Sample Number	Mean organisms ml <sup>-1</sup>	Standard Error
Days from start of overall experiment	Hours from the start of the logging phase			
37	140	CA6	71480	63955
38	169	*	12101100	1881000
44	313	CA7	413820	188100
51	477	CA8	1316700	474010
57	620	CA9	300960	112860
64	792	CA10	413820	150480
70	938	CA11	902880	300960
84	1269	CA12	225720	97810
91	1437	CA13	1279080	312245
98	1604	CA14	376200	112860
105	1776	CA15	71478	32729
112	1944	CA16	752400	376200
118	2090	CA17	62073	31604
121	2158	CA18	10420740	1805760
128	2326	CA19	44283	15059
134	2472	CA20	6621120	790020
141	2638	CA21	60190	12789
148	2809	CA22	8088300	940500
155	2977	CA23	1617660	150480
161	3121	CA24	97810	7558
168	3288	CA25	67715	29343
175	3453	CA26	45145	15040
184	3669	CA27	7185420	639540
191	3840	CA28	233245	105335
197	3981	CA29	338580	112860
205	4173	CA30	282150	109095
212	4340	CA31	1504800	451440
218	4483	CA32	338580	37620
226	4676	CA33	364915	112309
245	4844	CA34	44283	15050
239	4988	CA35	63955	26335
246	5157	CA36	203150	9781
253	5324	CA37	109100	45040
260	5492	CA38	564300	225720
266	5660	CA39	376200	353754
272	5811	CA40	225720	353735

---

<sup>2</sup> \*Number of bacteria *P. aeruginosa* ml<sup>-1</sup> of reservoir fluid

**Table 3 Mean total microbial counts by epifluorescence microscopy of outflow fluids from control experiment<sup>3</sup>**

Time		Sample Number	Mean organisms ml <sup>-1</sup>	Standard Error
Days from start of overall experiment	Hours from the start of the logging phase			
0	0		60161	37620
6	139	CB1	nc	
13	312	CB2	nc	
20	477	CB3	6035	3659
26	620	CB4	nc	
33	792	CB5	6428	1379
39	938	CB6	188100	35374
46	1100	CB7	nc	
53	1269	CB8	413820	150480
60	1437	CB9	262861	11285
67	1604	CB10	nc	
74	1776	CB11	127905	11285
81	1944	CB12	nc	
87	2090	CB13	263340	35374
90	2158	CB14	nc	
97	2326	CB15	nc	
103	2472	CB16	225720	127905
110	2638	CB17	nc	
117	2809	CB18	413820	75240
124	2976	CB19	nc	
130	3121	CB20	nc	
137	3288	CB21	127919	7558
144	3453	CB22	nc	
153	3669	CB23	225720	75240
160	3840	CB24	nc	
166	3981	CB25	188100	11271
174	4173	CB26	nc	
181	4340	CB27	112860	8037
187	4483	CB28	nc	
187	4484	*	8840700	169247
195	4676	CB29	176815	75623
202	4844	CB30	52670	18053
208	4988	CB31	48905	25205
215	5157	CB32	60190	12789
222	5324	CB33	150480	5882
229	5492	CB34	451440	150480
236	5660	CB35	1467180	376200
242	5811	CB36	752400	300960

<sup>3</sup> nc = no count available \*Number of 'dead' *P. aeruginosa* ml<sup>-1</sup> in reservoir

### 4.3 FLUID CHEMISTRY

The results of the fluid chemistry analysis for the control core are tabulated in Appendix 3 (prefix CB) and the biotic core (prefix CA) in Appendix 4.

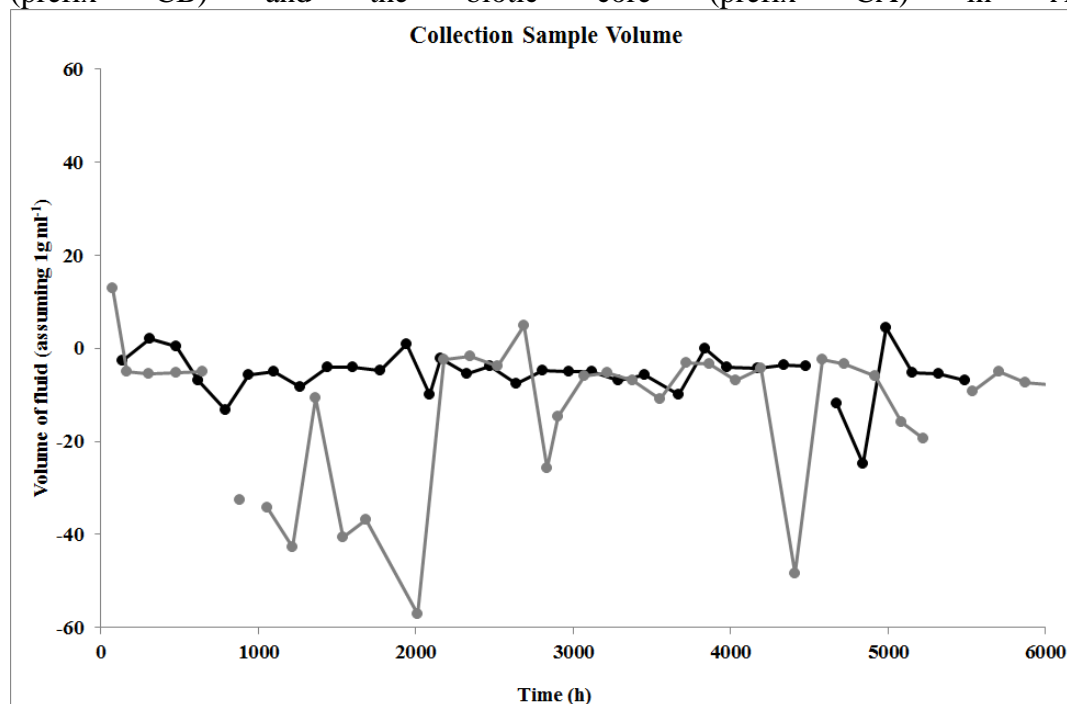


Figure 7 shows the difference in sample volumes collected during the biotic and control experiments. Figure 8 to Figure 17 illustrate changes in various parameters in the biotic and control experiments: namely sodium (Na) and chloride (Cl) (Figure 8 and 9), NPOC (Figure 10), pH (Figure 11), barium (Ba) (Figure 13), calcium (Ca) (Figure 13), and, aluminium (Al) (Figure 14), potassium (K) (Figure 15), molybdenum (Mo) (Figure 16) and tungsten (W) (Figure 17), nickel (Ni) (Figure 18) and zinc (Zn) (Figure 19).

Maximum concentrations of Mo and W (Figure 16 and Figure 17) were found at the start of the experiment and the concentrations of both analytes decreased rapidly in the first few weeks, as previously seen in experiments using syringe pumps (Harrison *et al.*, 2009). Microbial activity could be ruled out as the control core had significantly higher concentrations of Mo and W at the outset than the biotic core. The concentration of these ions decreased over time in both the control and biotic experiments until the lower limit of detection (LLD) by ICP-MS was reached. Similar, but rather less obvious, downward trends were seen in Ni and Zn concentrations during the course of the experiment (Figure 18 and 19). However, no trend was observed in other stainless steel related elements *e.g.* chromium (Cr) and copper (Cu), which would be expected in the corrosion of stainless steel. As neither Mo nor W were added to the groundwater or present in the core itself, it is therefore extremely likely that they originated from the cutting tool used to prepare the core for the experiments.

The initial increase in Ca (Figure 13) is followed by a decrease over time that stabilises after 3000 h at approximately  $7 \text{ mg l}^{-1}$ . Barium shows similar behaviour, but the concentrations are a factor of circa. 10 lower. The Ca and Ba were most likely to have originated from calcite and dolomite which are present in the core. Comparison of Figures 12 and 13 indicate that Ba and Ca follow similar trends throughout the biotic and control experiments. Barium is frequently found as a contaminant in Ca bearing mineral phases. Evidence of dissolution of silica from the core was inconclusive (Appendix 3, Appendix 4).

### 4.3.1 Biotic Core

A slow decrease in pH was observed in the biotic core from a starting value of 9.3 to 7.1 at the conclusion of the test (Figure 11). It was also noted that from 620 to 2090 hours from the start of the logging phase, Na and Cl concentrations (Figure 8) were unexpectedly low, whereas NPOC values were considerably higher (Figure 10). For Na, the overall average was  $5725 \text{ mg l}^{-1}$  (as  $\text{Na}^+$ ) compared to a mean value of  $2585 \text{ mg l}^{-1}$ , between *ca.* 24 and 87 days (620 and 2090 h) from the start of the logging phase. In a similar manner, Cl averaged  $9200 \text{ mg l}^{-1}$  but fell to  $325 \text{ mg l}^{-1}$  (as Cl<sup>-</sup>) over the same period (Figure 8). Figure 9 shows the very strong relationship ( $R^2 = 0.9783$ ) between the Na and Cl measured concentrations in the fluid exiting the BFA during the biotic experiment, which is related to the original saline groundwater used. The NPOC content showed an opposing pattern, averaging  $330 \text{ mg l}^{-1}$  before 24 days (620 h) from the start of the logging phase, increasing to a fairly constant  $2400 \text{ mg l}^{-1}$ , between *ca.* 24 and 87 days (620 and 2090 h) from the start of the logging phase. However, unlike Na and Cl, which remained fairly constant thereafter, NPOC gradually decreased until the end of the experiment (Figure 10). Other elements did not show this behaviour. One possible explanation was that the sample outlet became blocked with organic material. The volumes of sample collected in the syringe from the biotic experiment were lower than expected, as a result of a possible leak in the plastic tubing, considering a constant flow was supplied by the syringe pump (Figure 7). The sample volumes collected by the control core syringe showed less variability.

### 4.3.2 Control Core

The pH of the control test was more constant, averaging 7.22 (Figure 11). There were two anomalies towards the end of the control core experiment when the pH achieved a maximum of 8.12 and a minimum of 5.61; however the pH of the fluid remaining in the syringe pump was 7.19.

Plots of concentration of analytes in the column outflows against time showed no obvious trends for the majority of analytes other than those previously mentioned.

Figure 9 shows the very strong relationship ( $R^2 = 0.8545$ ) between the Na and Cl measured concentrations in the fluid exiting the BFA during the control experiment, which is related to the original saline groundwater used.

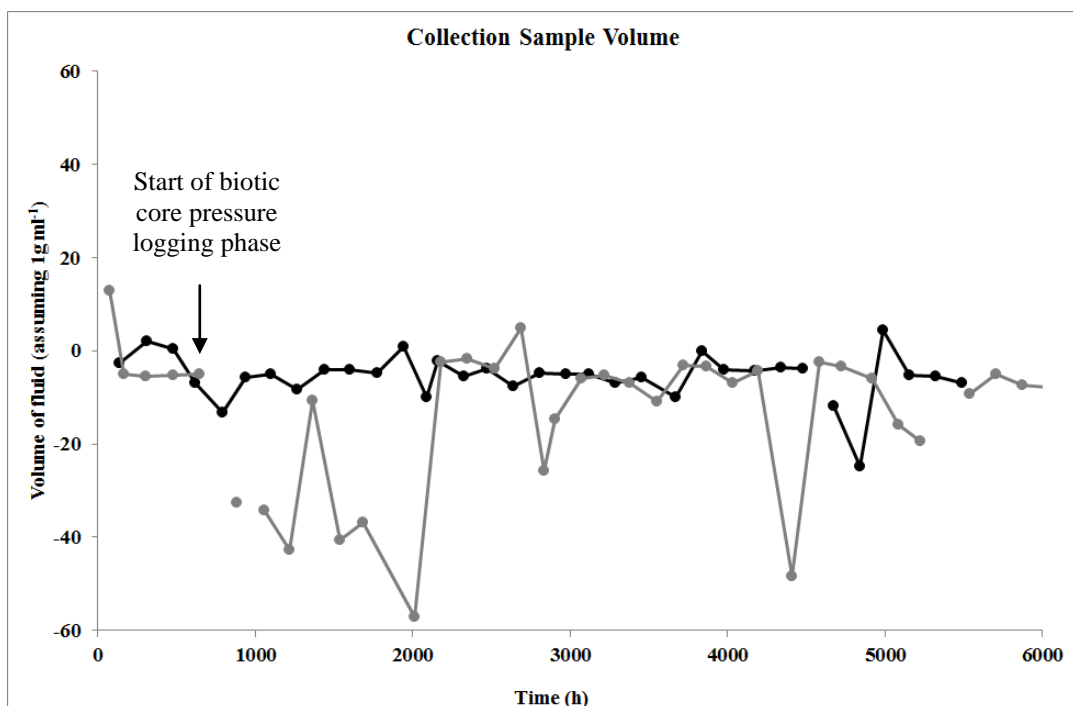


Figure 7 Shows the difference in collection syringe volumes from the biotic and control core experiments (determined by weight of liquid collected, assuming  $1 \text{ g ml}^{-1}$ ) from the start of the experiment<sup>4</sup>

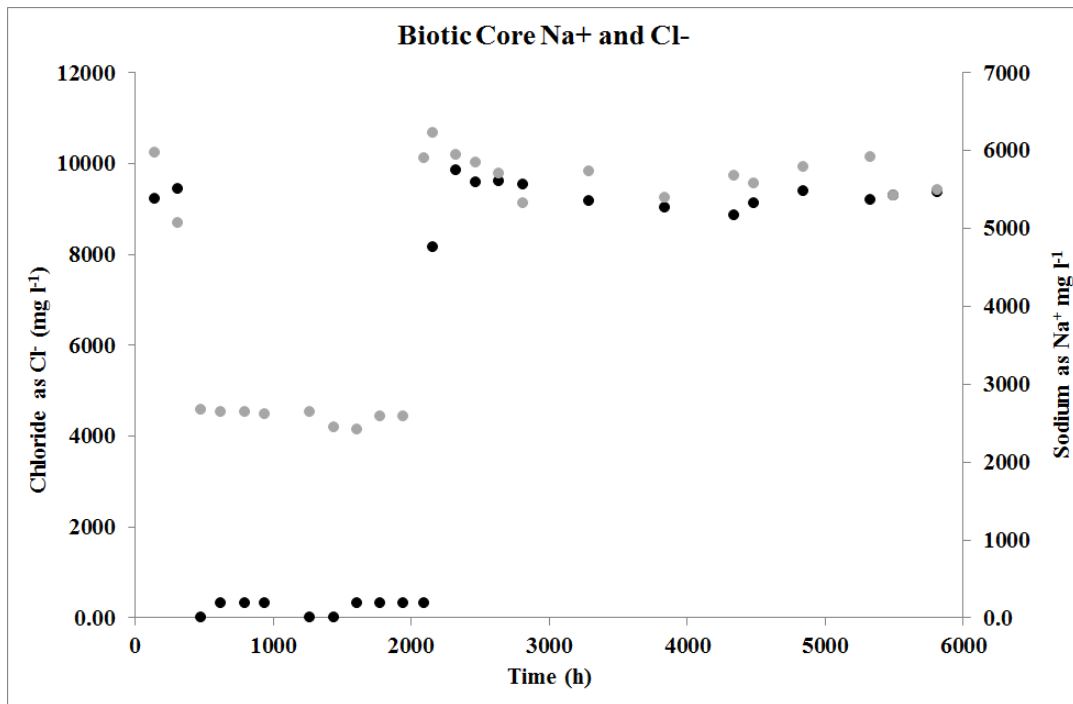


Figure 8 Concentrations of Na (grey circles) and Cl (black circles) in  $\text{mg l}^{-1}$  plotted against time from start of pressure logging phase of the biotic experiment in hours

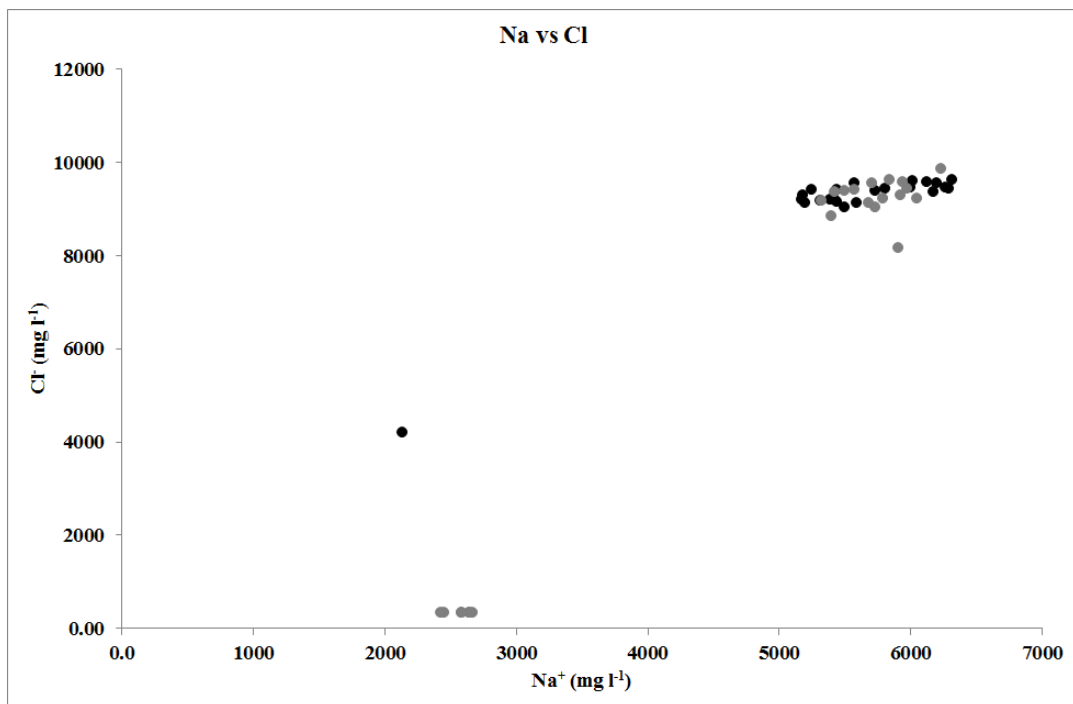
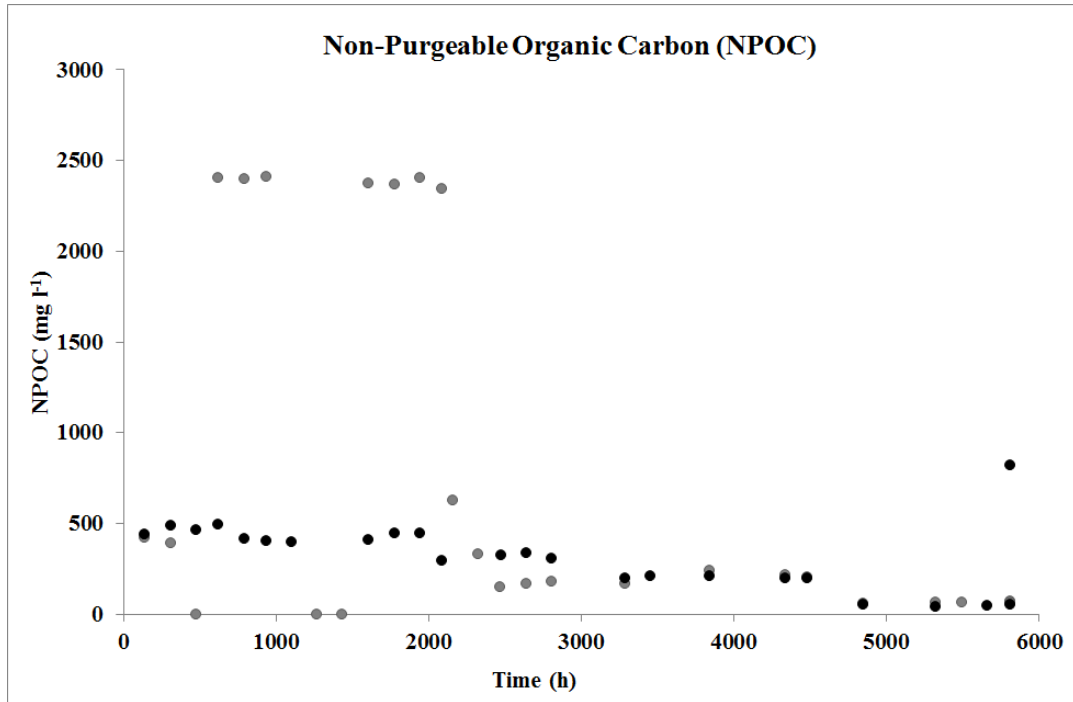
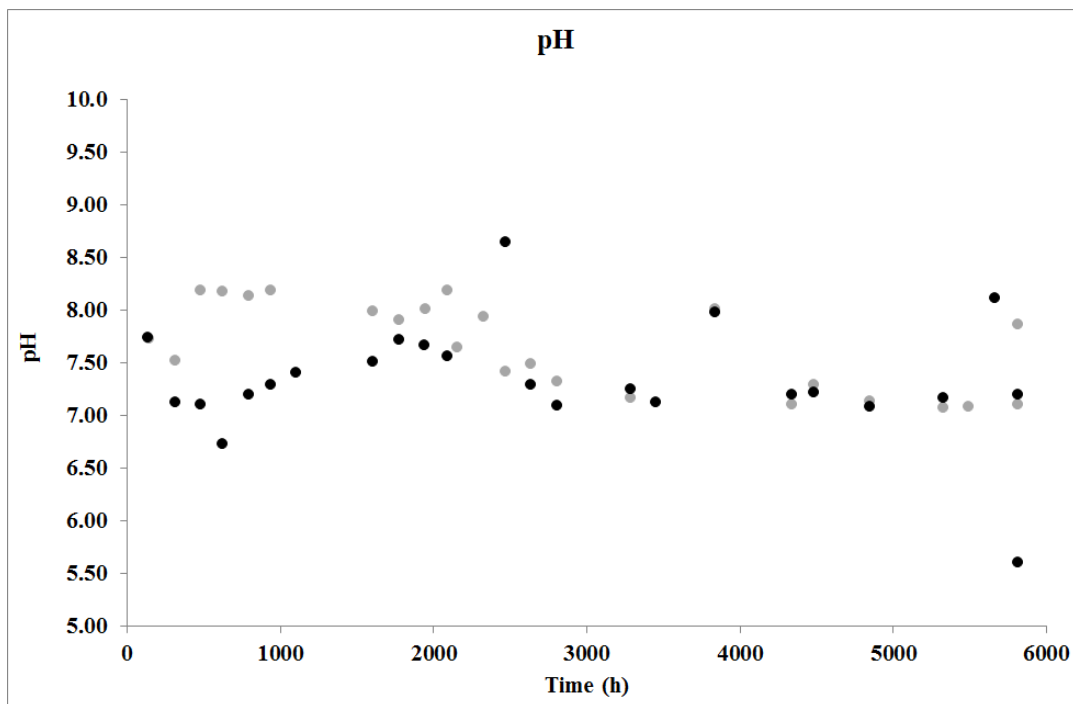


Figure 9 Plot of Na against Cl from start of logging phase in hours for the biotic core (grey circles) and the control core (black circles)

<sup>4</sup> The volume supplied to the core by the syringe pump was  $300 \mu\text{l h}^{-1}$  and the actual volume of liquid collected in the syringe was determined by weight. The grey circles/lines show the difference between supplied volume and collected volume in the biotic experiment, black circles/lines show those from the control core



**Figure 10** NPOC in mg l<sup>-1</sup> for the biotic core (grey circles) and the control core (black circles) plotted against time from start of pressure logging phase



**Figure 11** Plot of pH against time from start of logging phase in hours for the biotic core (grey circles) and the control core (black circles)

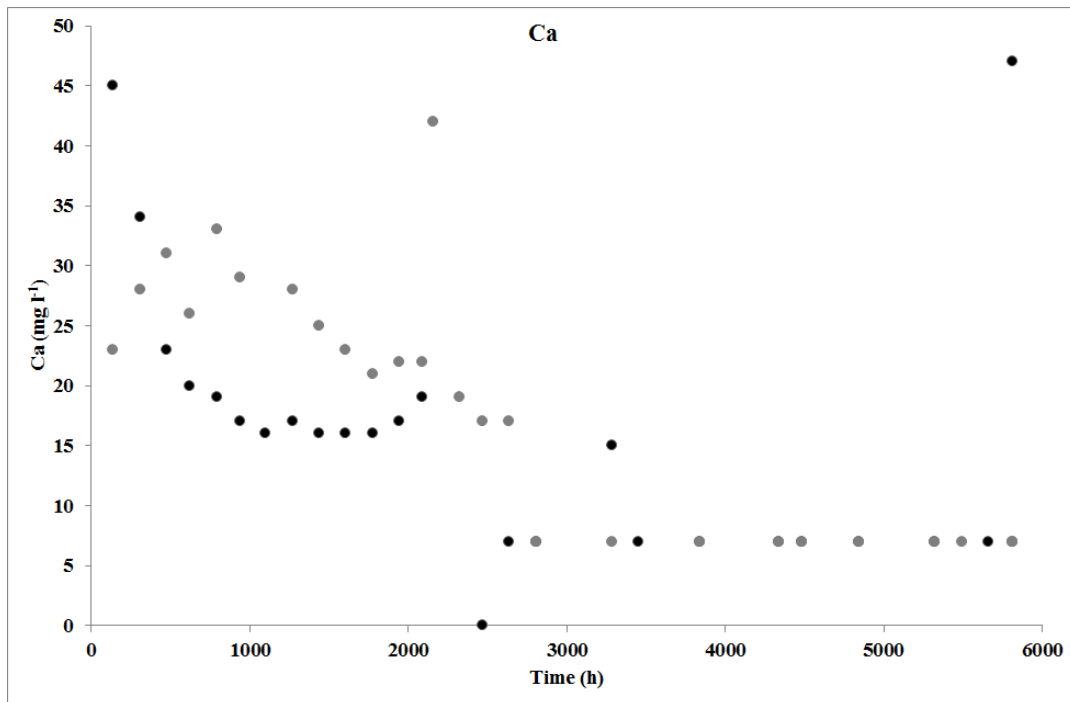


Figure 12 Plot of Ca against time from start of logging phase in hours for the biotic core (grey circles) and the control core (black circles)<sup>5</sup>

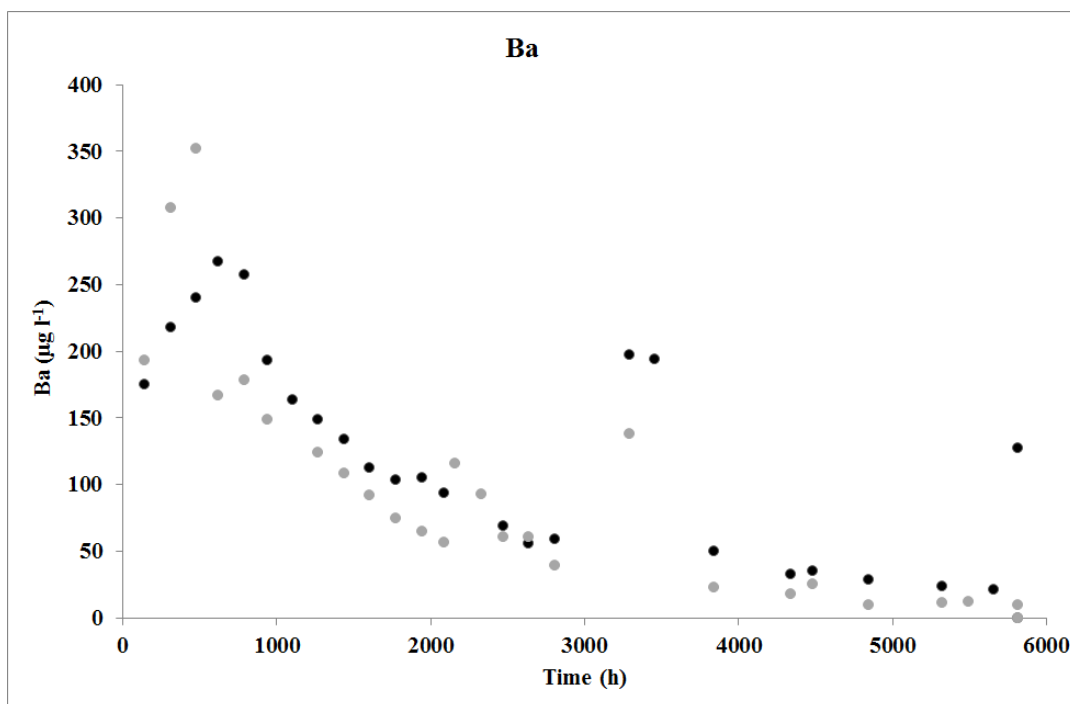


Figure 13 Plot of Ba against time from start of logging phase in hours for the biotic core (grey circles) and the control core (black circles)

<sup>5</sup> After 2500 h the majority of samples were below the method limit of detection (LOD) for Ca, therefore the LOD has been halved, as per standard analytical approaches, to allow the data to be plotted.

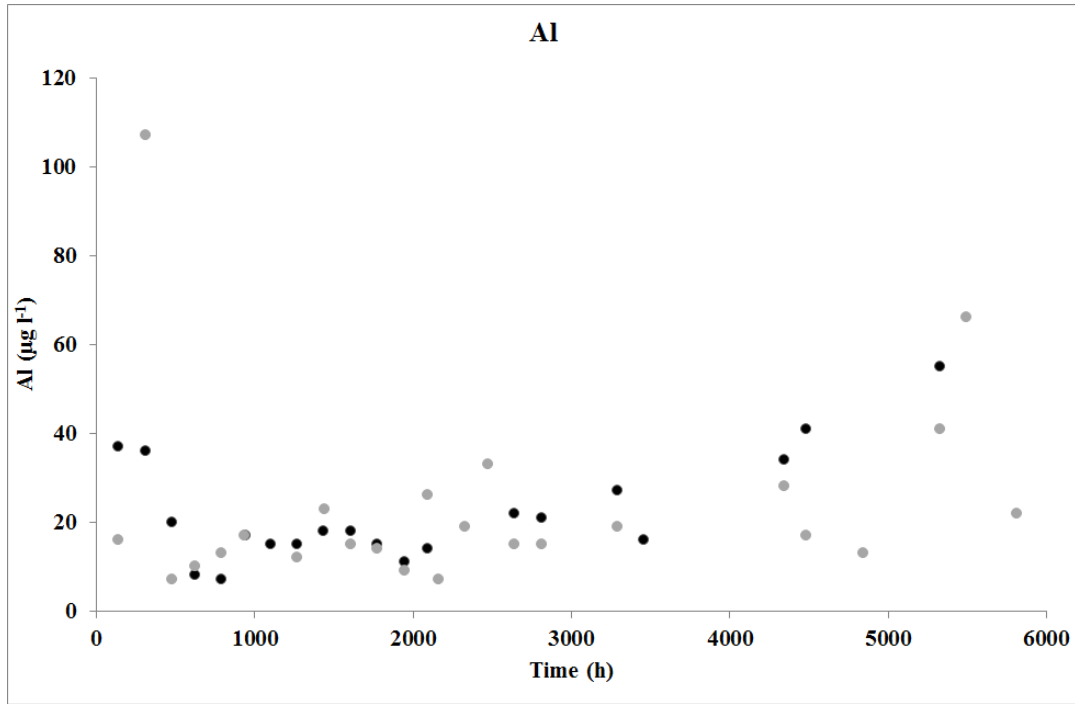


Figure 14 Plot of Al against time from start of logging phase in hours for the biotic core (grey circles) and the control core (black circles)

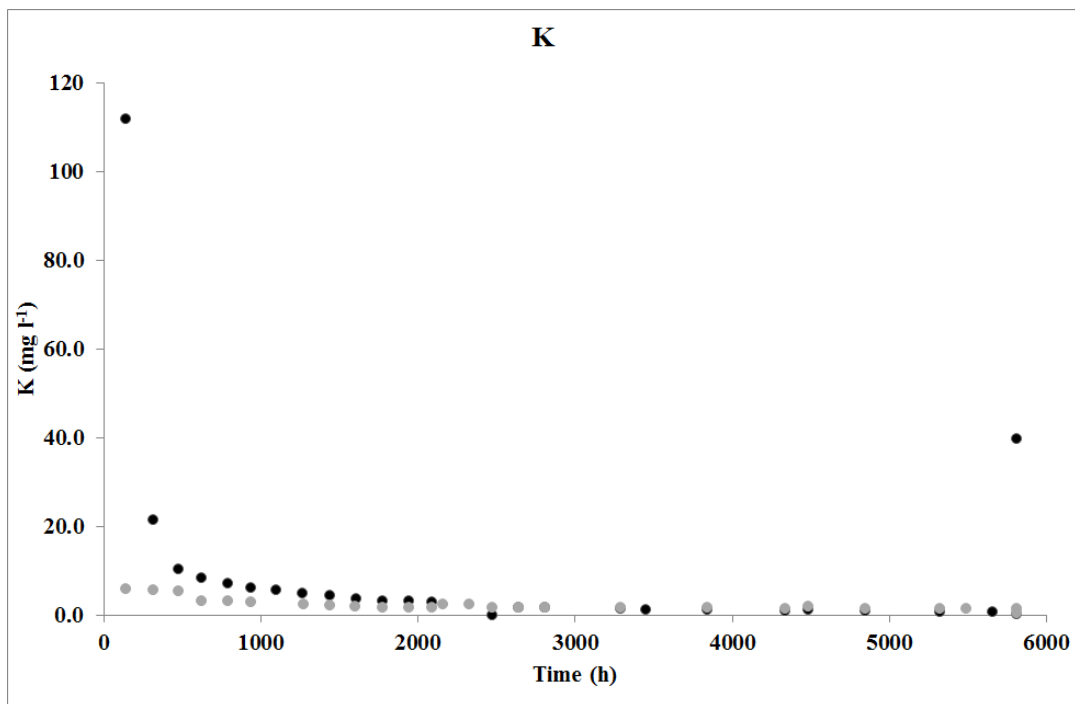
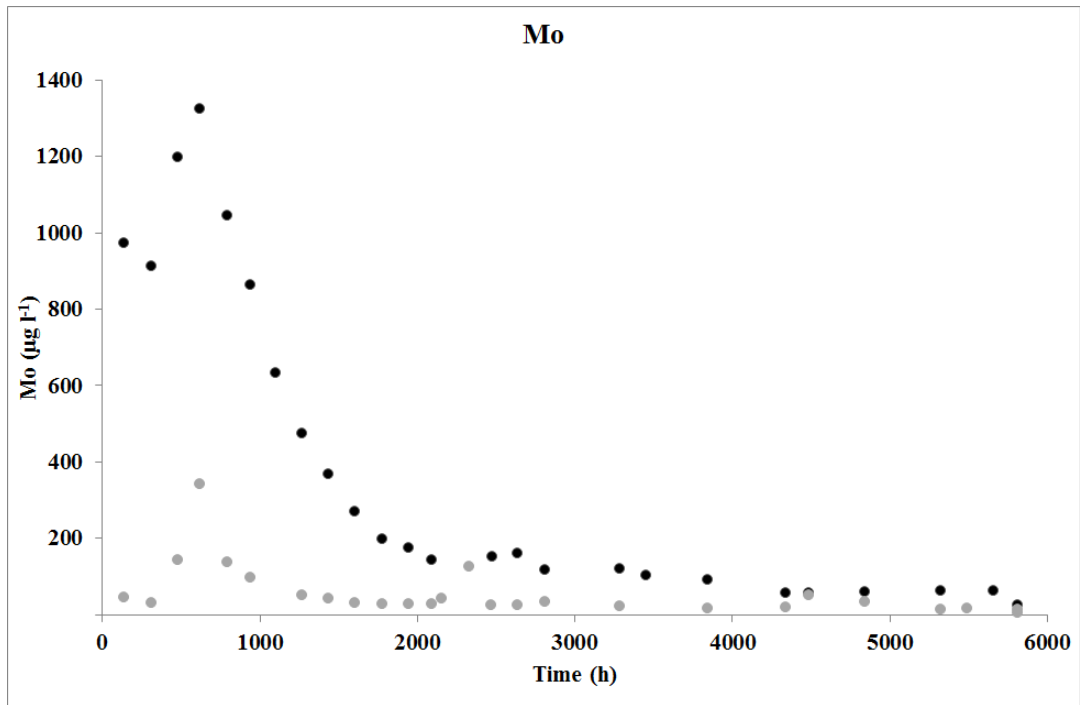
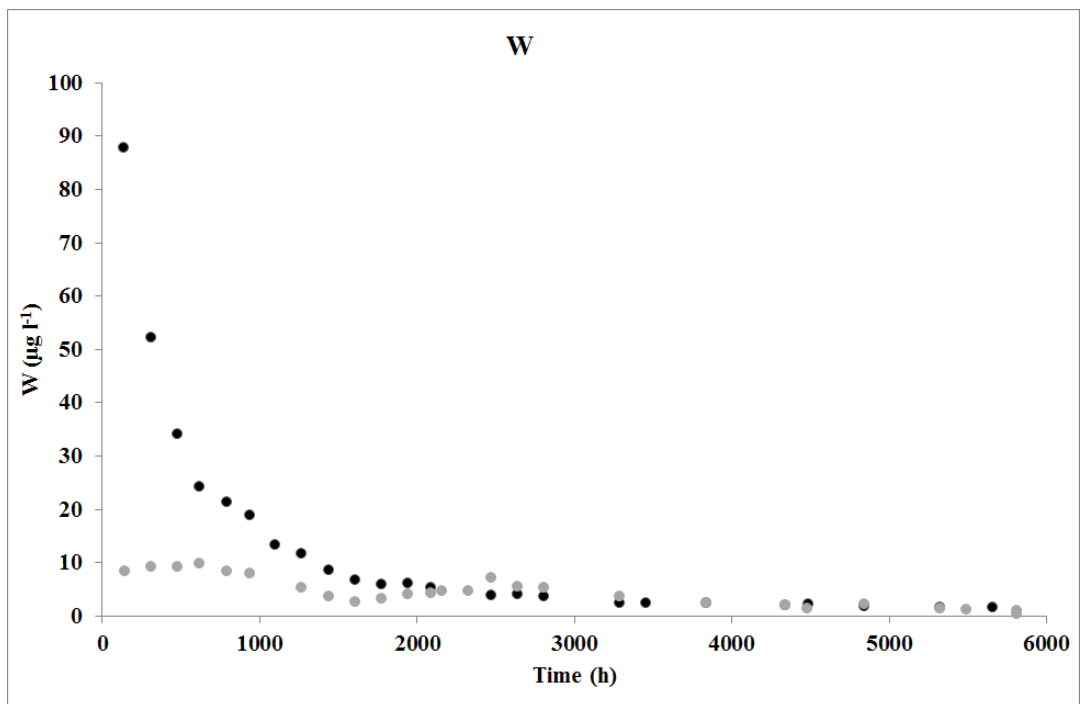


Figure 15 Plot of K against time from start of logging phase in hours for the biotic core (grey circles) and the control core (black circles)



**Figure 16** Plot of Mo against time from start of logging phase in hours for the biotic core (grey circles) and the control core (black circles)



**Figure 17** Plot of W against time from start of logging phase in hours for the biotic core (grey circles) and the control core (black circles)

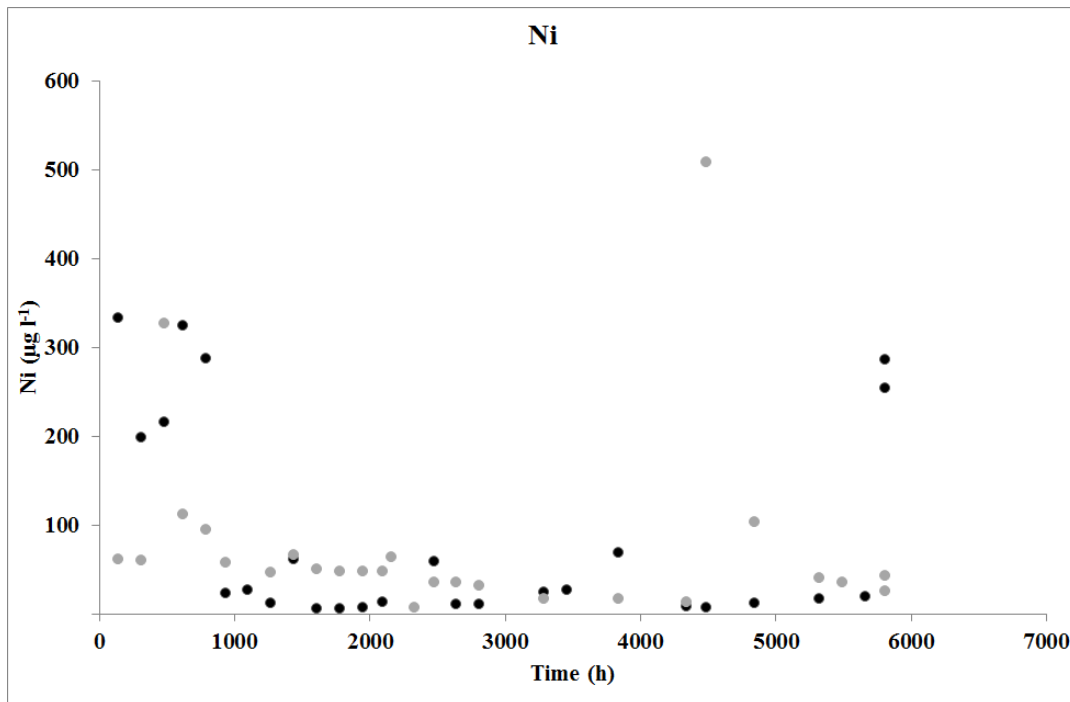


Figure 18 Plot of Ni against time from start of logging phase in hours for the biotic core (grey circles) and the control core (black circles)

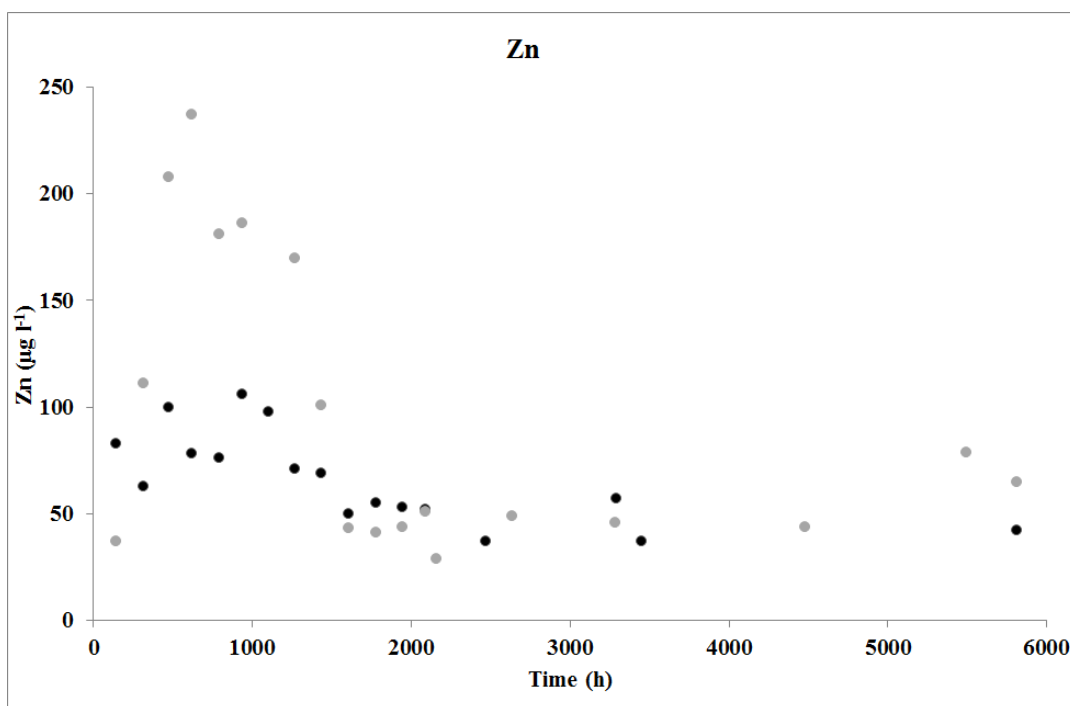


Figure 19 Plot of Zn against time from start of logging phase in hours for the biotic core (grey circles) and the control core (black circles)

#### 4.4 PHYSICAL MEASUREMENT RESULTS

Both biotic and control column experiments were performed at a constant flow rate and changes in injection and confining pressure were continuously logged by pressure transducers during the tests. Changes in injection pressure are depicted graphically in Figure 2020 (biotic experiment) and Figure 2121 (control experiment). An overlay of the biotic and control injection pressure

graphs from the start of the experiment to *ca.* 187 days (4484 h), when dead *P. aeruginosa* and associated organic material were injected into the control experiment, is given in Figure 2222. Each figure shows the experiment duration as time in hours along the x-axis and the recorded injection pump pressure in kPa along the y-axis. A secondary axis indicates the number of viable bacteria in each system, as bacterial counts  $\text{ml}^{-1}$ .

Prior to injection of the bacteria in the biotic experiment (Figure 2020), sterile groundwater was pumped through the column assembly for a nominal period (38 days – 912 h) with logging starting *ca.* 7 days (169 h) before injection. Post inoculation pressure increased compared to the control experiment (Figure 21), with an average pressure of 488 kPa. Prior to bacterial injection, initial changes in core permeability are considered to be a result of movement of fines, blocking pore spaces and resulting in localised pressure increases, followed by breakthrough and establishment of new pathways resulting from a pressure increase by the use of a constant flow rate. Rapid, saw-tooth like changes in pressure are evident over the post inoculation period although it should be noted that the regular 7 day (160 h) increases are due to pressure build up from fluid in collection syringes prior to sampling. Overall, these pressure profiles are symptomatic of a dynamic system exhibiting localised intermittent changes in permeability, brought about by the partial clogging of pore spaces by fines and/or biofilm followed by flushing because of an increase in localised hydraulic pressure.

The control experiment (Figure 2121) showed an increase in pressure over the initial 60 hours, followed by a stabilisation phase, up to *ca.* 14 days (350 h) of 15 kPa – over one order of magnitude less than the biotic experiment. Thus the presence of any indigenous organisms (and associated biofilm) does not appear to have the same impact on permeability as *P. aeruginosa*. The dynamic saw-tooth like changes in pressure in the biotic experiment also suggests that biofilm formation is a more dynamic process. The overlay of results from both biotic and control experiments (Figure 222) illustrates these pressure differences to 187 days (4484 h) when dead *P. aeruginosa* and associated organic material was injected. At this point in the control experiment (Figure 2121), there was an increase in pressure to a maximum of ~1500 kPa at *ca.* 208 days (5000 h). The pressure returns to 15kPa by 250 days (6000 h). This is attributed to their presence (with associated biofilm and organic material) bringing about partial and transitory clogging of pore spaces. The effect on pressure is over a period of *ca.* 63 days (1500 h).

A comparison of the injection pressure graphs from the biotic and control experiments (Figure 20 and 21) after 187 days (4484 h) show the effect on pressure of dead *P. aeruginosa* and associated organic (but inactive) material being introduced into the control. The biotic core (Figure 2020) continues to show rapid pressure oscillations, even when no more bacteria are being introduced into the flow from the pump, suggesting that the injected *P. aeruginosa* bacteria, probably with the indigenous microbes, have formed their own colonies within the core and are self-sustaining. The rapid oscillations seen in the control core (Figure 2121) after the introduction of organic material are short lived and the pressure flux reduces over time to levels prior to injection of dead bacteria. There are two possible explanations for this observation:

- The pressure within the control core increases rapidly when the dead bacteria and associated biofilm become trapped in the pore spaces, inducing locally high pressure zones. Subsequently, this build-up of pressure eventually causes break-through as a new network of fluid flow channels is established and organic material is flushed further into the core. This process of trapping and release repeats itself until a quasi-steady equilibrium state is reached, whereby further addition of organic material from the fluid from the pump causes localised pressure changes and the pressure returns to pre-injected conditions;

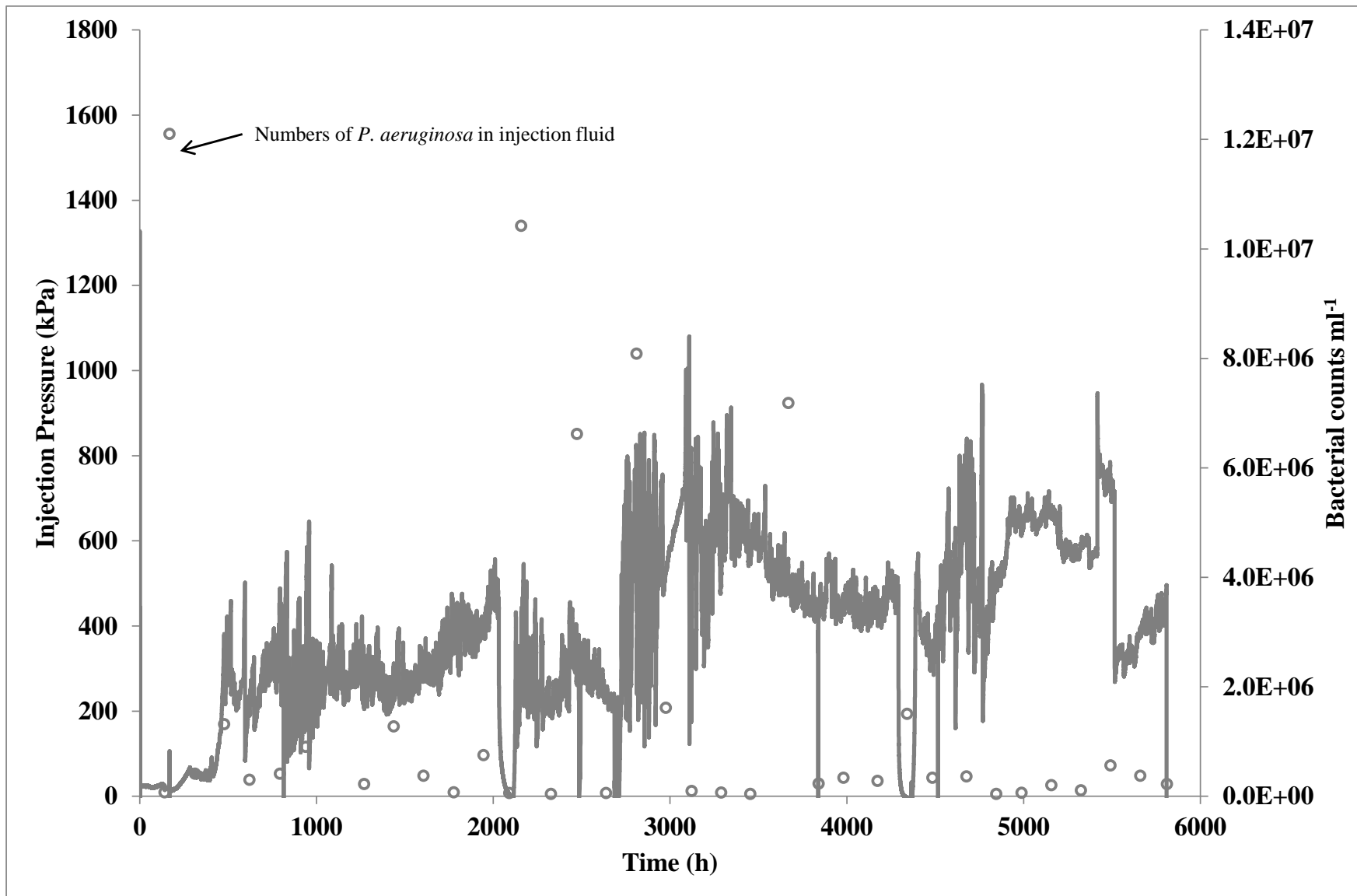


Figure 20 Biotic experiment: injection pressure and mean bacterial counts (open circles) plotted against pressure logging time in hours. Bacterial count in pump inflow fluid and remaining in pump at the end of the experiment is also given. *P. aeruginosa* injected at 169 h

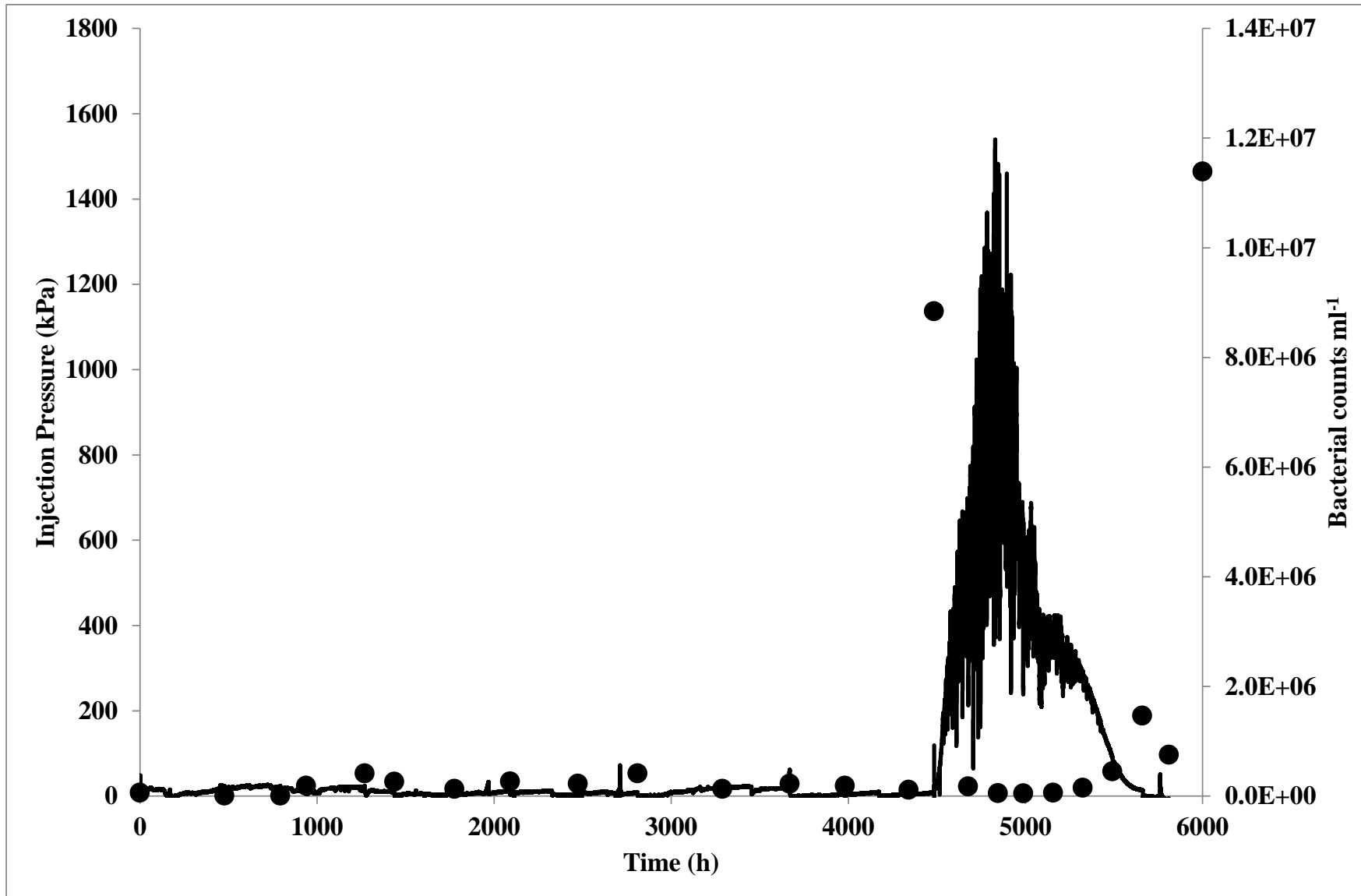


Figure 21 Control experiment: injection pressure and mean bacterial counts (circles) plotted against pressure logging time in hours. Results also shown following injection with killed *P. aeruginosa* and associated biofilm (injected at 4484 h) in pump in-flow fluid

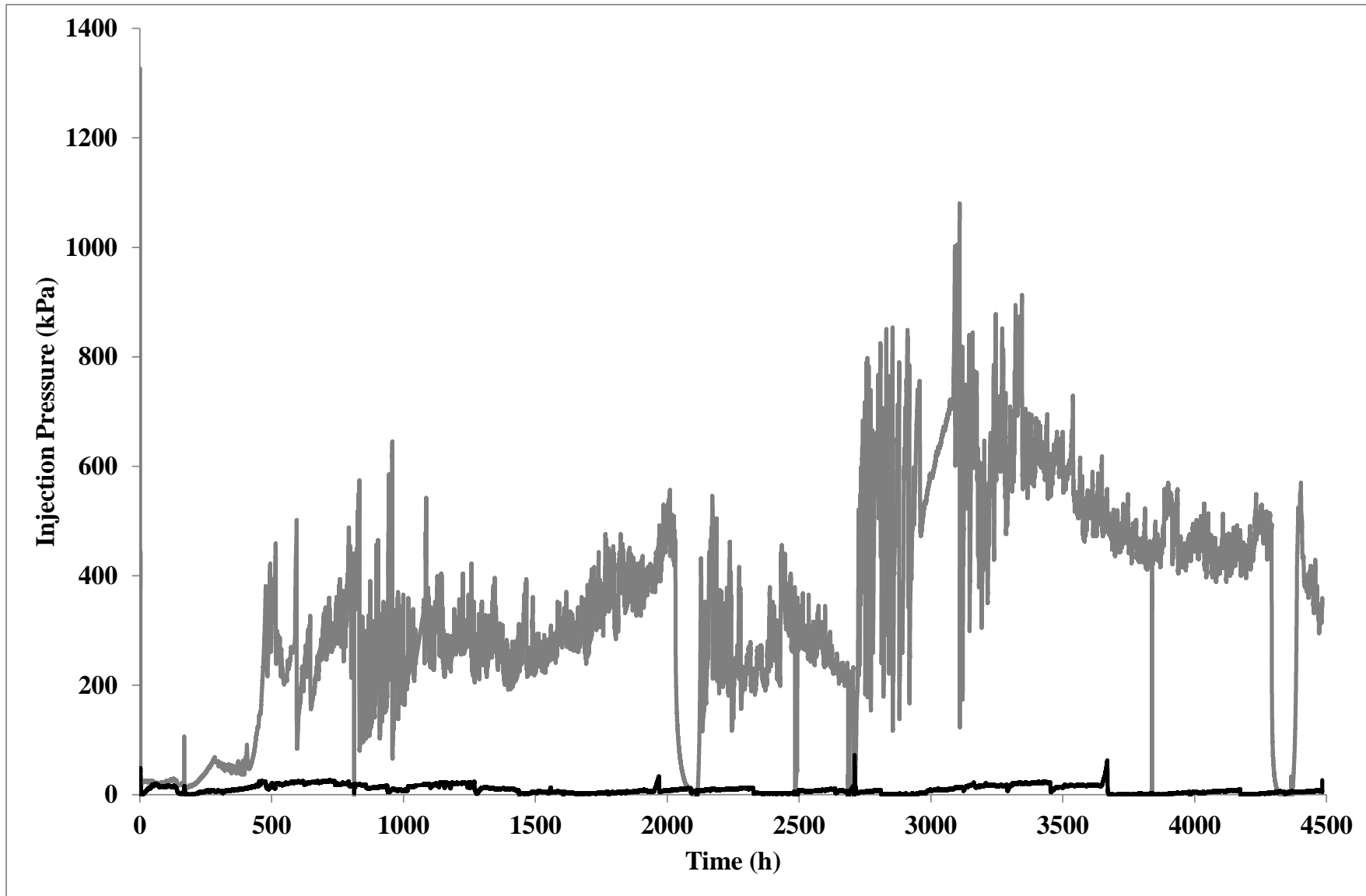


Figure 22 Comparison of injection pressure results in biotic (in grey) and control (in black) experiments plotted against pressure logging time (to 4484 h when dead organism were injected into the control experiment)



- The control core pressures return to pre-injection levels as, over time, the organic material within the syringe pump slowly settles on the base of the syringe (*i.e.* top of the piston). Therefore, the fluid being delivered from the top of the syringe into the core has a lower viscosity and contains less organic material.

## 4.5 MINERALOGICAL AND PETROGRAPHICAL CHARACTERISTICS OF THE SANDSTONE STARTING MATERIALS

### 4.5.1 Gamston borehole core sample

#### 4.5.1.1 PETROGRAPHY AND MODAL MINERALOGY

The sample of sandstone from the Sherwood Sandstone Group sequence in the Gamston borehole is broadly similar to sandstone samples previously examined from this borehole by Milodowski *et al.*, (1987) and Milodowski and Rushton (2008). Modal mineralogical data for the sandstone sample are given in Table 4. These data are in broad agreement with the results of quantitative whole-rock XRD analysis. XRD does indicate higher quartz content than modal analysis, possibly because a proportion of fine grained quartz detected by XRD may be unresolved and included by modal analysis in the illite/clay fraction (Table 4). In contrast, the modal analyses results indicate a higher content of kaolinite than XRD. This is possibly because the kaolinite is microporous, and modal analysis will include at least part of the microporosity in its volumetric estimates. In addition, minor iron oxide is evident from the petrographic observations and is included in the modal analysis but was not detected by XRD (Table 4).

The sandstone is defined as a subfeldspathic arenite (classification after Pettijohn *et al.*, 1987; Hallsworth and Knox 1999), composed of major detrital quartz, with subordinate detrital K-feldspar, and minor lithic grains (including micaceous schist, quartzite grains, and ferruginous mudstone clasts), detrital illite and other clay minerals (

Plate 9). It should be noted that the modal analysis, BSEM-EDXA-image analysis does not differentiate lithic clasts from the individual mineral components comprising them. Consequently, lithic clasts are not discriminated as a separate component in the modal analysis results.

The rock is moderately well-compacted (

Plate 9), displaying mild compactional deformation of mudstone clasts and mica flakes. Brittle fracturing and crushing of less-competent feldspar grains is also observed (Plate 10).

Detrital clay with disseminated fine iron oxide is also commonly present as fine grain-coating rims. These are most apparent where framework grains have been removed by dissolution, leaving the clay pellicle as a “ghost” moldic outline of the former grain margin (Plate 10). Discrete patches of clay are also present forming an apparent matrix squeezed between compacted detrital quartz and feldspar and filling intergranular pores. EDXA suggests that much of the clay is illitic in composition. The details of the clay mineralogy are described in Section 4.5.1.4.

The patchy nature of the intergranular clay and the recognition of partially-deformed clay and mudstone pellets suggest that much of this intergranular clay is “pseudomatrix” rather than true detrital clay, and results from the compactional deformation of plastic, clay-rich lithic grains. Other detrital components include very minor to trace amounts of albite, ilmenite, iron oxides (including magnetite), rutile, apatite and zircon.

The sandstone contains calcite (

Plate 9) and dolomite (

Plate 11) cements. Patches of late diagenetic ferroan calcite locally and partially fill intergranular pore spaces between compacted detrital grains (

Plate 11). Dolomite is more abundant than calcite and occurs as micronodules, or as a fine grained replacement of rounded detrital (carbonate or mudstone) clasts. These dolomite-cemented areas sometimes preserve a locally uncompacted grain fabric, and have previously been interpreted as early diagenetic (pedogenic) dolocrete cements (Milodowski *et al.*, 1987; Milodowski and Rushton, 2008). Euhedral overgrowths of later diagenetic ferroan dolomite may be developed around the margins of some of the earlier dolomite micronodules, and cements between compacted grains.

**Table 4 Modal mineralogical data for the Sherwood Sandstone Group samples from the Gamston borehole**

	Sample MPLN106		
	Normalised mineralogy %	Standard deviation	XRD %
Quartz	69.7	1.3	76.9
K-feldspar	13.4	2.3	13.9
Albite	0.2	0.3	0
Muscovite	0	0	Included in illite
Biotite	0	0	Included in illite
Kaolinite	4.17	1.46	1.0
Chlorite	0	0	0.5
Illite / clays	5.2	1.5	2.6
Dolomite	3.8	0.7	4.1
Calcite	1.7	0.9	0.7
Apatite	0.1	0.1	0
Ilmenite	0.1	0.1	0
TiO <sub>2</sub>	0.8	0.5	0
Iron oxides (incl. hematite magnetite, FeOOH)	1.0	Mineral	0
Zircon	<0.1	<0.1	
TOTAL	100.2	-	99.7
Porosity	15.3	1.1	-

In addition to authigenic carbonate cement, authigenic clay minerals are significant. The early grain coating illitic-smectitic clay rims (Plate 10) are often the sites for the nucleation of “wispy” growths of secondary illite-smectite clay mineralisation that may form pore-bridging clay menisci (

Plate 12).

Authigenic kaolinite is also an important component of the rock. It is closely associated with framework grain dissolution sites (Plate 13). It occurs as fine grained microcrystalline aggregates

or as coarser vermicular or book-like crystal aggregates (Plate 14), filling framework grain dissolution sites and locally extending into the adjacent primary intergranular pore sites. Fragments of corroded feldspar and remnants of altered felsic lithic grains may be found within these kaolinite-mineralised pores. This suggests that the kaolinite has formed by alteration and replacement of detrital feldspar and lithic clasts.

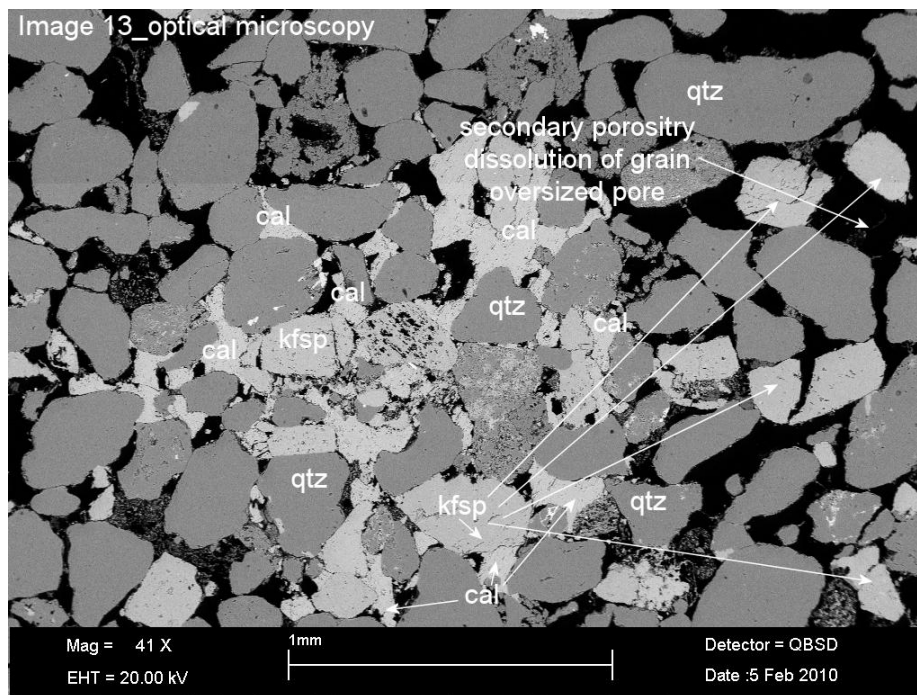


**Plate 9 BSE image of sandstone showing moderately compacted detrital fabric of quartz and K-feldspar grains, but with locally “oversized” pores indicative of secondary porosity formed by the dissolution of detrital framework grains. Patchy calcite cement appears partially corroded. Gamston borehole, sample MPLP106**

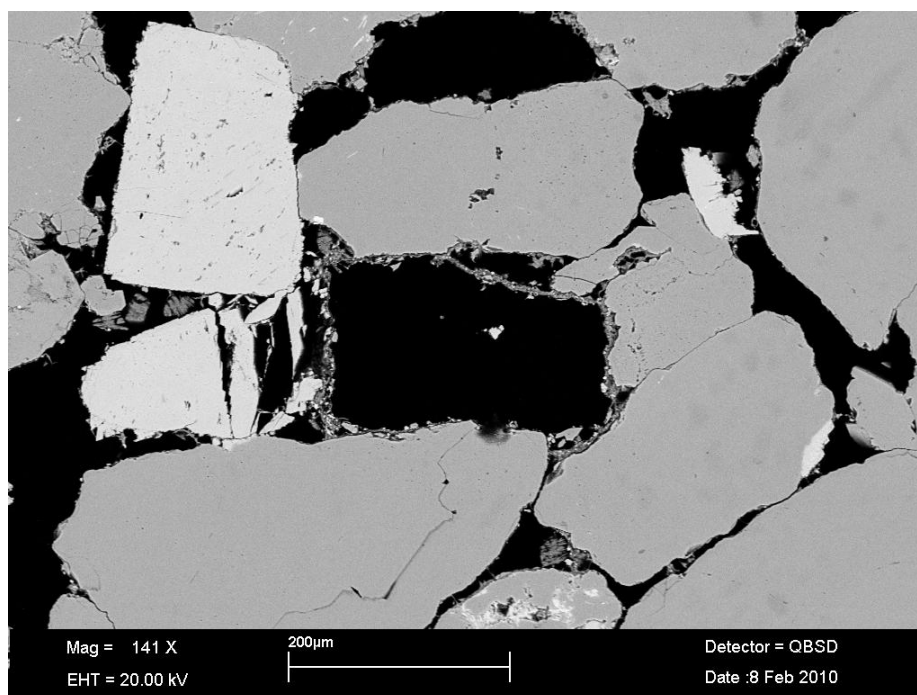


**Plate 10 BSE image of sandstone showing a thin “pellicle of illitic-smectitic-chloritic clay outlining an “oversized” secondary pore indicative formed by the dissolution of a detrital framework grain. Brittle deformation and crushing of a K-feldspar by compaction can also be seen. The clay coating was deposited on the surface of the original detrital grain (now removed by dissolution). Gamston borehole, sample MPLP106**

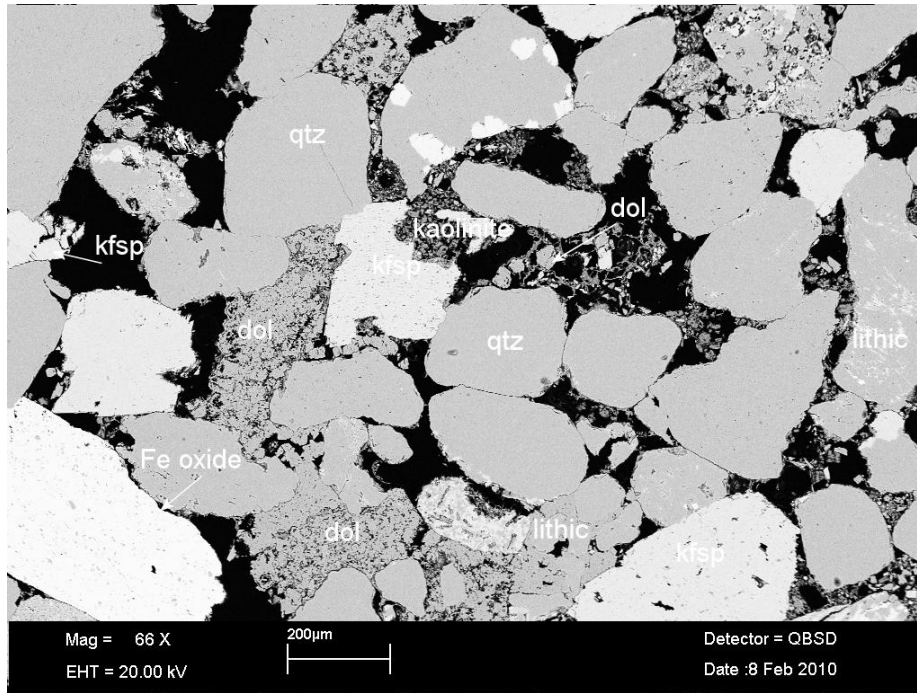


**Plate 11 BSEM image showing patchy micronodular dolomite cement (dolocrete) with overgrowths of later sub-hedral to euhedral dolomite adjacent to open pores. Authigenic kaolinite can be seen partially filling oversized, secondary pores representing framework grain alteration / dissolution sites. Gamston borehole, sample MPLP106**

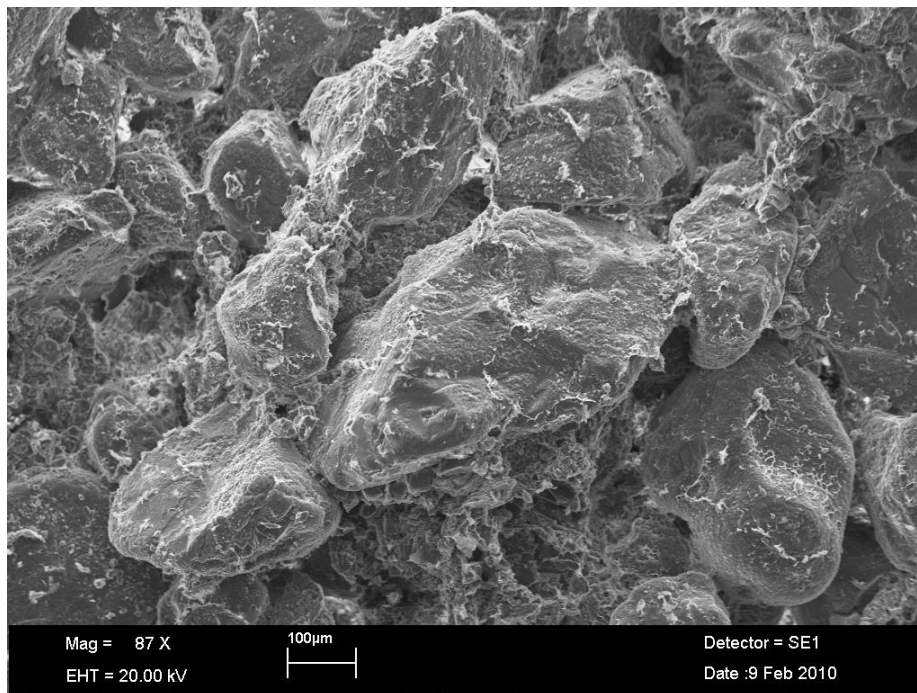


**Plate 12 SEI image showing detrital quartz grain surfaces coated with a thin pellicle of illitic or illite-smectite clay, with illite-smectite clay also forming a meniscus between grains at pore throats. Gamston borehole, sample MPLP106**

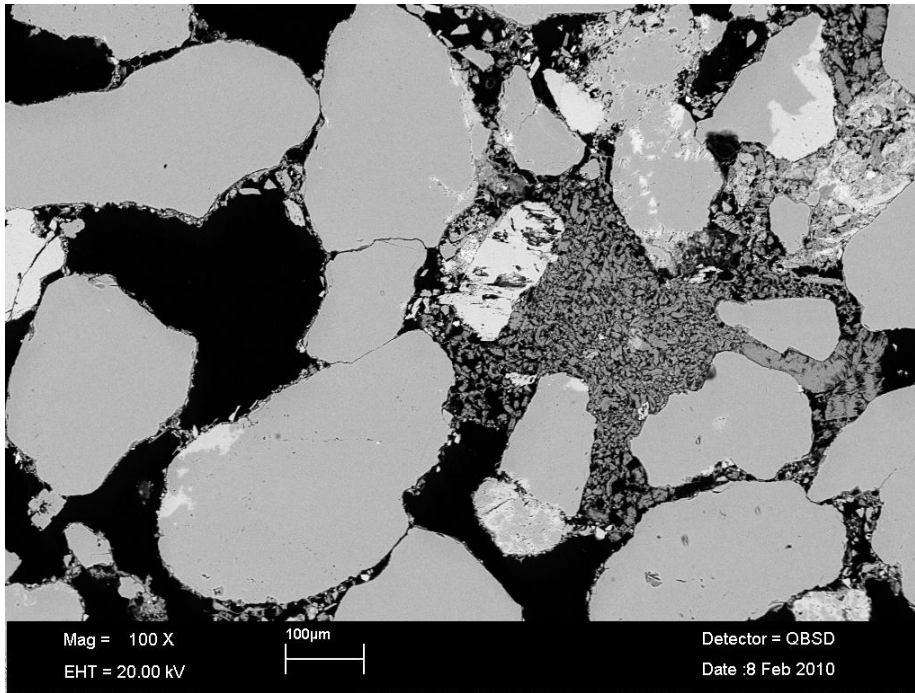


**Plate 13 BSEM image showing authigenic kaolinite filling oversized, secondary pore space, representing a framework grain alteration / dissolution site. Remnants of corroded detrital K-feldspar are enclosed within the kaolinite. Gamston borehole, sample MPLP106**

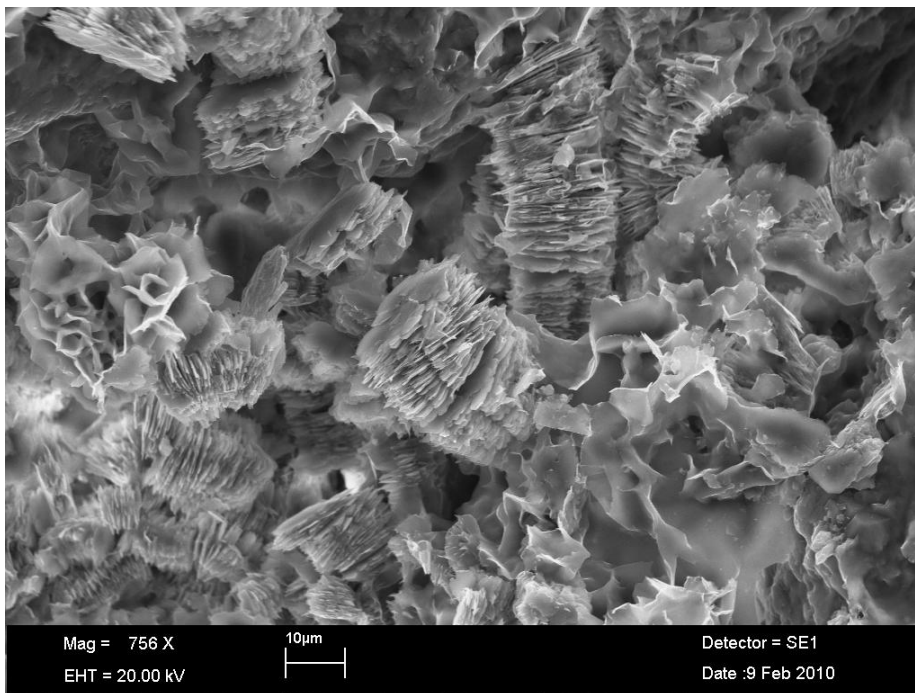


**Plate 14 SEI image showing showing vermicular or book-like crystals of authigenic kaolinite in secondary framework grain dissolution pore space. Wispy, flakey authigenic illite-smectite clay is also present, lining the pore space. Gamston borehole, sample MPLP106**

The development of quartz and K-feldspar cements is very limited in this rock. Rare, small, isolated euhedral overgrowths of authigenic quartz and feldspar are sometimes observed on grains with clean surfaces and that have limited or no grain-coating clay. The presence of an early grain coating clay appears to have inhibited the nucleation of major authigenic quartz and K-feldspar on many of the grains during burial diagenesis.

#### 4.5.1.2 POROSITY

The sandstone has good interconnected intergranular porosity. EDXA-image analysis determined a porosity of 15.3%. Most of the porosity is intergranular but a high proportion of the intergranular pores are oversized in comparison to the grain size of the sandstone (*e.g.* Plate 10 and

Plate 12). This indicates that these pores are of secondary origin and that they must result from the dissolution of unstable detrital grains (Schmidt and McDonald, 1979).

Petrographic observations suggest that much of the framework grain dissolution porosity is the result of alteration and dissolution of feldspars and feldspar-rich lithic clasts. The abundance of such framework grain dissolution porosity implies that the original sandstone had a significantly greater detrital feldspar and lithic clast content, possibly including plagioclase feldspar (which is seen in deeper buried sandstones from Cleethorpes No.1 borehole – Milodowski *et al.*, 1987; Milodowski and Rushton, 2008). As such, the original sandstone would probably have been closer to a feldspathic arenite or feldspathic-lithic arenite in composition (classification after Pettijohn *et al.*, 1987; Hallsworth and Knox 1999).

#### 4.5.1.3 WHOLE ROCK MINERALOGICAL ANALYSIS

The results of whole-rock XRD analyses of the initial Sherwood Sandstone Group sample from the Gamston borehole are summarised in Table 5 and labelled XRD traces are shown in the Appendix 1.

The whole rock XRD data are in broad agreement with the results from BSEM-EDXA-image analysis. The analysis indicates that the Sherwood Sandstone Group sandstone sample from the Gamston borehole is predominantly composed of quartz (76.9%) with minor amounts of K-feldspar (13.9%), dolomite (4.1%), ‘mica’ (undifferentiated mica species possibly including muscovite, biotite, illite, illite/smectite *etc.*; 2.6%) and ‘kaolin’ (one of the kaolin group minerals including halloysite, kaolinite *etc.*; 1.0%) and trace amounts of calcite, chlorite and pyrite.

**Table 5 Quantitative whole-rock XRD analysis from the Gamston borehole sample**

Sample name	MPL Code	Mineralogy (%)							
		calcite	chlorite	dolomite	‘kaolin’	K-feldspar	‘mica’	pyrite	quartz
Sherwood Sandstone Group (Castle Sandstone formation) Gamston borehole	MPLP106	0.7	0.5	4.1	1.0	13.9	2.6	<0.5	76.9

Key

‘mica’ = undifferentiated mica species including muscovite, biotite, illite and illite/smectite *etc.*;  
‘kaolin’ = one of the kaolin group minerals including halloysite, kaolinite *etc.*

#### 4.5.1.4 CLAY MINERALOGY

The results of XRD analysis of the <2 µm materials in the initial rock are summarised in Table 6 and labelled XRD traces are shown in the Appendix 1.

##### *'Non-swelling clays'*

The 'non-swelling clays' illite, kaolinite and chlorite were identified in sample:

Illite was identified by its characteristic air-dry d001 spacing of *c.*10.0Å which remains invariant after glycol-solvation and heating.

Chlorite was identified by its characteristic air-dry and glycol-solvated basal spacing peaks at 14.2, 7.1, 4.73 and 3.54Å and particularly the presence of a peak at *c.*13.5Å after heating at 550°C.

Kaolinite was identified by its characteristic air-dry basal spacings of *c.*7.1 and 3.58Å which remain invariant after glycol-solvation but which disappear after heating at 550°C due to the meta-kaolinite's X-ray amorphous state

##### *'Swelling clays'*

Illite-smectite mixed-layer clay was detected in the sample and is characterised by a broad d001/002 peak at *ca.*13.0Å on the air dry trace and a peak at *ca.*16.6Å on glycol-solvation. Heating to 550°C causes the peak to collapse to a *ca.* 9.6Å spacing.

A reflection at *c.*6.2°2θ after glycol-solvation suggests random interstratification of illite and smectite (R0-type mixed-layer mineral).

**Table 6 Semi-quantitative <2 um clay mineral XRD analyses from the Gamston borehole**

Sample name	MPL code	Clay mineralogy			Non-clay minerals
		major	minor	trace	
Sherwood Sandstone Group (Castle Sandstone formation) Gamston borehole	MPL P106	I/S mixed layer	kaolinite, illite	chlorite	quartz, K-feldspar

## 4.5.2 Cleethorpes No. 1 borehole core samples

### 4.5.2.1 PETROGRAPHY AND MODAL MINERALOGY

The two samples of sandstone from the Sherwood Sandstone Group sequence in the Cleethorpes No.1 geothermal borehole are very similar to other Sherwood Sandstone Group samples examined previously from this borehole by Milodowski *et al.*, (1987) and Milodowski and Rushton (2008). Modal mineralogical data for the sandstone sample are given in Table 7. These data show very good agreement with the results of the quantitative whole-rock XRD analysis on the same samples.

Both sandstones are defined as subfeldspathic arenites but sample MPLP510 contains significantly more albite and K-feldspar and is approaching a feldspathic arenite in composition (classification after Pettijohn *et al.*, 1987; Hallsworth and Knox 1999). They are composed of major detrital quartz (approximately 70:30 monocrystalline quartz : polycrystalline quartz), with subordinate detrital K-feldspar, and minor albitic plagioclase and lithic grains (mainly ferruginous mudstone clasts, but also chert grains and altered carbonate clasts), detrital illite and other clay minerals. Occasional detrital mica flakes (muscovite and biotite are also present. It

should be noted that the modal analysis, BSEM-EDXA-image analysis does not differentiate lithic clasts from the individual mineral components comprising them. Consequently, lithic clasts are not discriminated as a separate component in the modal analysis results.

*Sample MPLP510*

Sample MPLP510 is a finely laminated, clast-supported, fine to medium grained sandstone (Plate 15, Plate 16 and Plate 17). The laminae are moderately to well-sorted but vary in thickness from 3 mm for the darker, finer-grained and ferruginous more clay-rich laminae, to 5 mm for the cleaner sandier laminae. The grain fabric is also moderately- to well-compacted, with the development of dominantly concavo-convex and long grain boundaries in the cleaner sandstone laminae (Plate 17 and Plate 18). Triple-point grain contacts are also observed, and less competent mica flakes and mudstone clasts display evidence for both plastic and brittle deformation. The finer-grained laminae are significantly more compacted, with triple-point grain contacts being dominant (Plate 18).

This laminated fabric would be expected to exert significant directional control on the permeability and flow paths in the sandstone plugs used in the experiments. Permeability would be anticipated to be higher in the direction parallel to the lamination than perpendicular to the lamination.

**Table 7 Modal mineralogical data for the Sherwood Sandstone Group samples from the Cleethorpes No.1 borehole**

Mineral	Sample MPLP510			Sample MPLP511		
	Normalised mineralogy %	Standard deviation	XRD %	Normalised mineralogy %	Standard deviation	XRD %
Quartz	69.3	3.6	72.0	74.4	7.3	73.7
K-feldspar	17.5	2.9	16.9	12.4	3.4	13.1
Albite	3.4	1.7	4.6	1.4	0.4	3.0
Illite-clays	5.6	1.7	3.7	2.4	1.0	3.6
Dolomite	2.9	0.9	2.7	8.7	7.5	6.4
Apatite	0.1	0.1	0	0	0	0
Muscovite	1.0	1.0	Included in 'illite'	0.8	0.5	Included in 'illite'
Biotite	0.1	0.2	Included in 'illite'	0	0	Included in 'illite'
Ilmenite	0	0	0	0	0	0
TiO <sub>2</sub>	0		0	0	0	0
Iron oxides (incl. hematite magnetite, FeOOH)	0.1	0.2	<0.5	0	0	<0.5
TOTAL	100	-	99.9	100.1	-	99.8
Porosity	17.7	1.8	-	20.3	2.2	-

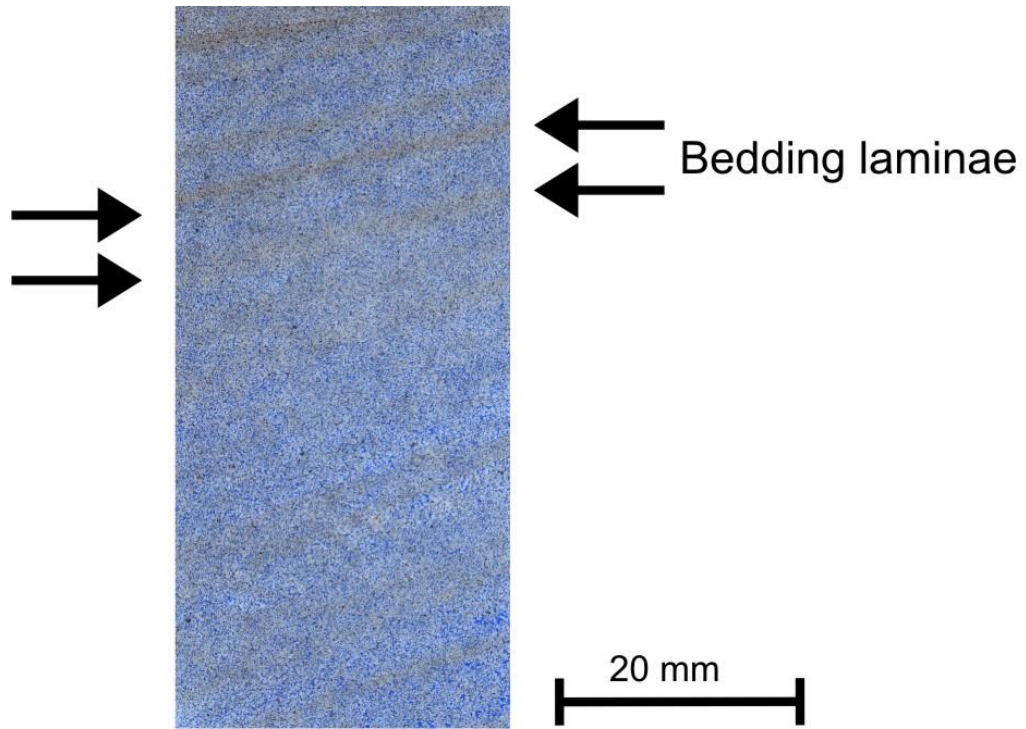


**Plate 15 Transmitted light scanned image of thin section of sandstone, showing finely-laminated fabric, with thin, dark, ferruginous clay laminae (arrowed). Blue dye resin impregnation reveals relatively uniform distribution of intergranular porosity within cleaner sandstone laminae, with lower porosity within the finer darker laminae. Sample MPLP510, Cleethorpes No.1 geothermal borehole**

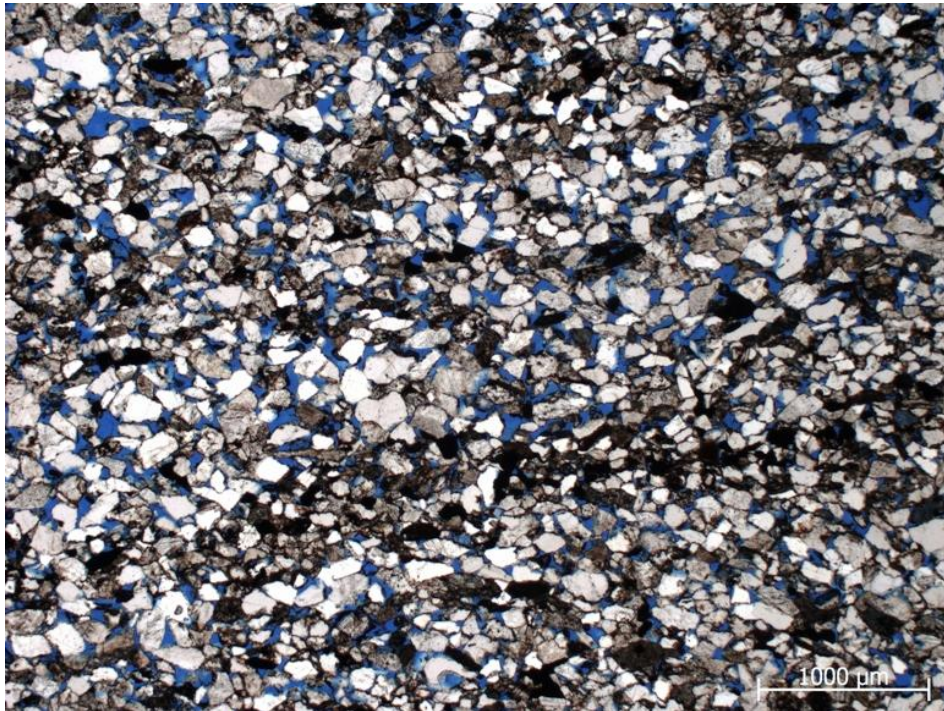


**Plate 16** Transmitted photomicrograph (plane polarised light) of thin section of sandstone, showing detail of finely-laminated sandstone fabric. The blue dye resin impregnation shows that intergranular porosity is significantly greater in the coarser, cleaner laminae and lower in the thin, dark, ferruginous clay-rich laminae. Many of the intergranular pores in the cleaner sandstone laminae are oversized, indicating that they are secondary and result from framework grain dissolution. Sample MPLP510, Cleethorpes No.1 geothermal borehole

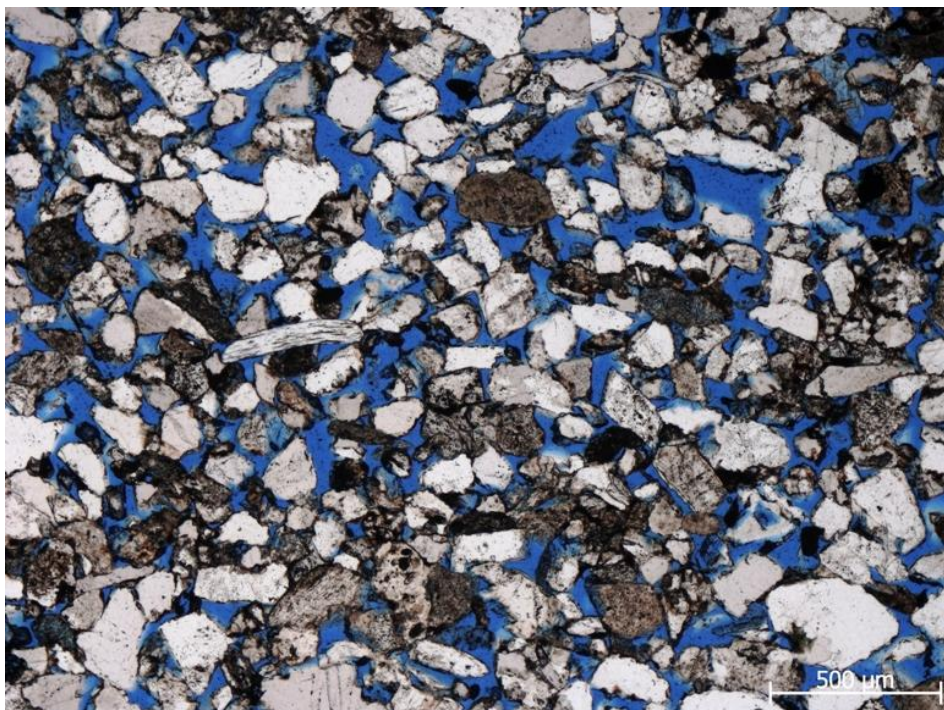


**Plate 17** Transmitted photomicrograph (plane polarised light) of thin section of sandstone, showing sandstone open, well-connected intergranular pore fabric, with moderately well-compacted sand grains, interspersed with “domains” with large oversized pores, indicative of major framework grain dissolution. Sample MPLP510, Cleethorpes No.1 geothermal borehole

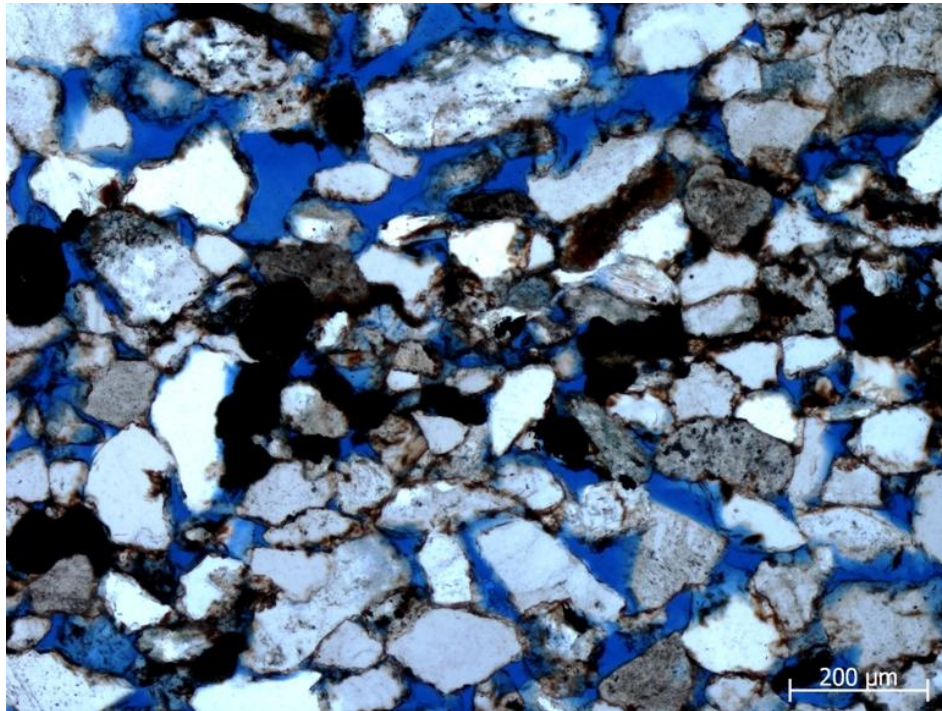


**Plate 18 Transmitted photomicrograph (plane polarised light) of thin section of sandstone, showing sandstone open, well-connected intergranular pore fabric, with moderately well-compacted sand grains, interspersed with “domains” with large oversized pores, indicative of major framework grain dissolution. The finer-grained ferruginous lamina running through the middle of the field of view shows very tight packing with the development of mainly long, concavo-convex, and triple-point grain contacts indicative of significant burial compaction. Sample MPLP510, Cleethorpes No.1 geothermal borehole**

The sandstone has been significantly modified by diagenesis. Dolomite cement occurs in discontinuous patches (Plate 19). Two generations of dolomite can be differentiated:

- Early, “nodular” to “patchy” non-ferroan dolomite cement that often displays a radial and displacive fabric, and appears to separate uncompacted detrital grains. This dolomite is typically full of inclusions of fine grained ferruginous detrital material and clay, and appears to have developed before significant compaction of the rock. It has been interpreted previously to represent pedogenic dolomite or “dolocrete” (Milodowski *et al.*, 1987; Milodowski and Rushton, 2008); and,
- Later diagenetic slightly ferroan dolomite overgrowths on the earlier dolomite, with euhedral rhombic terminations into open pore space. Locally this dolomite was seen locally to poikilotopically enclose compacted detrital grains. This later dolomite is typically free of fine grained detrital inclusions.

In addition to authigenic dolomite, quartz and K-feldspar cements commonly form syntaxial authigenic overgrowths on detrital grains (Plate 20). These overgrowths are best developed on clean detrital grain surfaces which have little or now detrital clay coating. However, many grains are coated with a thin pellicle of illitic or illitic and chloritic clay (Plate 21), which inhibits overgrowth development. This clay coating is usually impregnated with fine grained iron oxide (hematite), and is interpreted as early (syndimentary or pedogenic) infiltrated clay. Fine, wispy secondary authigenic illite or illite-smectite has nucleated on the surface of this infiltrated clay pellicle (Plate 21).

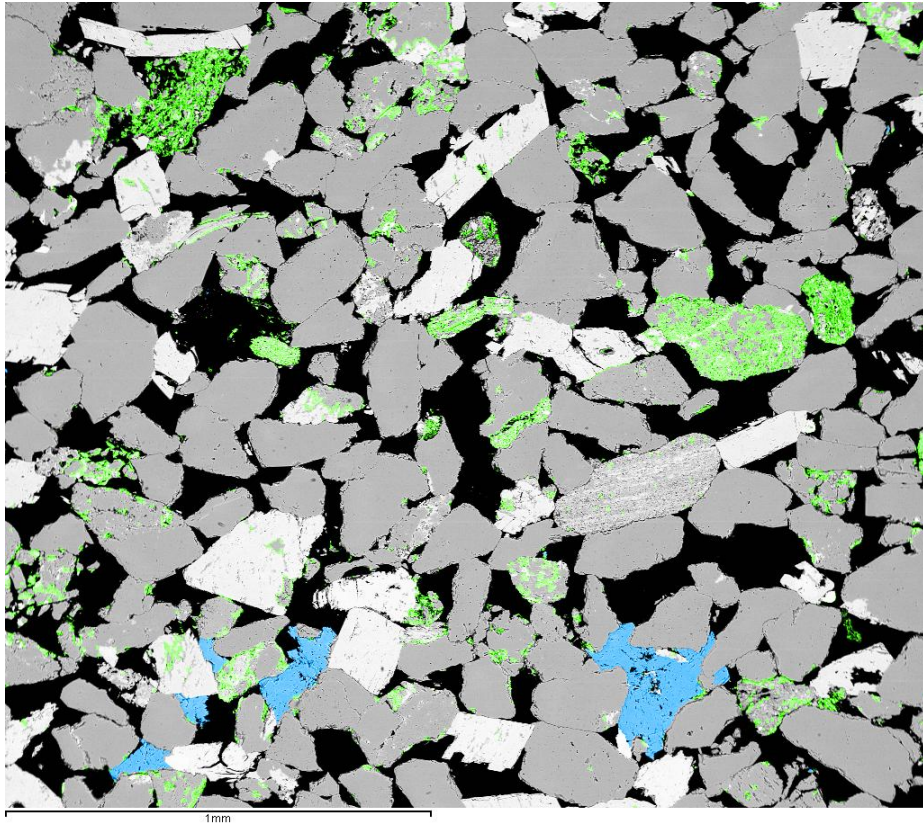


**Plate 19 BSEM photomicrograph with EDXA-modal mineral distribution map overlay. The colours correspond to different phases: grey – quartz, black – porosity, white – K feldspar (and trace albite), laminated grey/white are lithic clasts, blue-represents dolomite cement and green – scattered clay minerals (both illitic clay and mica within lithic clasts). Sample MPLP510, Cleethorpes No.1 geothermal borehole**

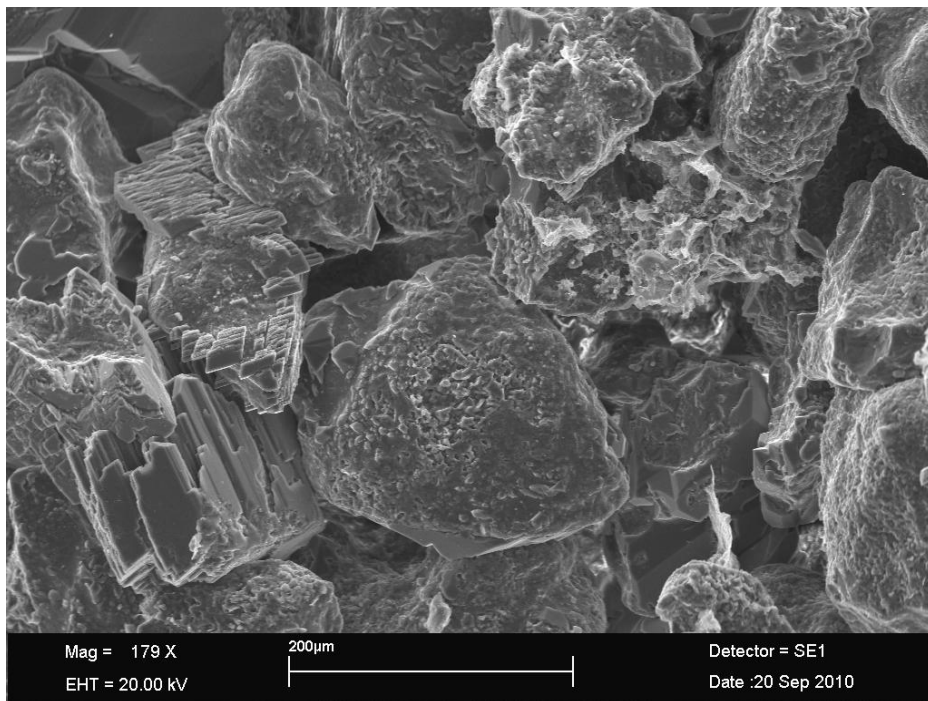


**Plate 20 SEM photomicrograph (SEI) showing euhedral authigenic K-feldspar and quartz overgrowth cements locking the grain framework together. The overgrowth surfaces are generally very smooth and clean. Sample MPLP510, Cleethorpes No.1 geothermal borehole**

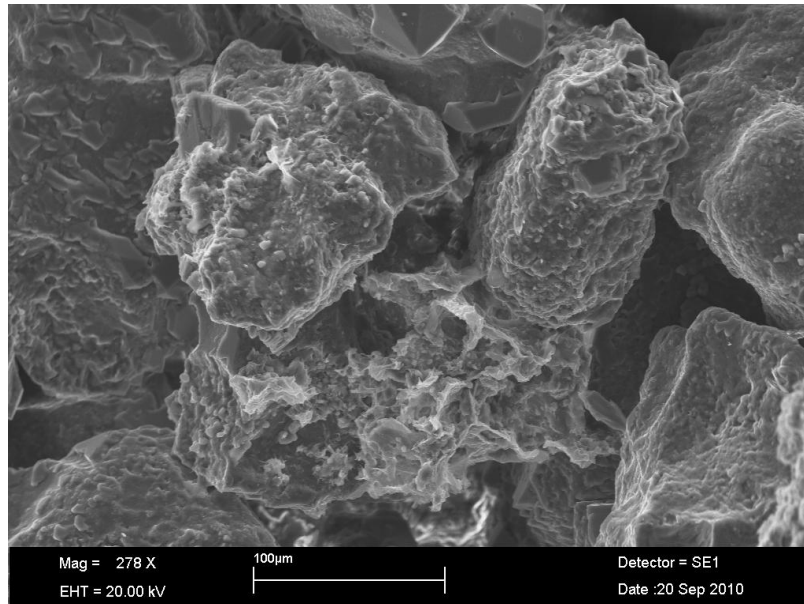


**Plate 21 SEM photomicrograph (SEI) showing detrital clay coatings on detrital grains, with authigenic illite-smectite forming wispy protrusions from some coatings. Sample MPLP510, Cleethorpes No.1 geothermal borehole**

*Sample MPLP511*

Sample MPLP 511 is a loosely cemented, moderately sorted and moderately to locally strongly compacted sandstone. It has a more homogenous fabric than sample MPLP510, with only faint traces of bedding lamination (Plate 22 and Plate 23). Superficially, the grain fabric appears very open but close examination shows that the detrital grains display dominantly concavo-convex, and long grain boundaries, with triple-point grain contacts being moderately common. This implies a significant degree of burial compaction has occurred. The open pore fabric is anomalous and is indicative of major framework grain dissolution.

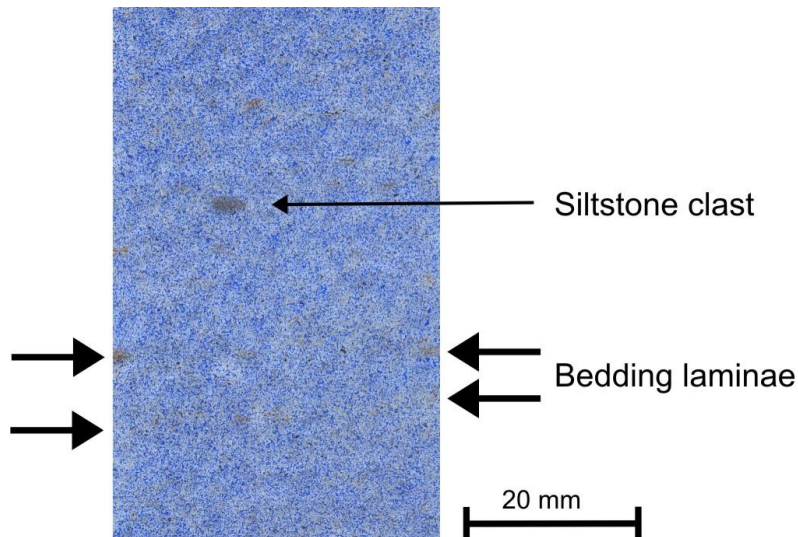


**Plate 22 Transmitted light scanned image of thin section of sandstone, showing only traces of a discontinuous finely-laminated bedding fabric, with thin, dark, ferruginous clay laminae (arrowed). Blue dye resin impregnation reveals relatively uniform distribution of intergranular porosity. Sample MPLP511, Cleethorpes No.1 geothermal borehole**

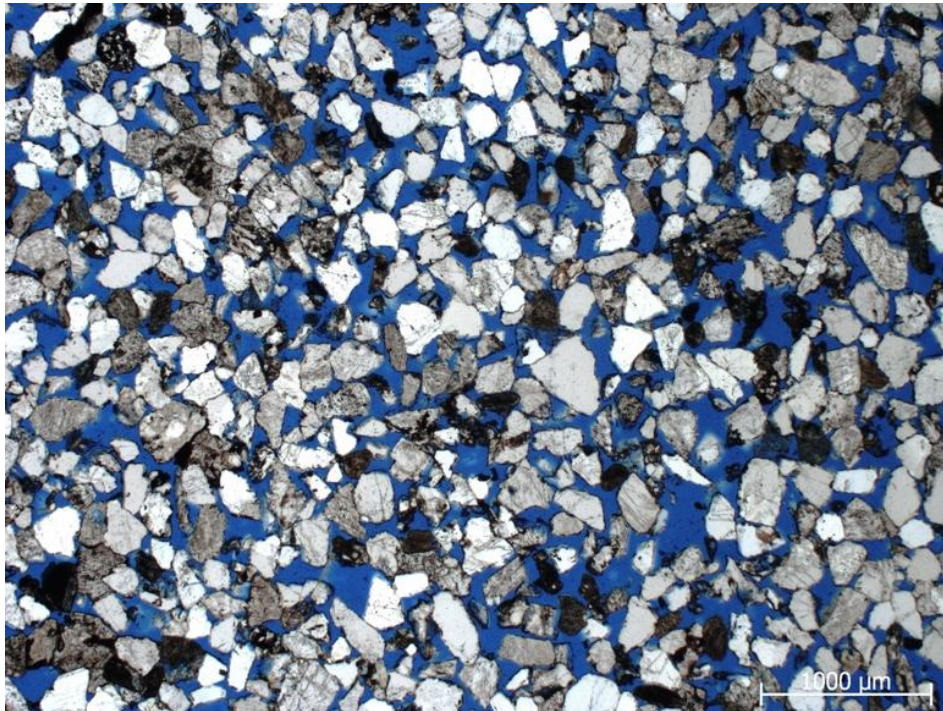


**Plate 23** Transmitted photomicrograph (plane polarised light) of thin section of sandstone, showing sandstone open, very porous well-connected intergranular pore fabric, with moderately well-compacted sand grains, interspersed with “domains” with large oversized pores, indicative of major framework grain dissolution. Sample MPLP511, Cleethorpes No.1 geothermal borehole

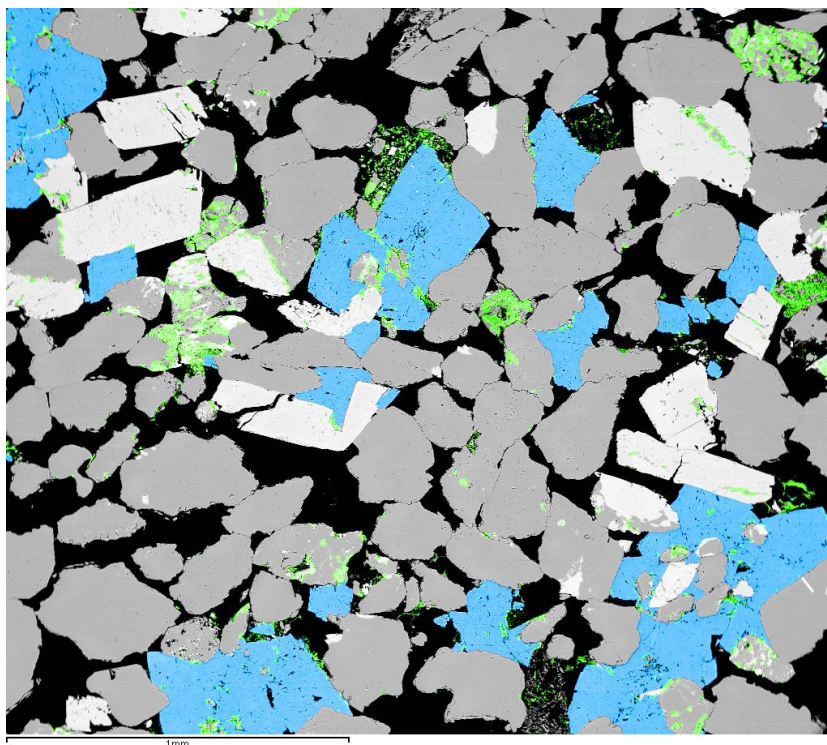


**Plate 24** BSEM photomicrograph with EDXA-modal mineral distribution map overlay. The colours correspond to different phases: grey – quartz, black – porosity, white – K feldspar (and trace albite), laminated grey/white are lithic clasts, blue-represents dolomite cement and green – scattered clay minerals (both illitic clay and mica within lithic clasts). Sample MPLP511, Cleethorpes No.1 geothermal borehole

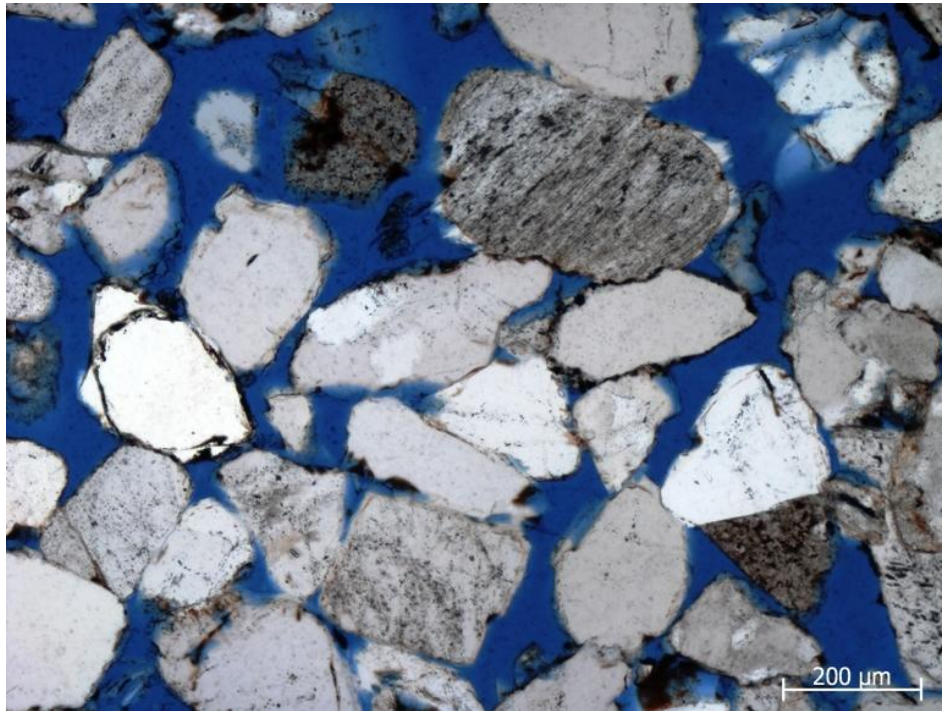


**Plate 25** Transmitted photomicrograph (plane polarised light) of thin section of sandstone, showing well-developed euhedral quartz overgrowths (clear) on detrital quartz grains. Sample MPLP511, Cleethorpes No.1 geothermal borehole

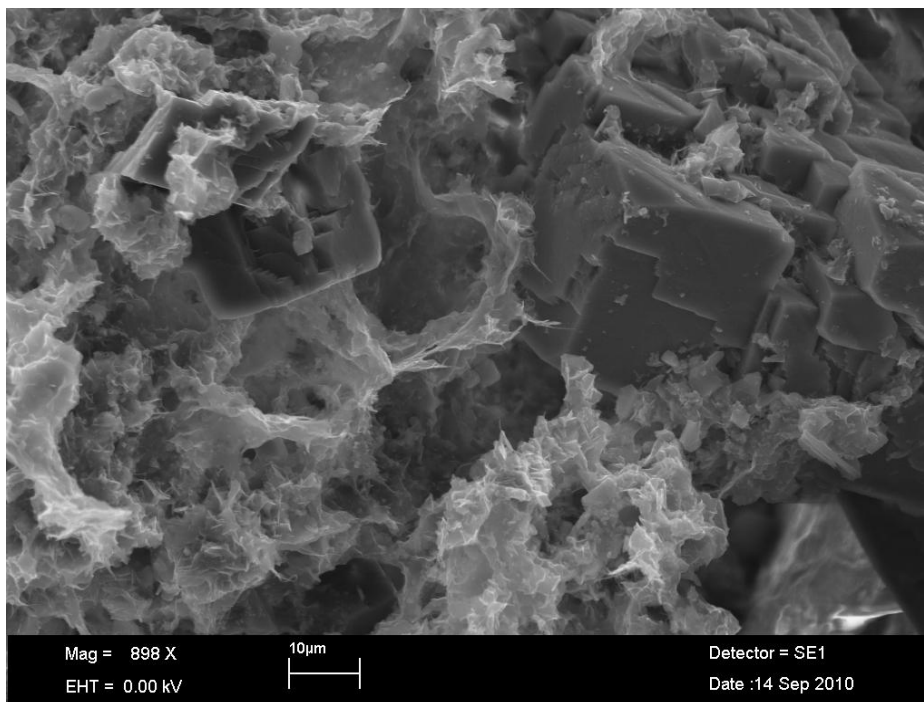


**Plate 26** SEM photomicrograph (SEI) showing the typical morphology of authigenic wispy illite-smectite clay that locally abundantly developed and associated with the dissolution of unstable detrital minerals. Sample MPLP511, Cleethorpes No.1 geothermal borehole

Mineralogically, this sandstone shows broadly similar mineralogical and diagenetic features to those observed in sample MPLP510. However, it has a lower feldspar content and a greater amount of dolomite cement (Plate 24). Many of the quartz and K-feldspar grains display well-developed euhedral overgrowths of authigenic quartz and K-feldspar (Plate 25). These are typically larger than those seen in sample MPLP510, probably because their growth was not as inhibited due the lower amount of grain-coating clay.

Grain-coating clay pellicles are present but are less obvious than in sample MPLP51. The clay rims are impregnated with fine iron oxide, and appears to have largely infiltrated into the sandstone after deposition. Delicate, wispy authigenic illite has grown on top of these clay pellicles. The wisps of illite appear to be the “roots” of attachment of pore-lining illite fibres that have broken down and collapsed back onto the grain surfaces as a result of the drying out of the core after drilling. This authigenic illite or illite-smectite is locally very abundant in some pores, where it is closely associated with the breakdown of unstable detrital silicates (Plate 26).

#### 4.5.2.2 POROSITY

The two sandstone samples from the Cleethorpes No.1 borehole have good interconnected intergranular porosity. EDXA-image analysis determined porosity values of 17.7% for the finely laminated sandstone sample MPLP510. The better sorted and cleaner sandstone represented by sample MPLP511 was shown by EDXA-image analysis to have a higher porosity of 20.3%. Detailed mercury-injection porosimetry data for the two sandstones is provided in Appendix 2. This gave higher values for total porosity of 23.7% and 27.7%, respectively for MPLP510 and MPLP511. The higher porosity values determined from mercury-injection core porosimetry reflect the fact that this technique measures the fine microporosity within the clay material and fine intragranular pores that was probably underestimated or unresolved by the BSEM-EDXA modal analysis measurements.

Most of the porosity is intergranular but a very high proportion of the intergranular pores are large oversized pores, in comparison to the grain size and packing state of the sandstone (*e.g.* Plate 23 and Plate 24). This indicates that these pores are of secondary origin and that they must result from the dissolution of unstable detrital grains (Schmidt and McDonald, 1979).

Petrographic observations (Section 4.5.2.1.) suggest that much of the framework grain dissolution porosity is the result of alteration and dissolution of feldspars and feldspar-rich lithic clasts. The abundance of such framework grain dissolution porosity implies that the original sandstone had a significantly greater detrital feldspar and lithic clast content, possibly including plagioclase feldspar. As in the case of the sandstone from the Gamston borehole, these two sandstones would also originally have been closer to a feldspathic arenite or feldspathic-lithic arenite in composition (classification after Pettijohn *et al.*, 1987; Hallsworth and Knox 1999)

The pore fabric and interconnectivity of the intergranular pore network is strongly influenced by the primary sedimentary lamination in sample MPLP510. The porosity within the fine, ferruginous clay-rich laminae is almost completely lost through extensive compaction, whereas in the cleaner, well-sorted and sandier laminae, the porosity is much greater. Consequently, this fabric will potentially exert a significant control on fluid flow through the sandstone core plugs during the experiments. Permeability will potentially be much higher parallel to the lamination, and therefore flow is likely to be channelled parallel to the lamination

The sandstone sample MPLP511 appears to have a much more homogeneous fabric, with only weakly-developed or weakly-preserved sedimentary lamination. Therefore, this sandstone is likely to have a much more uniform distribution of permeability.

#### 4.5.2.3 WHOLE ROCK MINERALOGICAL ANALYSIS

Whole-rock X-ray diffraction analysis indicates that the two Sherwood Sandstone Group samples from the Cleethorpes No.1 geothermal borehole are predominantly composed of quartz (*ca.*72-74%) with minor amounts of K-feldspar (*ca.*13-17%), dolomite (*ca.*3-6%), albite (*ca.*3-5%), ‘mica’ (undifferentiated mica species possibly including muscovite, biotite, illite, illite/smectite *etc.*; *ca.*3%) and ‘chlorite’ (*ca.*1.0%) and trace amounts of hematite.

The results of whole-rock XRD analyses of the initial Sherwood Sandstone Group sample from the Cleethorpe No.1 geothermal borehole are summarised in Table 8 and labelled XRD traces are shown in the Appendix 1.

**Table 8 Quantitative whole-rock XRD analysis from the Cleethorpes No.1 borehole samples**

Sample Name	BGS Code	Mineralogy							
		albite	chlorite	dolomite	hematite	'kaolin'	K-feldspar	'mica'	quartz
Sherwood Sandstone Group	MPLP510	4.6	0.7	2.7	<0.5	nd	16.9	3.0	72.0
Sherwood Sandstone Group	MPLP511	3.0	0.8	6.4	<0.5	nd	13.1	2.8	73.7
Basal Permian Sandstone	MPLP512	1.2	3.7	nd	2.9	6.1	2.1	14.5	69.5

Key

nd = not detected

#### 4.5.2.4 CLAY MINERALOGY

The results of XRD analysis of the <2 µm materials in the initial rock are summarised in Table 9 and labelled XRD traces are shown in the Appendix 1.

**Table 9 Summary of semi-quantitative <2 µm clay mineral XRD analyses from the Cleethorpes No.1 borehole samples**

Sample Name	BGS Code	Clay Mineralogy		Non-clay minerals
		major	minor	
Sherwood Sandstone Group	MPLP510	chlorite, illite	I/S mixed layer	quartz, K-feldspar, albite, hematite
Sherwood Sandstone Group	MPLP511	chlorite, illite	I/S mixed layer	quartz, K-feldspar, albite, hematite
Basal Permian Sandstone	MPLP512	kaolinite, illite	I/S mixed layer, chlorite	quartz, K-feldspar, albite, hematite

#### *'Non-swelling clays'*

The 'non-swelling clays' illite, and chlorite were identified in the two Sherwood Sandstone Group samples MPLP510 and MPLP511, and in the sample from the Basal Permian Sandstone. Kaolinite was only identified in the Basal Permian Sandstone sample MPLP512.

Illite was identified by its characteristic air-dry d001 spacing of c.10.0Å which remains invariant after glycol-solvation and heating. Illite is a major clay mineral component in all three sandstone samples from the Cleethorpes No.1 borehole.

Chlorite was identified by its characteristic air-dry and glycol-solvated basal spacing peaks at 14.2, 7.1, 4.73 and 3.54Å and particularly the presence of a peak at ca.13.5Å after heating at 550°C. It was identified as a major component of the clay mineral assemblage of the two Sherwood Sandstone Group samples but only as a minor component in the sample from the Basal Permian Sandstone.

Kaolinite was identified by its characteristic air-dry basal spacings of *ca.*7.1 and 3.58Å which remain invariant after glycol-solvation but which disappear after heating at 550°C due to the meta-kaolinite's X-ray amorphous state

#### 'Swelling clays'

A broad peak to the low angle side of the illite  $\sim 10$  Å peak, which shows a limited degree of swelling after ethylene glycol solvation to *ca.*11.7Å, possibly represents an interlayered illite/smectite (I/S) phase. In the Cleethorpes No.1 borehole illite/smectite mixed-layer clay is a minor component of the clay mineral assemblage. This differs from the Gamston borehole where illite/smectite mixed-layer clay is the major clay mineral component. The lower proportion of "swelling clay" components in the clay mineral assemblage of the Cleethorpes No.1 borehole may be a reflection of its deeper burial depth.

## 4.6 MINERALOGICAL AND ESEM ANALYSIS OF THE POST-EXPERIMENTAL MATERIALS

### 4.6.1 Dead *P. aeruginosa*

In the original sample of inoculation fluid containing dead bacterial culture (section 2.5), biofilm residues were visible to the unaided eye as suspended diaphanous sheets. A subsample was carefully collected, via pipette, to include some of this matter.

When in a wet state within the ESEM, biofilm material was not morphologically or texturally recognisable; the biofilm does not impose any recognisable structures at the liquid surface, suggesting that surface tension effects dominate over any biofilm effects.

During drying cycles, moisture was noted to be retained whilst at humidities >80% (the humidity is taken from the theoretical water vapour pressure-temperature phase diagram, Figure 5). Below 80% humidity, drying was observed as a gradual reduction in volume. Only once the humidity was taken to around 60% was complete drying achieved; at this humidity stable residues were noted to comprise of a mix of crystalline forms and patches of morphologically indistinct to crumpled sheets of amorphous material (Plate 27A). This amorphous material was interpreted to be the biofilm residues. These residues were observed to rehydrate readily at humidities  $\geq 80\%$  and <100% (Plate 27B) and to be susceptible to beam damage when dry (further collapse and shrinkage) even whilst imaging at low accelerating voltages (7.5 kV). No bacterial forms were recognised.

In conclusion, the biofilm is virtually undetectable texturally or morphologically when wet. In a dry state it is identifiable but morphologically indistinct. It collects in amorphous clumps and sheets on surfaces, and is highly susceptible to beam damage.

The noted tendency to retain water and to rehydrate at relatively low humidities (at which pure water would be expected to evaporate) is due, at least in part, to the fact that the wetting agent is a solution and not pure water (see discussion in Section 3.3.4.2: note on use of 0.25M NaCl solution as a wetting fluid in ESEM mode). It is also possible that the biofilm is a hydrophilic constituent whose tendency to retain water is a property that could be used to infer its presence where other physical evidence is lacking.



**Plate 27 SEI photomicrograph of dead *P. aeruginosa* sample (under ESEM). A: Precipitated crystals, two elongate in form, emergent from an amorphous mass of biogenic material, most likely biofilm residue, which is unevenly spread across the striations of the sample holder's milled surface. B: At 85% theoretical water vapour relative humidity, partial rehydration has occurred, resulting in crystal dissolution and an expansion of the biogenic material**

## 4.6.2 Post-experimental materials

### 4.6.2.1 INLET FRIT – BIOTIC EXPERIMENT

An examination of the inner (sample-facing) surface of the inlet frit shows that it has a texture of highly varied pore sizes defined by a metallic matrix with a 'grain' size of 50-150  $\mu\text{m}$  (Plate 28). Pores are up to 50  $\mu\text{m}$  across (Plate 28). Examination of the pore walls revealed widespread crenulated and bladed deposits of probable Fe oxide/hydroxide (Plate 29 and Plate 30) that support the visible evidence of corrosion (Plate 7). With only minor probable biofilm residues identified (Plate 30). It seems likely that the frit was not blocked by biofilm at the end of the experiment.

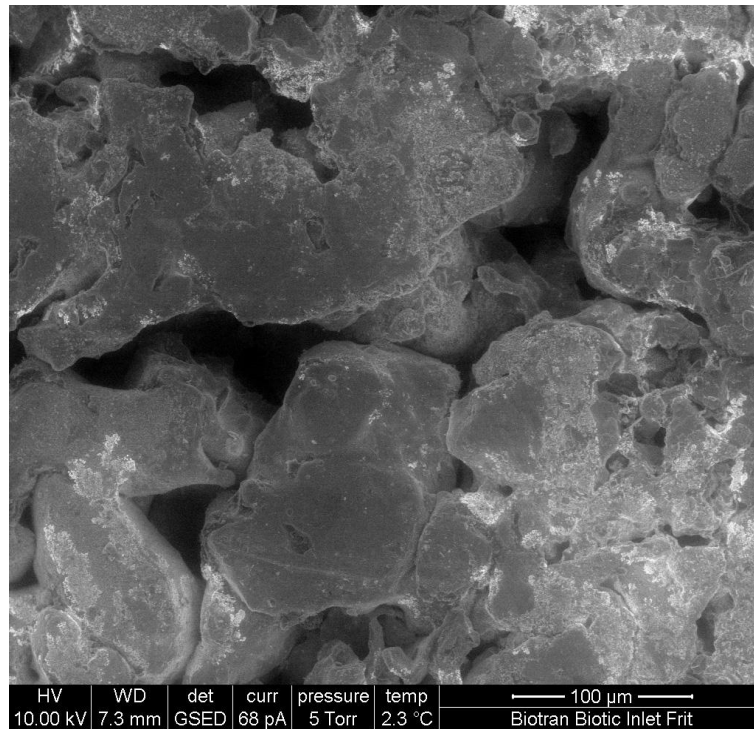


**Plate 28 SEI photomicrograph of the inner face of the inlet frit (under ESEM). This shows the structure of the metallic matrix and pores of the frit**

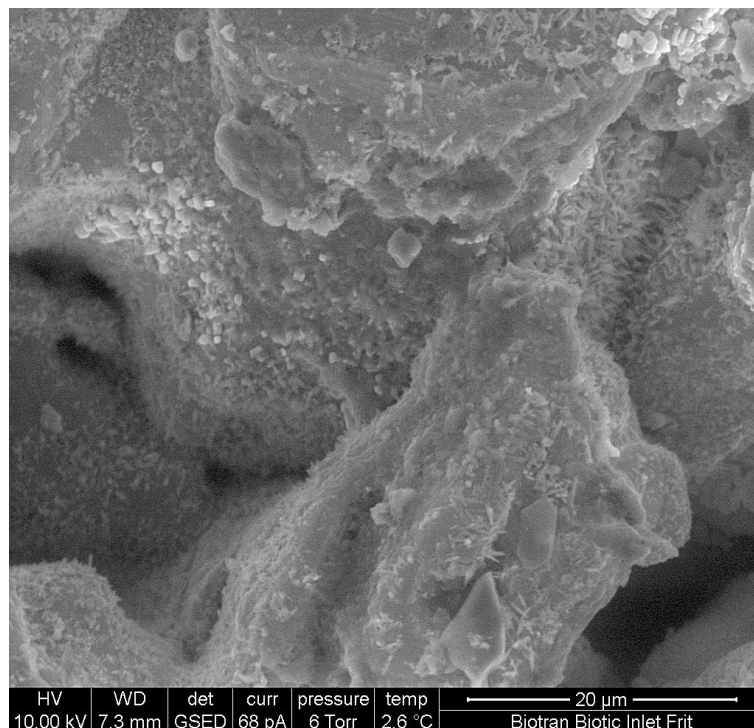


**Plate 29 SEI photomicrograph of the inner face of the inlet frit (under ESEM). The widespread bladed pore-lining bladed deposit is most likely of iron oxide/hydroxide**

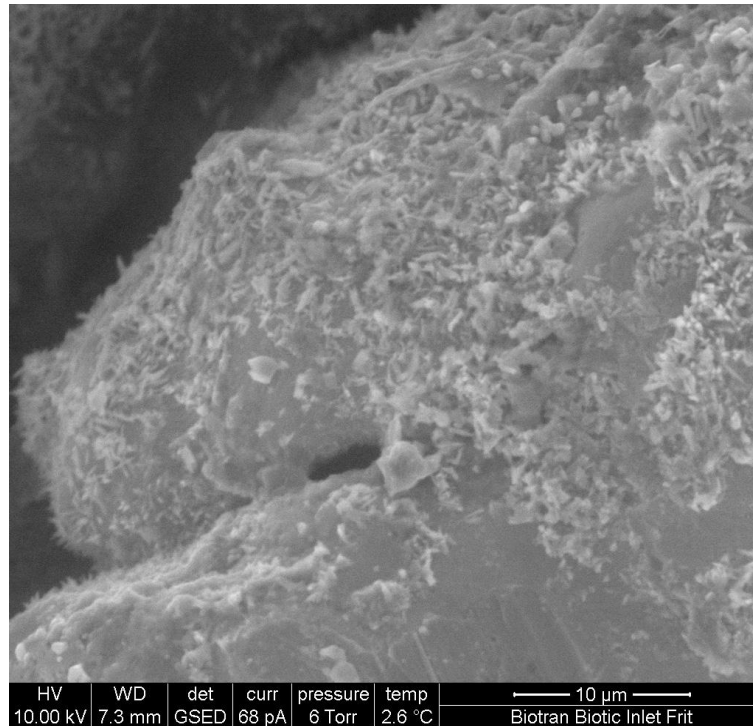


**Plate 30 SEI photomicrograph of the inner face of the inlet frit (under ESEM). Typical bladed deposit of probable iron oxide/hydroxide on pore walls with scattered angular mineral debris. Fingered amorphous sheet at top right is a probable biofilm residue**

#### 4.6.2.2 ROCK MATERIALS

The various samples and different preparations show that biogenic materials are very difficult to identify and image directly. Characteristics observed during drying cycles, however, suggest that there are significant differences to the way that wetting liquids behave between the different samples that cannot be explained solely by the differences in liquid compositions (distilled water, 0.25M NaCl brine). These characteristics can potentially, therefore, be used to give an indication of the distributions and abundances of experimentally derived biogenic materials in addition to direct physical evidence observed.

##### *Liquid behaviour in ESEM mode*

When starting from a completely saturated state and held at 100% humidity (relative to water), rock chips typically displayed some evaporation, resulting from local heating from the electron beam, with the final liquid distribution normally stabilising after 5-10 minutes. Subsequent reductions in the theoretical humidity were performed in steps by modifying the ESEM stage temperature and chamber pressure; after each step change, final liquid distribution was typically established within 10 minutes. The observed behaviours of the wetting liquids with samples from the biotic and control cores are summarised below, and in Table 10 and Plate 31.

In summary:

- The material from the biotic experiment has a greater propensity to retain liquid, irrespective of its composition, compared to that from the control experiment. This contrast is shown more strongly with the use of distilled water as the ESEM wetting liquid;
- With 0.25M NaCl brine as the ESEM wetting liquid, no or little evaporation occurs at 100% humidity, and there is only limited evaporation at humidities down to 80%. Complete drying requires a <80% humidity;

- With distilled water as the ESEM wetting liquid, samples dry rapidly at 80% humidity, with control experiment samples virtually completely dry inside 10 minutes in contrast to most biotic samples which retain a thin pore lining;
- With distilled water as the ESEM wetting liquid, samples do not re-hydrate after drying without setting sample and chamber conditions to over-saturate with respect to liquid water; and,
- One of the biotic experiment samples examined (from the outlet end) was an exception to the generalised observations above. With distilled water as the ESEM wetting liquid, at 80% humidity it dried almost completely, behaviour more like a typical control experiment sample (Plate 32).

**Table 10 Summary of differences in rock materials from biotic and control experiments**

Wetting Liquid\Experiment	Biotic	Control
<b>0.25M NaCl brine</b>	<p>From an initial saturated state:</p> <ul style="list-style-type: none"> <li>• At 80% humidity the liquid content is reduced. Remaining pore water coats most pore walls, fills some pores and locally fills pore throats – Plate 31C.</li> <li>• The finer pore structure of finer grained sample portions notably retain more pore water – Plate 31A.</li> <li>• At 65% humidity the samples are mostly completely dry.</li> </ul> <p>Rehydration is partial and localised at &lt;100% humidity.</p>	<p>From an initial saturated state:</p> <ul style="list-style-type: none"> <li>• At 80% humidity the liquid content is reduced. Remaining pore water is a patchy, incomplete pore coating, fills fine pores and locally fills pore throats – Plate 31B.</li> <li>• At 65% humidity the samples are mostly completely dry.</li> </ul> <p>Rehydration is partial and localised at &lt;100% humidity.</p>
<b>Distilled H<sub>2</sub>O</b>	<p>From an initial saturated state:</p> <ul style="list-style-type: none"> <li>• At 100% humidity the wetting pore water is retained as a pore-filling.</li> <li>• At 80% pore water content is reduced. Remaining liquid remains as a thin pore coating meniscus after 10 mins – Plate 31E. Evaporation continues, particularly under the beam.</li> <li>• No rehydration apparent when returned to 100% humidity.</li> </ul>	<p>From an initial saturated state:</p> <ul style="list-style-type: none"> <li>• At 100% humidity the wetting pore water evaporates from pores steadily until it is present only as a thin and patchy pore coating – Plate 31D.</li> <li>• At 80% humidity the remaining pore water evaporates leaving the sample virtually dry – Plate 31F.</li> </ul> <p>No rehydration apparent when returned to 100% humidity.</p>

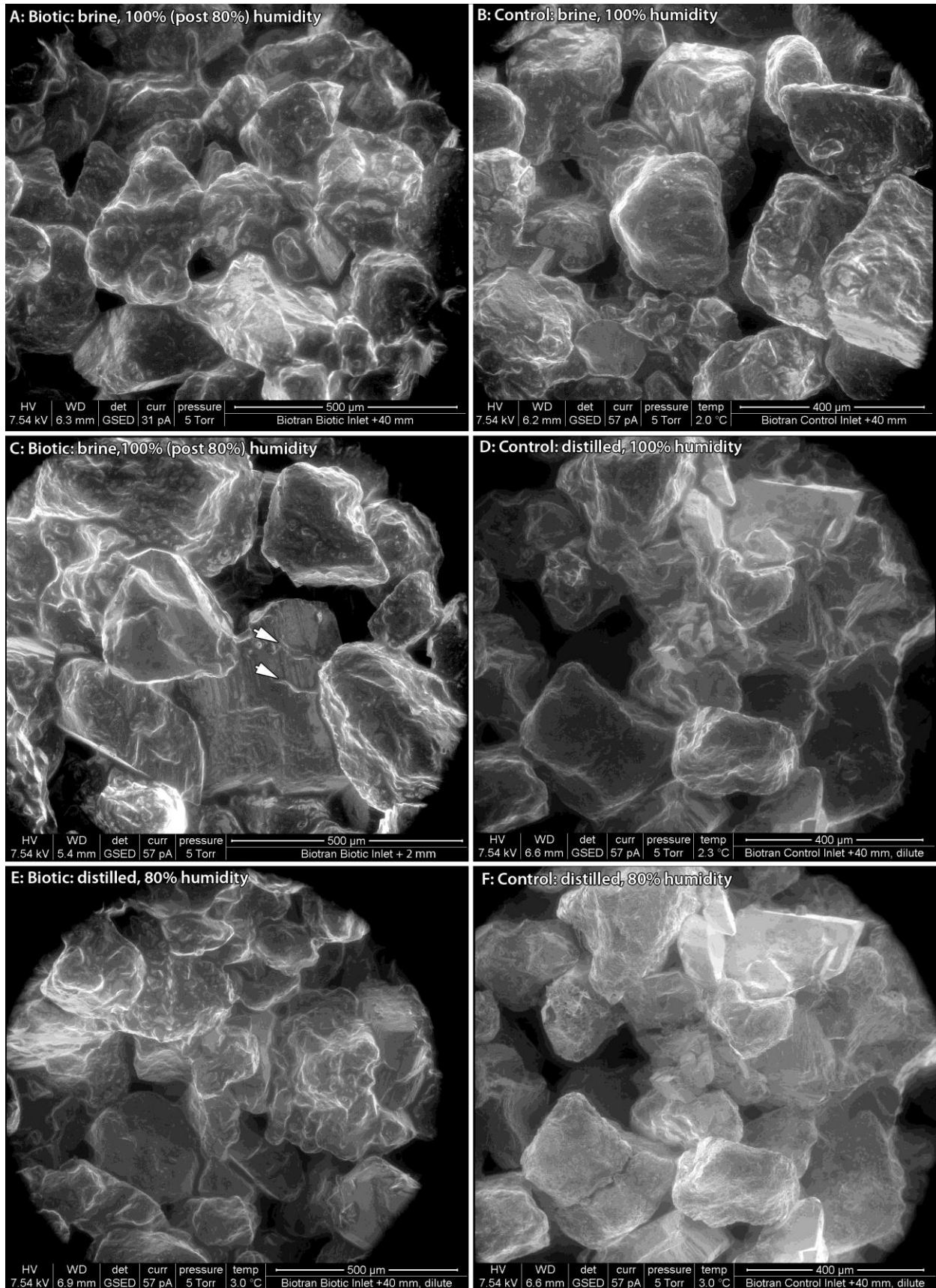


**Plate 31 SEI photomicrographs (under ESEM). Samples from the biotic core (A, C, E) and the control core (B, D, F) are shown at different humidities and with different wetting liquids (details on images). All samples are from central portions of the cores except that in C. Liquid is typically imaged as a darker phase coating pore walls, draped between grains and locally filling pores. A shows the highest liquid content, A and C contrast finer and**

coarser grained sample portions, F is almost completely dry. Arrows in C highlight ridged forms

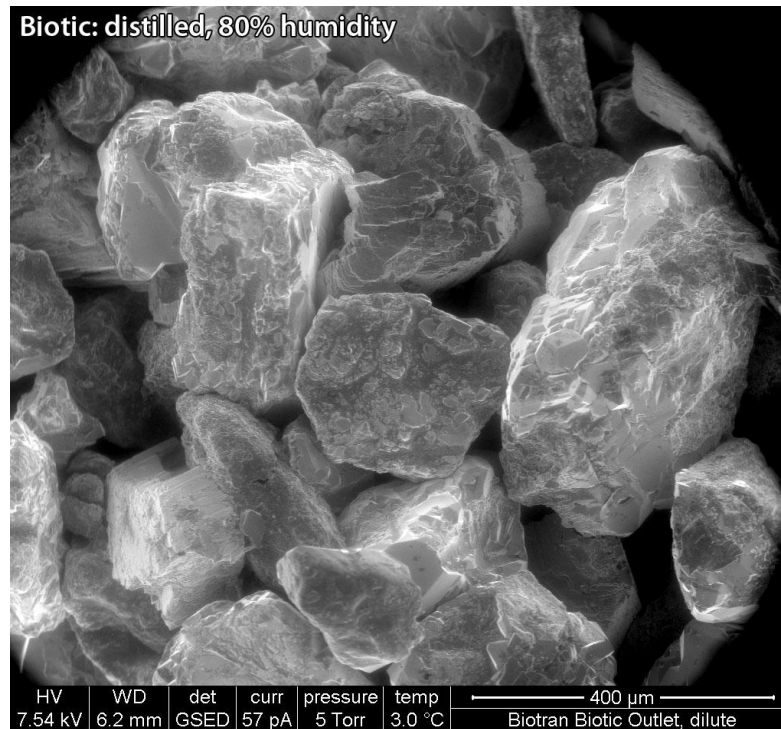


**Plate 32 SEI photomicrographs of biotic sample from outlet face, prepared with diluted brine, distilled water used as the ESEM wetting liquid. Within a couple of minutes of reducing the humidity to 80%, the sample dried almost completely**

#### *Possible biogenic deposits*

Drawing on similar work with *P. aeruginosa* by Turner and Rushton (2012) it has been possible to identify probable bacterially derived biofilm and rare bacterial forms, lining the pore walls of the experimental products through ESEM examination. Some of these textures were observed in both the biotic and the control post-experimental products. Clear differences were, identified between the two that suggest the biogenic materials are more abundant in the biotic experimental products.

Comparisons of the pore walls between samples from the control and biotic experiments typically show that the latter are coated by more abundant coating materials than the former (Plate 33). In the biotic products the coating materials include amorphous films and blotches that are more commonly associated with mineral fines (Plate 33, Plate 34 and Plate 35). This association with trapped mineral fines was noted as a common characteristic of biofilm by Turner and Rushton (2012).

Rare textures such as ridges of wetting phase residues bridging pore margins under partially dried conditions are indicative of the presence of underlying supportive structures. In some cases mineral fines are part of these supportive structures. In the example shown below (Plate 35), however, further drying revealed no such solid phase, suggesting that other material is responsible for supporting the texture; this is consistent with the presence of biofilm.

A variety of fibrous forms were noticed associated with amorphous deposits and/or residual wetting phase (Plate 36, Plate 37 and **Error! Reference source not found.**). Where brine was used as the wetting phase, many of these were identified as halite crystals developing during drying (Plate 36). Other examples are fibres of illitic clay (Plate 37) similar to those observed in the pre-test sample material (Plate 27). A patch of amorphous deposit with an associated fibrous portion that was demonstrated to be susceptible to beam damage (**Error! Reference source not**

**found.**) represents the strongest evidence observed for the presence of biofilm that has bridged porosity.

Probable bacterial forms were only recognised in one sample (biotic outlet) as oval forms 2-3  $\mu\text{m}$  in length associated with an area of probable biofilm (Plate 38).

No significant difference on the abundance or distribution of probable biogenic deposits was noted with respect to distance along the length of the test plugs in either the control or the biotic experimental products. One sample portion of the biotic outlet end displayed characteristics similar to the control experimental products, suggesting that it has a lower content of biogenic deposits. However, this suggests a patchy distribution rather than any systematic variation.

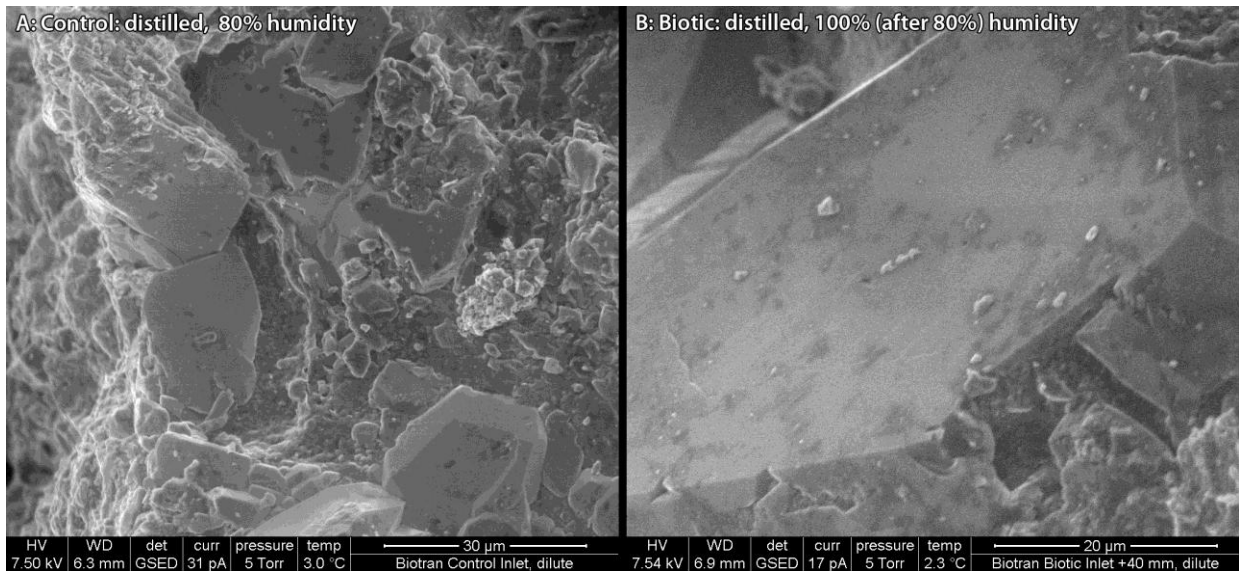


**Plate 33 SEI photomicrographs (under ESEM). A: Control sample from the inlet face, showing sparsely scattered pore-lining materials after drying. B: Biotic sample 40 mm in from the end face, showing widespread pore-lining material again in the dry state. In the latter, mineral fines are typically associated with a widespread amorphous film-like deposit**

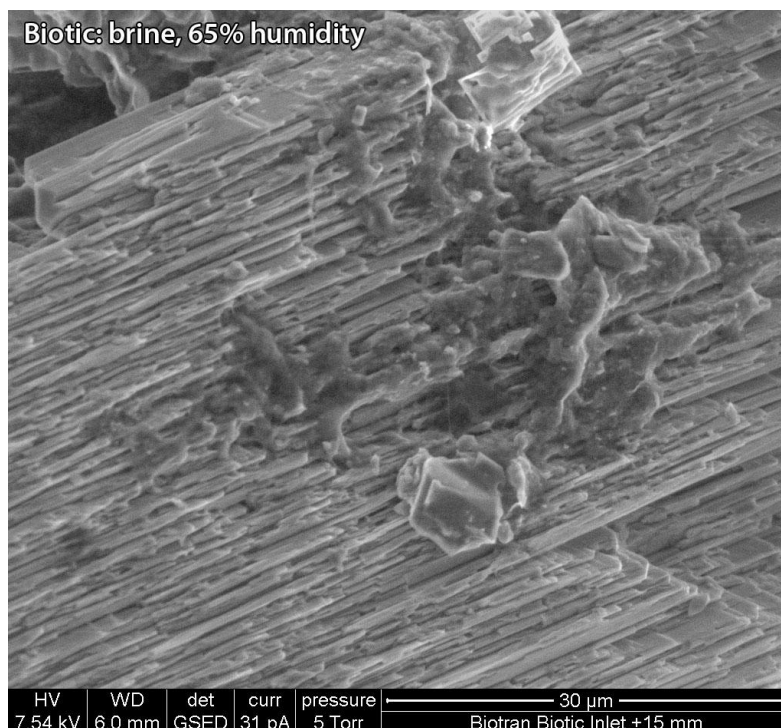


**Plate 34 SEI photomicrographs (under ESEM) of biotic sample, 15 mm in from the inlet face, in a dry condition. This shows an amorphous globular deposit draped across the stepped form of a K-feldspar overgrowth, with associated mineral fines**

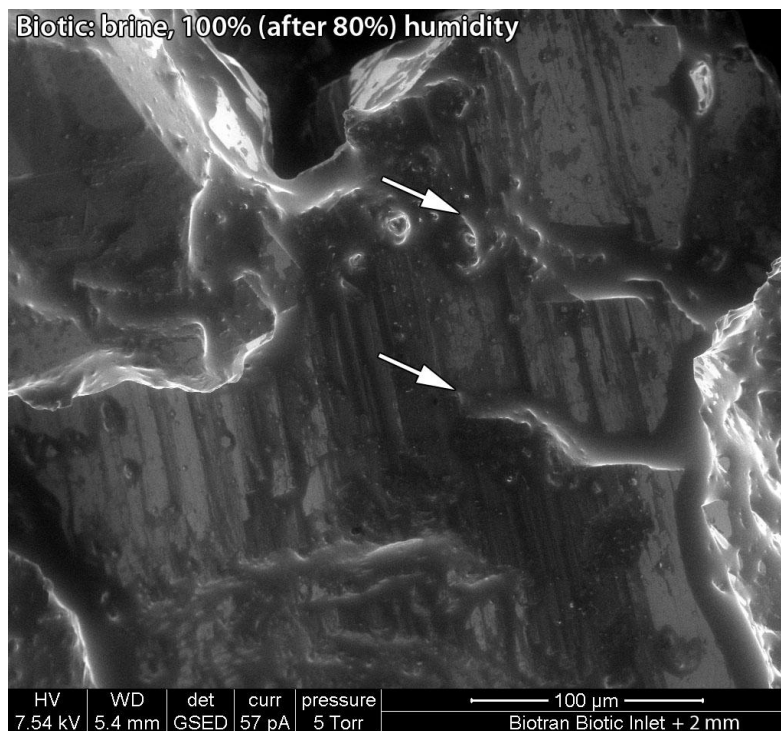


**Plate 35 SEI photomicrographs (under ESEM) of biotic sample, from 2 mm inside the inlet face, partially dry using brine as the ESEM wetting liquid. Brine remains as a thin film on pore walls, here largely defined by K-feldspar overgrowth, and as thicker pools in pore throats. Arrows show two ridges that bridge across the pore margin that are most likely supported by biofilm**

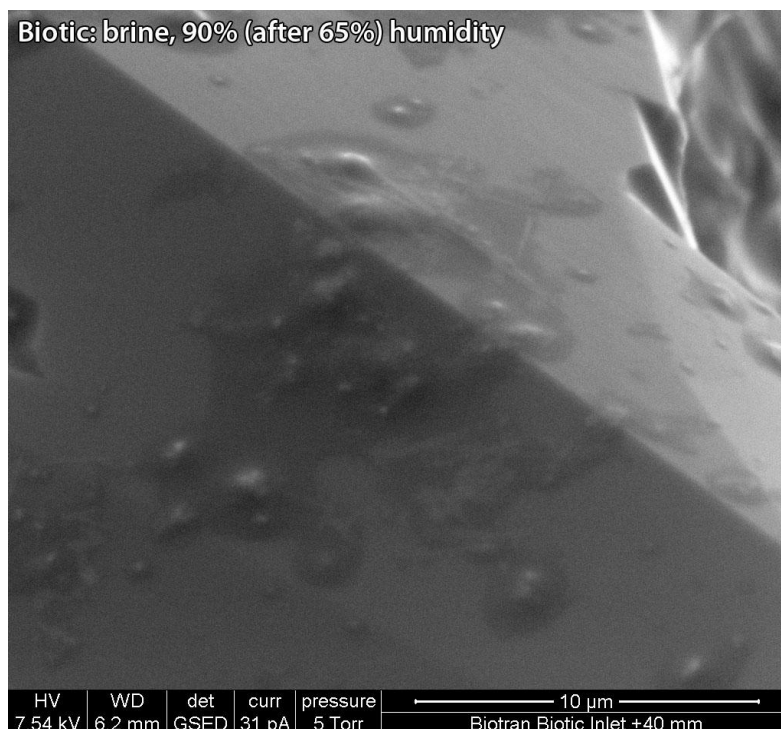


**Plate 36 SEI photomicrographs (under ESEM) of biotic sample, 40 mm from inlet face, slightly rehydrated after drying, brine used as the ESEM wetting liquid. Fibrous forms visible within this patch of amorphous pore-lining deposit are incipient halite crystals**

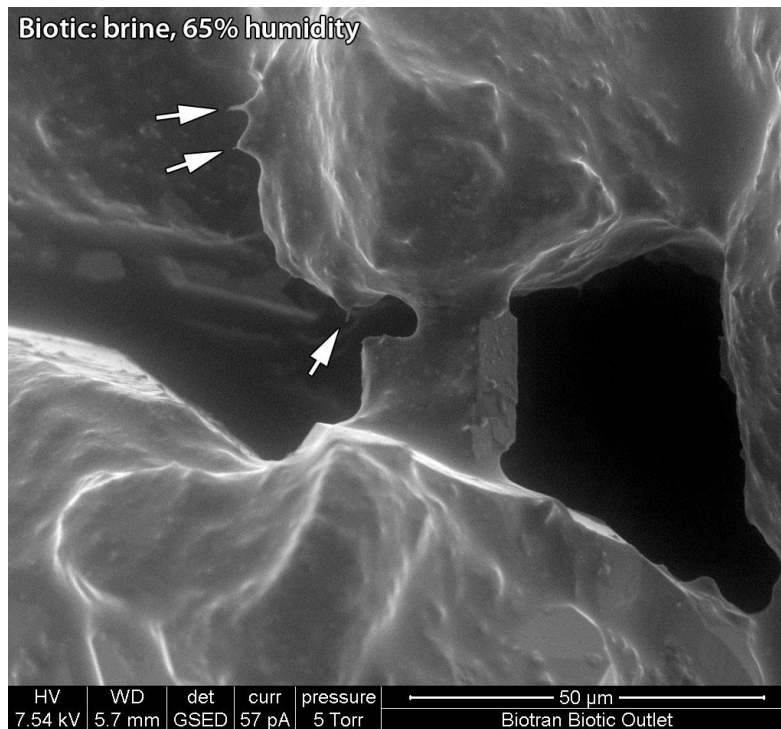


**Plate 37 SEI photomicrographs (under ESEM) of biotic sample from outlet face, still wet with a thin film of brine coating pore walls. Indicated fibrous forms emergent from the pore-lining film deposit are most likely illitic clay fibres**



**Plate 38 SEI photomicrographs (under ESEM) of biotic sample, at outlet face, distilled-water-wet sample at 100% humidity after a period at 80% humidity. The probable biofilm deposit, including the fibrous portion (unlabelled arrow), showing a fragmented form; this is taken as evidence of beam damage. There are also scattered probable bacterial forms**

### 4.6.3 Clay mineralogical analysis of the post-experimental material

Subsamples were taken near the column inlet (0-3cm) from the reacted biotic experiment and from the control column, followed by clay (<2 $\mu$ m) mineral separation and X-ray diffraction analysis. No obvious changes in clay mineralogy were observed suggesting that the introduction of microbes did not, or to only a very limited amount, effect the clay mineralogical composition.

## 5 Discussion

The flow-through column experiments showed that *P. aeruginosa* and indigenous microbes were able to survive in saline fluids in intact Sherwood Sandstone under pressurised conditions (4000 kPa) over a period of 235 days (5642 h) (from injection) with approximately  $10^5$  organisms ml<sup>-1</sup> present in the outlet fluids.

In the biotic experiment (Figure 2020), post inoculation pressure increased compared to the control experiment (Figure 218), with an average pressure of 488 kPa. Prior to bacterial injection, initial changes in core permeability are considered to be a result of movement of fines, blocking pore spaces and resulting in localised pressure increases, followed by breakthrough and establishment of new pathways resulting from a pressure increase by the use of a constant flow rate. However, rapid, saw-tooth like changes in pressure are evident over the post inoculation period although it should be noted that the regular 7 day (160 h) increases are due to pressure build up from fluid in collection syringes prior to sampling. These pressure profiles are symptomatic of a dynamic system exhibiting localised intermittent changes in permeability, and are likely to have been brought about by the partial clogging of pore spaces by fines and/or biofilm followed by flushing because of an increase in localised hydraulic pressure as noted in previous studies (Harrison *et al.*, 2011).

The control experiment (Figure 2121) showed an increase in pressure over the initial 60 hours, followed by a stabilisation phase, up to *ca.* 14 days (350 h) of 15 kPa – over one order of magnitude less than the biotic experiment. Thus the presence of any indigenous organisms (and associated biofilm) does not appear to have the same impact on permeability as *P. aeruginosa*. The overlay of results from both biotic and control experiments (Figure 222) illustrates these pressure differences to 187 days (4484 h) when dead *P. aeruginosa* and associated organic material was injected. At this point in the control experiment (Figure 2121), there was an increase in pressure to a maximum of ~1500 kPa at *ca.* 208 days (5000 h). The pressure returns to 15kPa by 250 days (6000 h). This is attributed to their presence (with associated biofilm and organic material) bringing about partial and transitory clogging of pore spaces which last over a period of *ca.* 63 days (1500 h).

A comparison of the injection pressure graphs from the biotic and control experiments (Figure 20 and 21) after 187 days (4484 h) shows the effect on pressure of dead *P. aeruginosa* and associated organic (but inactive) material being introduced into the control. The biotic core (Figure 2020) continues to show rapid pressure oscillations which suggests that the injected *P. aeruginosa* bacteria, probably with the indigenous microbes, have formed a self-sustaining community within the core. The rapid oscillations seen in the control core (Figure 2121) after the introduction of organic material are short lived and the pressure flux reduces over time to levels prior to injection of dead bacteria. This may be because the pressure within the control core increases rapidly when the dead bacteria and associated biofilm become trapped in the pore spaces, inducing locally high pressure zones. Subsequently, this build-up of pressure eventually causes break-through as a new network of fluid flow channels is established and organic material is flushed further into the core. This process of trapping and release repeats itself until a quasi-steady equilibrium state is reached, whereby further addition of organic material from the fluid from the pump causes localised pressure changes and the pressure returns to pre-injected conditions. Alternatively, there may have been some settlement of the organic material within

the syringe pump itself so that the fluid delivered to the BFA may have a lower viscosity and contain less organic material. Further work is therefore needed to clarify the observations in the control experiment.

Fluid chemistry results show that, overall, for most elements there is an increase followed by a steady decline in element concentrations throughout both experiments. This decline does not appear to impact on the physical and microbiological results. The release of Ca and Ba were most likely to have originated from the dissolution of calcite and dolomite which are present in the core. Evidence of dissolution of silica from the core was inconclusive.

A slow decrease in pH was observed in the biotic core from a starting value of 9.3 to 7.1 at the conclusion of the test. It was also noted that from 620 to 2090 hours from the start of the logging phase, Na and Cl concentrations (Figure 8) were unexpectedly low, whereas NPOC values were considerably higher (Figure 10). For Na, the overall average was  $5725 \text{ mg l}^{-1}$  (as  $\text{Na}^+$ ) compared to a mean value of  $2585 \text{ mg l}^{-1}$ , between *ca.* 24 and 87 days (620 and 2090 h) from the start of the logging phase. In a similar manner, Cl averaged  $9200 \text{ mg l}^{-1}$  but fell to  $325 \text{ mg l}^{-1}$  (as Cl) over the same period (Figure 8). Figure 9 shows the very strong relationship ( $R^2 = 0.9783$ ) between the Na and Cl measured concentrations in the fluid exiting the BFA during the biotic experiment, which is related to the original saline groundwater used. The NPOC content showed an opposing pattern, averaging  $330 \text{ mg l}^{-1}$  before 24 days (620 h) from the start of the logging phase, increasing to a fairly constant  $2400 \text{ mg l}^{-1}$ , between *ca.* 24 and 87 days (620 and 2090 h) from the start of the logging phase. However, unlike Na and Cl, which remained fairly constant thereafter, NPOC gradually decreased until the end of the experiment (Figure 10). Other elements did not show this behaviour. Possible explanations for these changes in Na, Cl and NPOC concentration between 24 and 87 days (620 and 2090 h) are:

- A leakage at the sample collection point; and/or,
- Errors in the sample preparation and analysis.

However, these changes do not seem to have an impact on the physical and microbiological results.

The pH of the control test was more constant, averaging 7.22 (Figure 11). Plots of concentration of analytes in the column outflows against time showed no obvious trends for the majority of analytes other than those previously mentioned. Again, there is a very strong relationship ( $R^2 = 0.8545$ ) between the Na and Cl measured concentrations in the fluid exiting the BFA during the control experiment, which is related to the original saline groundwater used (Figure 9).

It has been possible to identify probable bacterially derived biofilm and rare bacterial forms lining pore walls through petrographic ESEM examination of the experimental products. By combining the observations made during ESEM analyses of the test samples with those made of a sample of biofilm and with the theoretical considerations of the behaviour of liquids of different compositions under ESEM conditions, it is possible to observe the likely effects of the presence of biofilm as well as identify likely remnants of biofilm in dried or nearly dried sample material. Some of these textures were observed in both the biotic and the control post-experimental products. The biogenic materials are more abundant in the biotic experimental products. Possible associated bacterial forms provide scant evidence for the bacterial origins of the observed deposits in the biotic experimental products.

Additional evidence for the presence of more abundant biofilm in the post-experimental biotic test sample is in the systematically greater propensity for the biotic experimental products to retain pore-lining liquid, compared to the control experimental products. In the static conditions of the ESEM, the biofilm would seem to act as an agent that increases the retention of aqueous liquids on pore walls. Effectively, biofilm is increasing the attraction between pore surfaces and the liquid. This increased affinity will mean that a layer of an aqueous liquid will be immobilised or at least have its mobility significantly reduced. The presence of such a layer of surface-bound liquid would effectively constrict pores and pore throats. Assuming that this retention effect is

strong enough to also apply in dynamic conditions (*i.e.* with liquid flow), then this is a mechanism that would be expected to reduce the permeability of the rock additional to any physical constriction of pore throats resulting from the presence of bacteria and biofilm. A tendency for the biofilm to trap mobilised mineral fines noted both in this study and by Turner and Rushton (2012), presents another mechanism whereby pore structures can be constricted and fragmented, reducing the effective permeability of the host sediment.

Biofilm growth occurred in the biotic experiment and was observed at the end of the experimental period. The biofilm significantly covered the pore walls of the material. Probable biofilm formation was also observed in the control experiments, probably resulting from the presence of indigenous organisms, but is less abundant and displays a lesser propensity for aqueous liquid retention and fines entrapment than that observed in the biotic experimental products. No evidence of dissolution effects or alteration of the sandstone starting materials was observed in either the biotic or control experiments from the mineralogical observations.

## 6 Conclusions

In 2010-2011, the focus of the study was on the Sherwood Sandstone, a rock type with a generic application. In the UK, there are uncertainties regarding the host geology for the deep geological disposal facility (GDF) for low and intermediate level waste (L/ILW). Consequently, some UK microbiological research programmes target, for investigation, a “generic” rock type with a mineralogy that could be considered broadly similar to that of a potential host geology that might be expected in the UK, with an acid/intermediate character containing quartz, feldspars, muscovite/chlorite/illite and iron oxides. This study has targeted calcite-dolomite-cemented feldspathic sandstone from the Sherwood Sandstone Group for examination, and this report describes pilot studies investigating changes in far-field transport properties that are due to microbial activity within intact core material. The Sherwood Sandstone Group is the UK’s second most important aquifer formation (second only in size to the Chalk), thus representing a major water resource. It is also one of UK’s principal oil and gas reservoirs, and a target formation for natural gas storage. In addition it contains the largest deep saline aquifers that have potential for the geological storage of carbon dioxide, in the southern North Sea and Irish Sea areas offshore of the UK.

This study has shown that *P. aeruginosa* and indigenous microbes can survive and thrive in pressurised flow through column experiments which utilised Sherwood Sandstone material (from Lincolnshire, UK) over a period of 235 days (5642 h) (from injection). Numbers of organisms in the biotic experiment appear to stabilise at  $\sim 10^5 \text{ ml}^{-1}$  throughout the experiment.

Fluctuations in injection pressure within the cores were detected during the biotic and control column experiments over the experimental period. In the biotic experiment, post inoculation pressure increased with an average injection pressure of 488 kPa. In general, injection pressure stabilised at approximately 15 kPa in the control experiment – over one order of magnitude less than the biotic experiment – even though indigenous organisms were detected in the outflow fluid. This, combined with the observation that rapid saw-tooth like changes in pressure were only observed under biotic conditions, suggests that the indigenous organisms, on their own, do not affect the transport properties in the same way as the injected *P. aeruginosa*. The short but rapid saw-tooth like changes in pressure are only observed under biotic conditions. However, it should be noted that there is a regular 7 day (160 h) cycling of pressure build-up which is related to sampling protocol. As noted previously by Harrison *et al.*, (2011) small changes in the pressure profile of the control columns appear to be related to small changes in permeability and could be the result of partial blocking of pore spaces by fines and the subsequent flushing of material as new pathways were established.

Post experimental imaging of the post-experimental rock features showed *P. aeruginosa* derived biofilms significantly covering the pore walls of the sandstone host. However, there was no evidence of dissolution or alteration effects when compared to the starting materials.

Overall, fluid chemistry results show a steady decline in element concentrations throughout the experiments. There are changes in Na, Cl and NPOC concentrations in the biotic column experiments for period between 24 and 87 days (620 and 2090 h) although this appears to be as result of leakage or sampling errors. The release of Ca and Ba observed is most likely to have originated from the dissolution of calcite and dolomite which are present in the core. Evidence of dissolution of silica from the core was inconclusive. The source of Mo and W is likely to be the cutting tool used to prepare the core for the experiments. It is therefore recommended that more sensitive analyses of the original sandstone material to help identify the sources of subtle changes in fluid chemistry. This could be achieved by X-ray fluorescence (XRF) and/or total digestion with inductively coupled plasma (ICP) analyses. However, all fluid chemistry changes do not appear to have influenced the physical and microbial results.

These results suggest that, whilst microbial activity does not appear to impact on overall chemistry results, their effects on physical transport properties is profound in terms of fluid flow. This is shown by the quantitative changes in permeability, as demonstrated by increases of the monitored injection pressure in the biotic experiment. Additionally, whilst biofilms form on mineral surfaces which can be imaged, they do not alter the surfaces in any way. Taken together, this would suggest that the production of biofilms is the primary cause of changes in fluid flow which is also observed in studies in other rock types such as mudstones (Harrison *et al.*, 2009; 2011). Microbial activity is likely, therefore, to complicate the physical transport of contaminants in the geological environment. This is likely to be rock type and site/concept specific and the following examples could include:

- Radioactive waste – the effects of microbes on the transport of an alkaline fluid generated from a cementitious repository into the excavation damaged zone and into the host rock;
- Carbon capture and storage - the effects of microbes on the transport of CO<sub>2</sub> and any associated contaminants, such as as H<sub>2</sub>S, NO<sub>x</sub> and SO<sub>x</sub>, in saturated water in storage reservoirs.

## Appendix 1 X-ray diffraction traces

### X-RAY DIFFRACTION TRACES

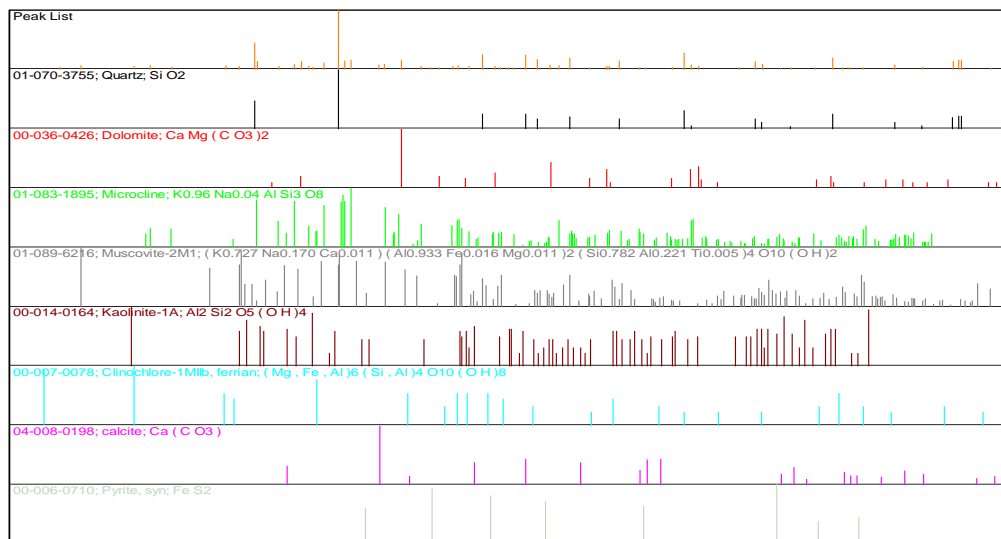
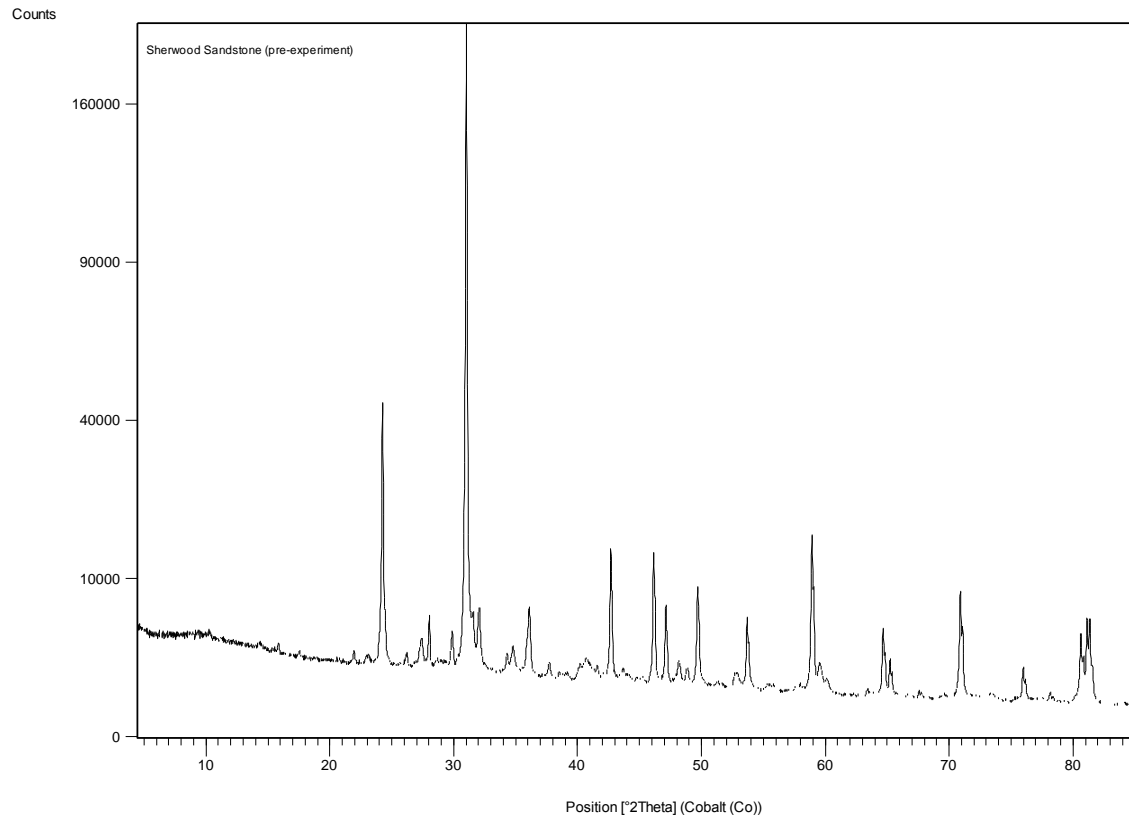
#### KEY

Vertical axis – Intensity (counts per second)

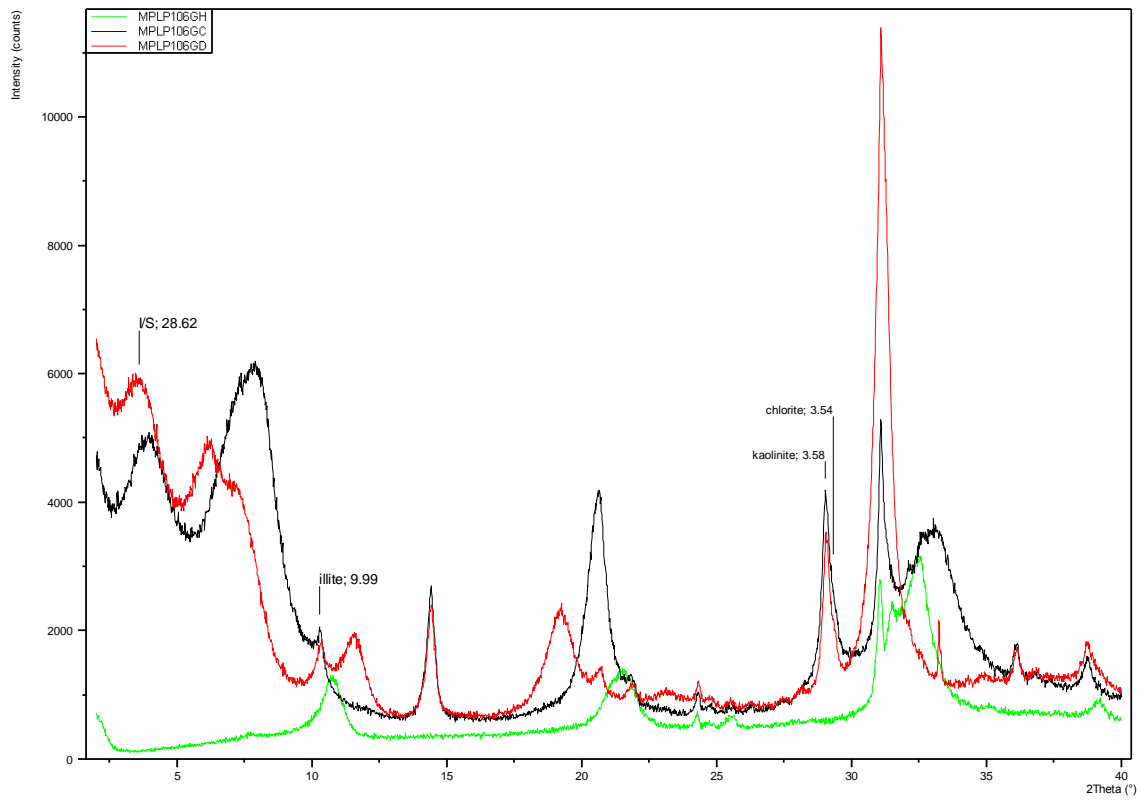
Horizontal axis -  $^{\circ}2\theta$  Co-K $\alpha$

For the whole-rock trace, the upper figure shows the sample diffraction trace. The lower figure shows stick pattern data for the extracted sample peaks (orange) and the identified mineral standard data. Vertical axis – intensity (counts), horizontal axis -  $^{\circ}2\theta$  Co-K $\alpha$

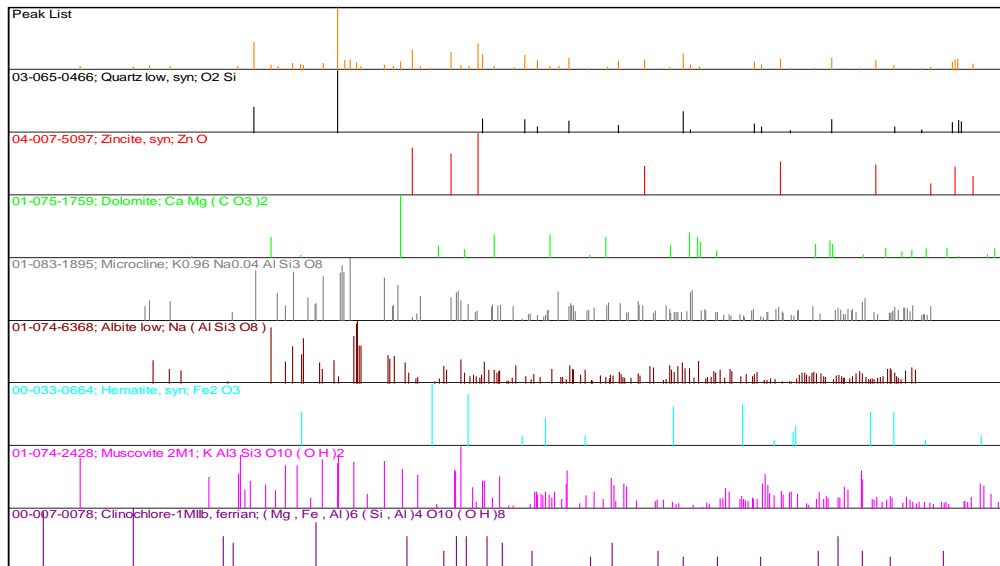
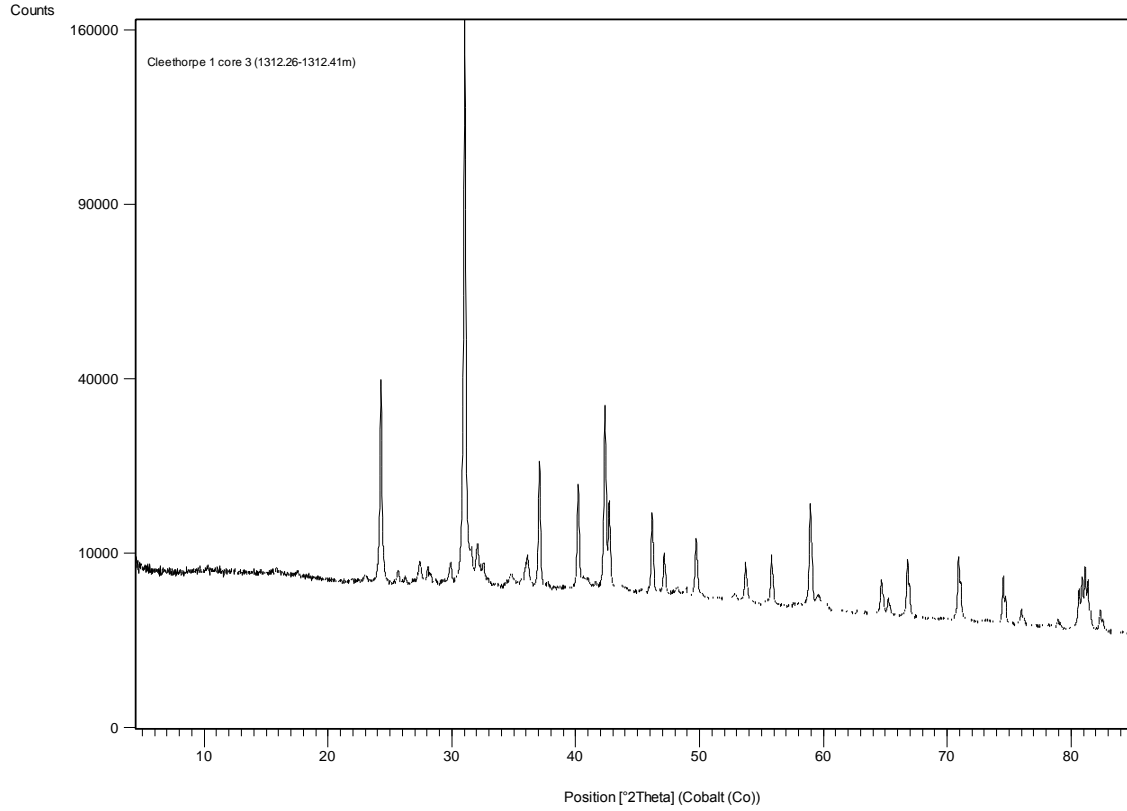
For the  $<2 \mu\text{m}$  trace, black trace (air-dry), red trace (glycol-solvated), green trace (heated  $550^{\circ}\text{C}/2 \text{ h}$ ). Only the most intense/diagnostic peak of each identified mineral is labelled with its corresponding  $d(\text{\AA})$  spacing. Vertical axis – intensity (counts), horizontal axis -  $^{\circ}2\theta$  Cu $\alpha$



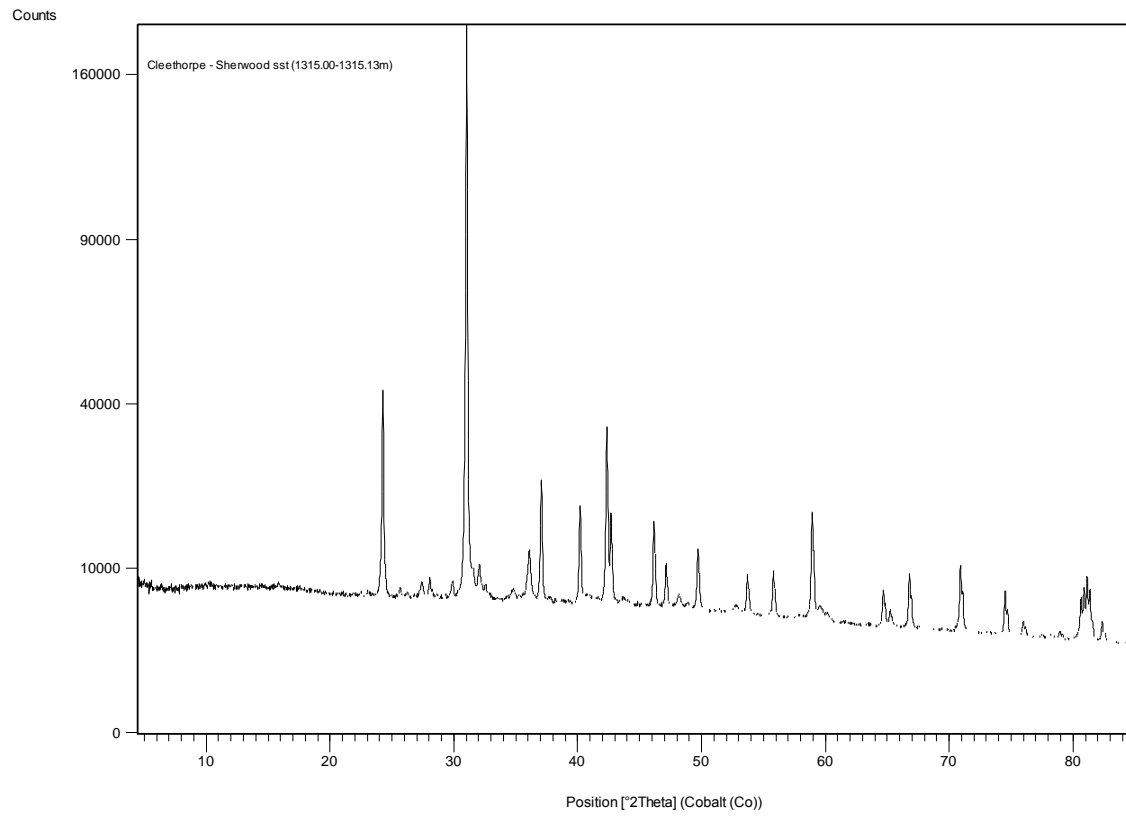
Gamston Borehole: Sherwood Sandstone Group – whole rock



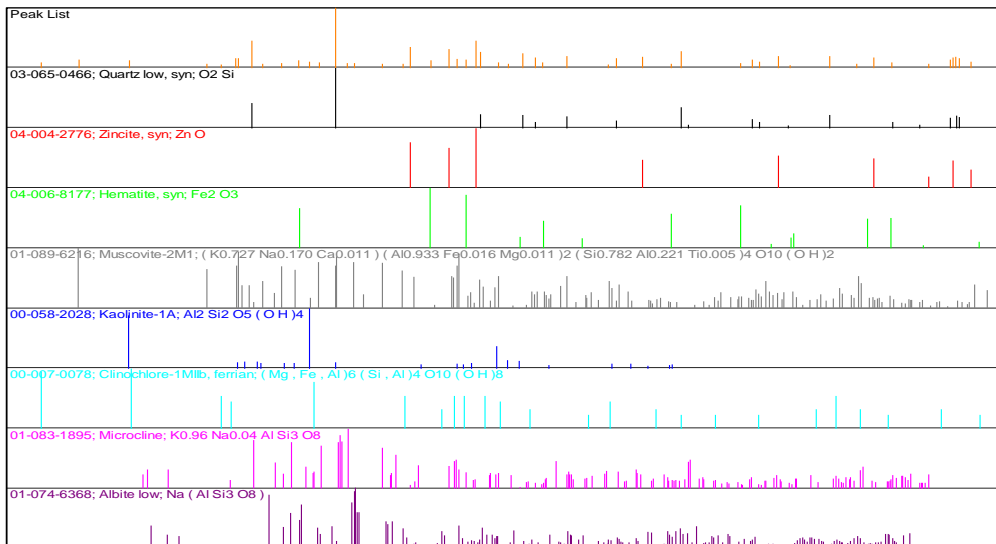
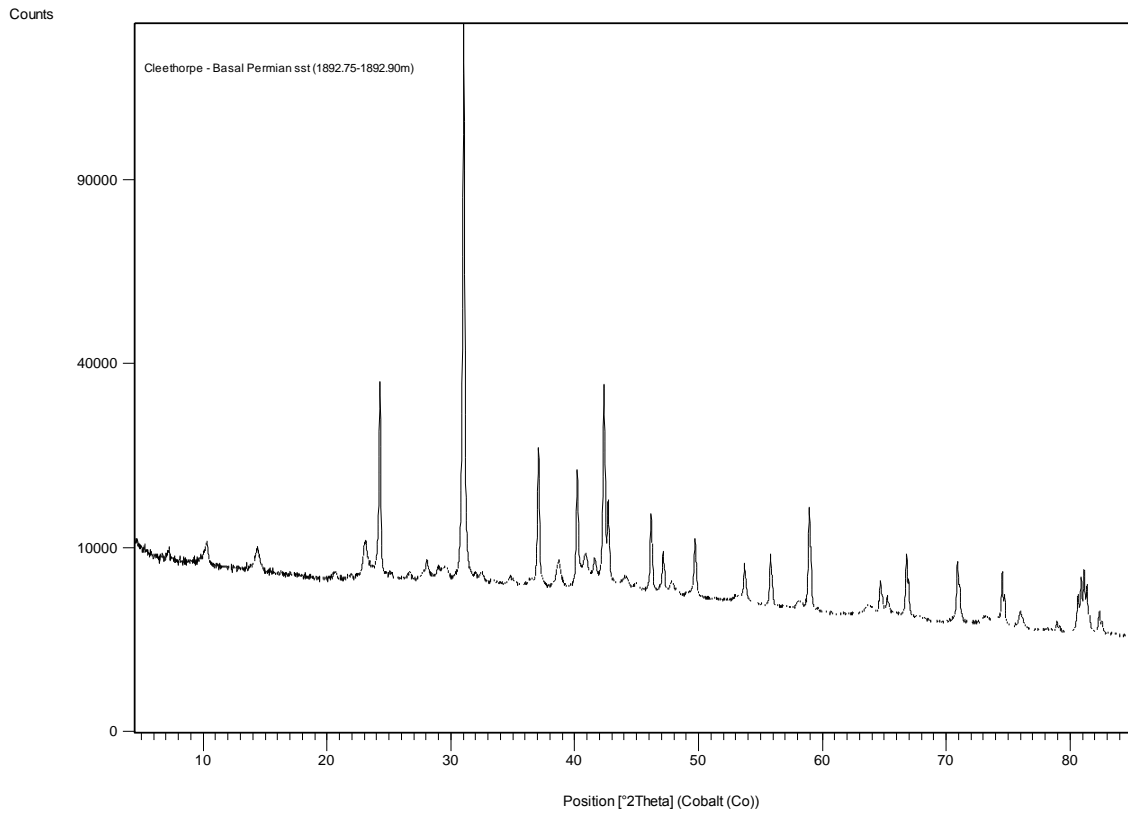
Gamston borehole: Sherwood Sandstone Group - <2 μm clay fraction



Cleethorpes No.1 borehole sample MPLP510: Sherwood Sandstone Group - whole rock



Cleethorpes No.1 borehole sample MPLP511: Sherwood Sandstone Group - whole rock



Cleethorpes No.1 borehole sample MPLP512: Basal Permian Sandstone - whole rock

# Appendix 2 Mercury injection core porosimetry data

**Cleethorpes No. Borehole: Sherwood Sandstone Group core sample MPLP 511**



MICROMERITICS INSTRUMENT CORPORATION

AutoPore IV 9500 V1.09      Serial: 1041      Port: 1/1      Page 1

Sample ID: CLE-1312  
 Operator: ASB  
 Submitter: ASB  
 File: C:\9500\DATA\BLANKS\CLE-1312.SMP

LP Analysis Time: 01/08/2011 10:02:21PM      Sample Weight: 4.9400 g  
 HP Analysis Time: 01/08/2011 11:06:31PM      Correction Type: Blank  
 Report Time: 01/08/2011 11:06:23PM      Show Neg. Int: No

**Summary Report**

**Penetrometer parameters**

Penetrometer:	0074 - (11) 5 Bulb, 1.836 Stem, Solid		
Pen. Constant:	27.820 $\mu\text{L/pF}$	Pen. Weight:	58.3830 g
Stem Volume:	1.8360 mL	Max. Head Pressure:	4.4500 psia
Pen. Volume:	7.3800 mL	Assembly Weight:	130.3000 g

**Hg Parameters**

Adv. Contact Angle:	130.000 degrees	Rec. Contact Angle:	130.000 degrees
Hg Surface Tension:	485.000 dynes/cm	Hg Density:	13.5335 g/mL

**User Parameters**

Param 1: 0.000      Param 2: 0.000      Param 3: 0.000

**Low Pressure:**

Evacuation Pressure: 50  $\mu\text{mHg}$   
 Evacuation Time: 5 mins  
 Mercury Filling Pressure: 0.51 psia  
 Equilibration Time: 10 secs

**High Pressure:**

Equilibration Time: 10 secs

Blank Correction Sample: C:\9500\DATA\BLANKS\BK11-074.SMP  
 Blank Correction ID: BK11-074

(From Pressure 0.10 to 60000.00 psia)

**Intrusion Data Summary**

Total Intrusion Volume = 0.1166 mL/g  
 Total Pore Area = 0.870  $\text{m}^2/\text{g}$   
 Median Pore Diameter (Volume) = 19369.0 nm  
 Median Pore Diameter (Area) = 17.3 nm  
 Average Pore Diameter (4V/A) = 535.9 nm  
 Bulk Density at 0.51 psia = 2.0321 g/mL  
 Apparent (skeletal) Density = 2.6628 g/mL  
 Porosity = 23.6872 %  
 Stem Volume Used = 31 %

**Pore Structure Summary**

Threshold Pressure: 7.89 psia (Calculated)  
 Characteristic length = 22936.6 nm  
 Conductivity formation factor = 0.052  
 Permeability constant = 0.00442  
 Permeability = 121.8364 mdarcy  
 BET Surface Area = 230.0000  $\text{m}^2/\text{g}$   
 Pore shape exponent = 1.00  
 Tortuosity factor = 2.144  
 Tortuosity = 5.6916  
 Percolation Fractal dimension = 2.983  
 Backbone Fractal dimension = 2.902

**Mayer Stowe Summary**

Interstitial porosity = 47.6300 %  
 Breakthrough pressure ratio = 3.3512

**Material Compressibility**

Linear Coefficient = N/A 1/psia  
 Quadratic Coefficient = N/A 1/psia<sup>2</sup>

**Cleethorpes No. Borehole: Sherwood Sandstone Group core sample MPLP 512**



**MICROMERITICS INSTRUMENT CORPORATION**

AutoPore IV 9500 V1.09                      Serial: 1041                      Port: 1/1                      Page 1

Sample ID: CLE-1315  
 Operator: ASB  
 Submitter: ASB  
 File: C:\9500\DATA\BLANKS\CLE-1315.SMP

LP Analysis Time: 01/08/2011 10:50:42PM                      Sample Weight: 6.8200 g  
 HP Analysis Time: 01/08/2011 12:07:32PM                      Correction Type: Blank  
 Report Time: 01/08/2011 12:07:32PM                      Show Neg. Int: No

**Summary Report**

**Penetrometer parameters**

Penetrometer: 0613 - (11) 5 Bulb, 1.836 Stem, Solid  
 Pen. Constant: 28.098  $\mu\text{L}/\rho\text{F}$                       Pen. Weight: 59.3840 g  
 Stem Volume: 1.8360 mL                      Max. Head Pressure: 4.4500 psia  
 Pen. Volume: 7.4626 mL                      Assembly Weight: 119.5300 g

**Hg Parameters**

Adv. Contact Angle: 130.000 degrees                      Rec. Contact Angle: 130.000 degrees  
 Hg Surface Tension: 485.000 dynes/cm                      Hg Density: 13.5335 g/mL

**User Parameters**

Param 1: 0.000                      Param 2: 0.000                      Param 3: 0.000

**Low Pressure:**

Evacuation Pressure: 50  $\mu\text{mHg}$   
 Evacuation Time: 5 mins  
 Mercury Filling Pressure: 0.52 psia  
 Equilibration Time: 10 secs

**High Pressure:**

Equilibration Time: 10 secs

Blank Correction Sample: C:\9500\DATA\BLANKS\BK11-613.SMP  
 Blank Correction ID: BK11-613

(From Pressure 0.10 to 60000.00 psia)

**Intrusion Data Summary**

Total Intrusion Volume = 0.1433 mL/g  
 Total Pore Area = 0.555  $\text{m}^2/\text{g}$   
 Median Pore Diameter (Volume) = 36167.4 nm  
 Median Pore Diameter (Area) = 23.7 nm  
 Average Pore Diameter (4V/A) = 1032.5 nm  
 Bulk Density at 0.52 psia = 1.9362 g/mL  
 Apparent (skeletal) Density = 2.6794 g/mL  
 Porosity = 27.7368 %  
 Stem Volume Used = 53 %

**Pore Structure Summary**

Threshold Pressure: 4.78 psia (Calculated)  
 Characteristic length = 37818.5 nm  
 Conductivity formation factor = 0.092  
 Permeability constant = 0.00442  
 Permeability = 584.1792 mdarcy  
 BET Surface Area = 230.0000  $\text{m}^2/\text{g}$   
 Pore shape exponent = 1.00  
 Tortuosity factor = 2.124  
 Tortuosity = 4.5258  
 Percolation Fractal dimension = 2.990  
 Backbone Fractal dimension = 2.962

**Mayer Stowe Summary**

Interstitial porosity = 47.6300 %  
 Breakthrough pressure ratio = 3.3512

**Material Compressibility**

Linear Coefficient = N/A 1/psia  
 Quadratic Coefficient = N/A 1/psia<sup>2</sup>

## Appendix 3 Fluid Chemistry Data (Control Core)

LIMS Code	Sample Code	Date/Time	Time from the start of the logging phase (hrs)	pH	Ca	Mg	Na	K	HCO <sub>3</sub> <sup>-</sup>	Cl <sup>-</sup>	SO <sub>4</sub> <sup>2-</sup>	NO <sub>3</sub> <sup>-</sup>	Cation Total	Anion Total	Balance	Br <sup>-</sup>	NO <sub>2</sub> <sup>-</sup>	HPO <sub>4</sub> <sup>2-</sup>	F <sup>-</sup>	NPOC
	CONTROL				mg l <sup>-1</sup>	mg l <sup>-1</sup>	mg l <sup>-1</sup>	mg l <sup>-1</sup>	meq l <sup>-1</sup>	meq l <sup>-1</sup>	%	mg l <sup>-1</sup>	mg l <sup>-1</sup>	mg l <sup>-1</sup>	mg l <sup>-1</sup>	mg l <sup>-1</sup>				
12629-0001	CB1	11/11/2010 09:05	139	7.74	45	11.2	6002	112	88.0	9469	98.9	56.2	267.1	270.1	-0.55	<4.00	<2.00	<20.0	<2.00	438
12629-0002	CB2	18/11/2010 14:05	312	7.12	34	7.1	5576	21.5	87.5	9565	37.0	427	245.4	277.9	-6.21	<4.00	<2.00	21	<2.00	489
12629-0003	CB3	25/11/2010 10:15	477	7.10	23	5.1	6176	10.4	65.0	9366	<10.0	<4.00	270.5	264.2	1.18	<4.00	<2.00	<20.0	<2.00	463
12629-0004	CB4	01/12/2010 10:00	620	6.73	20	4.5	6198	8.3	55.1	9563	22.0	26.3	271.2	270.7	0.10	<4.00	<2.00	<20.0	<2.00	491
12629-0005	CB5	08/12/2010 14:00	792	7.20	19	3.8	6316	7.0	54.7	9630	<10.0	8.49	276.2	271.8	0.80	<4.00	<2.00	<20.0	<2.00	414
12629-0006	CB6	14/12/2010 15:45	938	7.29	17	3.7	6289	6.1	54.4	9435	<10.0	7.95	274.9	266.3	1.59	<4.00	<2.00	<20.0	<2.00	404
12629-0007	CB7	21/12/2010 10:00	1100	7.41	16	4.0	6269	5.5	57.8	9463	<10.0	10.4	274.0	267.1	1.27	<4.00	<2.00	<20.0	<2.00	397
12629-0008	CB8	28/12/2010 10:25	1269	n/s	17	4.4	6256	4.8	n/s	n/s	n/s	n/s	273.5	n/s	n/s	n/s	n/s	n/s	n/s	
12629-0009	CB9	04/01/2011 10:30	1437	n/s	16	4.5	6280	4.3	n/s	n/s	n/s	n/s	274.5	n/s	n/s	n/s	n/s	n/s	n/s	
12629-0010	CB10	11/01/2011 10:00	1604	7.51	16	4.3	5802	3.6	60.0	9440	<10.0	<4.00	253.6	266.3	-2.44	<4.00	<2.00	<20.0	<2.00	410
12629-0011	CB11	18/01/2011 13:30	1776	7.72	16	4.4	5735	3.2	44.0	9390	89.6	26.2	250.7	267.2	-3.18	<4.00	<2.00	<20.0	<2.00	446
12629-0012	CB12	25/01/2011 13:30	1944	7.66	17	4.9	6123	3.1	63.4	9581	13.1	13.3	267.7	270.8	-0.57	<4.00	<2.00	<20.0	<2.00	442
12629-0013	CB13	31/01/2011 15:30	2090	7.56	19	4.8	6013	2.8	63.4	9594	<10.0	5.58	n/s	270.7	n/s	<4.00	<2.00	<20.0	<2.00	295
12744-0013	CB16	16/02/2011 14:00	2472	8.64	n/s	n/s	n/s	n/s	61.6	9442	<5.00	<2.00	234.6	266.4	-6.34	<2.00	<1.00	<10.0	<1.00	325
12744-0014	CB17	23/02/2011 11:30	2638	7.29	<14	4.3	5436	1.7	62.9	9415	5.74	<2.00	236.9	265.7	-5.74	<2.00	<1.00	<10.0	<1.00	337
12744-0015	CB18	02/03/2011 15:00	2809	7.09	<14	4.3	5249	1.7	72.4	9415	<5.00	<2.00	228.7	265.6	-7.46	<2.00	<1.00	<10.0	<1.00	309
12744-0016	CB21	22/03/2011 14:00	3288	7.25	15	6.0	5176	1.5	133.2	9192	<5.00	<2.00	226.4	259.6	-6.82	<2.00	<1.00	<10.0	5.92	199
12744-0017	CB22	29/03/2011 11:00	3453	7.13	<14	5.7	5198	1.1	123.5	9119	5.46	<2.00	226.6	257.7	-6.42	<2.00	<1.00	<10.0	6.42	209
12744-0018	CB24	14/04/2011 14:00	3840	7.98	<14	5.1	5585	1.1	100.3	9132	<5.00	<2.00	243.4	257.6	-2.84	<2.00	<1.00	<10.0	<1.00	207
12744-0019	CB27	05/05/2011 10:00	4340	7.20	<14	4.6	5440	1.0	97.2	9149	<5.00	<2.00	237.0	258.1	-4.25	<2.00	<1.00	<10.0	<1.00	197
12744-0020	CB28	11/05/2011 09:00	4483	7.22	<14	4.5	5387	1.2	95.0	9189	<5.00	<2.00	234.7	259.3	-4.97	3.62	<1.00	<10.0	<1.00	194
12744-0021	CB30	26/05/2011 10:00	4844	7.08	<14	4.4	5312	0.8	123.3	9173	12.4	39.5	231.5	259.7	-5.74	<2.00	<1.00	<10.0	<1.00	52.0
12744-0022	CB33	15/06/2011 10:00	5324	7.17	<14	4.6	5499	0.7	115.4	9034	<5.00	<2.00	239.6	254.8	-3.08	<2.00	<1.00	<10.0	<1.00	40.4
12744-0023	CB35	29/06/2011 10:00	5660	8.12	<14	4.5	5422	0.6	123.0	9206	7.93	<2.00	236.2	259.9	-4.76	<2.00	<1.00	<10.0	<1.00	45.7
12744-0024	CB36	05/07/2011 10:00	5811	5.61	47	38.6	2134	39.8	217.5	4197	6.35	3.54	102.2	118.8	-7.52	18.5	<1.00	<10.0	<1.00	818
12744-0025	CB final (pump)	05/07/2011 10:00	5811	7.19	<14	<0.1	5181	0.2	65.3	9306	<5.00	<2.00	225.6	262.5	-7.57	<2.00	<1.00	<10.0	<1.00	54.7

## Fluid Chemistry Data (Control Core) continued

LIMS Code	Sample Code	Total P	Total S	Si	SiO <sub>2</sub>	Ba	Sr	Mn	Total Fe	Reduced Fe	Oxidised Fe	Li	Be	B	Al	Ti	V	Cr	Co	Ni	Cu
		mg l <sup>-1</sup>	mg l <sup>-1</sup>	mg l <sup>-1</sup>	mg l <sup>-1</sup>	µg l <sup>-1</sup>															
12629-0001	CB1	<0.4	30	2.7	5.69	175	345	95.0	96	<100	96	72	<0.03	4057	37	0.8	<3	23.1	32.6	333	35
12629-0002	CB2	<0.4	<30	2.4	5.16	218	182	73.8	11	<100	11	22	<0.03	1797	36	0.9	<3	0.9	21.2	199	7
12629-0003	CB3	<0.4	<30	2.1	4.45	240	78.4	73.9	142	<100	142	12	<0.03	680	20	1.6	<3	1.2	5.67	216	3
12629-0004	CB4	<0.4	<30	2.1	4.41	267	50.2	103	285	<100	285	<12	<0.03	<550	8	1.1	<3	1.0	4.32	324	3
12629-0005	CB5	<0.4	<30	2.1	4.39	257	38.7	79.2	172	<100	172	<12	<0.03	<550	7	1.2	<3	0.3	4.63	287	<2
12629-0006	CB6	<0.4	<30	2.0	4.17	193	29.9	11.8	<4	<100	<4	<12	<0.03	<550	17	1.8	6	0.2	0.24	23	2
12629-0007	CB7	<0.4	<30	1.9	3.98	163	25.4	16.3	7	<100	7	<12	<0.03	<550	15	1.3	12	0.3	0.45	27	<2
12629-0008	CB8	<0.4	<30	1.8	3.87	149	23.0	10.6	20	<100	20	<12	<0.03	<550	15	0.4	13	2.0	0.18	12	<2
12629-0009	CB9	<0.4	<30	1.7	3.55	134	19.8	30.0	52	<100	52	<12	<0.03	<550	18	0.6	7	10.0	1.24	62	<2
12629-0010	CB10	<0.4	<30	1.9	4.02	113	16.6	7.4	4	<100	4	<12	<0.03	<550	18	0.5	8	0.2	0.10	6	<2
12629-0011	CB11	<0.4	<30	1.5	3.10	103	16.0	7.7	8	<100	8	<12	<0.03	<550	15	0.4	7	0.3	0.08	6	<2
12629-0012	CB12	<0.4	<30	1.5	3.29	105	15.9	8.2	<4	<100	<4	<12	<0.03	<550	11	0.4	6	0.2	0.19	7	<2
12629-0013	CB13	<0.4	<30	1.5	3.14	93.5	14.5	15.3	7	n/s	7	<12	<0.03	<550	14	0.6	4	3.7	0.58	13	<2
12744-0013	CB16	<0.2	<50	<4.5	<10	69.0	<16	23	<14	574	n/s	<20	<0.5	<650	<12	<2	<7	0.8	1.62	59	12
12744-0014	CB17	<0.2	<50	<4.5	<10	56.0	<16	8	<14	59	n/s	<20	<0.5	<650	22	<2	<7	0.7	0.15	11	<3
12744-0015	CB18	<0.2	<50	<4.5	<10	59.0	<16	8	<14	47	n/s	<20	<0.5	<650	21	<2	<7	1.0	0.35	11	<3
12744-0016	CB21	<0.2	<50	<4.5	<10	197	16	16	<14	<50	<14	<20	<0.5	<650	27	<2	<7	0.6	1.21	25	3
12744-0017	CB22	<0.2	<50	<4.5	<10	194	18	17	<14	52	n/s	<20	<0.5	<650	16	<2	<7	<0.5	2.01	27	4
12744-0018	CB24	<0.2	<50	<4.5	<10	50.0	<16	30	<14	57	n/s	<20	<0.5	<650	<12	<2	<7	1.3	1.77	69	<3
12744-0019	CB27	<0.2	<50	<4.5	<10	33.0	<16	9	<14	<50	<14	<20	<0.5	<650	34	<2	<7	<0.5	0.39	8	<3
12744-0020	CB28	<0.2	<50	<4.5	<10	35.0	<16	<7	64	<50	64	<20	<0.5	<650	41	<2	<7	12.2	0.51	7	6
12744-0021	CB30	<0.2	<50	<4.5	<10	29.0	<16	7	<14	<50	<14	<20	<0.5	<650	<12	<2	<7	<0.5	0.30	12	<3
12744-0022	CB33	<0.2	<50	<4.5	<10	24.0	<16	23	<14	66	n/s	<20	<0.5	<650	55	<2	<7	4.5	0.43	17	<3
12744-0023	CB35	<0.2	<50	<4.5	<10	21.0	<16	23	45	56	n/s	<20	<0.5	<650	<12	<2	<7	3.5	0.75	19	<3
12744-0024	CB36	<0.2	<50	<4.5	<10	127	73	5001	29308	29723	n/s	<20	<0.5	31761	<12	<2	<7	0.7	63.5	286	<3
12744-0025	CB final from pump	<0.2	<50	<4.5	<10	<2	<16	52	2112	2202	n/s	<20	<0.5	<650	<12	<2	<7	11.3	2.96	254	5

## Fluid Chemistry Data (Control Core) continued

LIMS Code	Sample Code	Zn	Ga	As	Se	Rb	Y	Zr	Mo	Cd	Cs	La	Ce	Pr	Nd	Hf	Ta	W	Tl	Pb	Th	U
		µg l <sup>-1</sup>																				
12629-0001	CB1	83	<1	374	7	68.2	<0.2	<0.5	973	0.9	5.17	0.01	<0.04	<0.05	<1	<0.3	<0.1	87.9	0.7	1.6	<0.6	1.98
12629-0002	CB2	63	<1	8	18	25.4	<0.2	<0.5	913	0.5	2.77	<0.01	<0.04	<0.05	<1	<0.3	<0.1	52.3	0.4	0.5	<0.6	0.34
12629-0003	CB3	100	<1	6	20	16.1	<0.2	<0.5	1198	0.6	1.96	<0.01	<0.04	<0.05	<1	<0.3	<0.1	34.2	0.2	0.4	<0.6	0.01
12629-0004	CB4	78	<1	4	21	13.5	<0.2	<0.5	1323	0.6	1.73	<0.01	<0.04	<0.05	<1	<0.3	<0.1	24.3	0.2	<0.4	<0.6	0.01
12629-0005	CB5	76	<1	4	19	11.6	<0.2	<0.5	1045	0.6	1.52	0.01	<0.04	<0.05	<1	<0.3	<0.1	21.4	0.1	<0.4	<0.6	<0.01
12629-0006	CB6	106	<1	9	17	9.5	<0.2	<0.5	863	0.4	1.28	<0.01	<0.04	<0.05	<1	<0.3	<0.1	18.8	0.1	<0.4	<0.6	<0.01
12629-0007	CB7	98	<1	11	17	8.0	<0.2	<0.5	633	0.3	1.07	<0.01	<0.04	<0.05	<1	<0.3	<0.1	13.3	<0.1	<0.4	<0.6	<0.01
12629-0008	CB8	71	<1	12	14	6.9	<0.2	<0.5	473	0.3	0.91	<0.01	<0.04	<0.05	<1	<0.3	<0.1	11.7	<0.1	<0.4	<0.6	<0.01
12629-0009	CB9	69	<1	9	10	6.1	<0.2	<0.5	369	0.2	0.80	<0.01	<0.04	<0.05	<1	<0.3	<0.1	8.6	<0.1	<0.4	<0.6	0.02
12629-0010	CB10	50	<1	8	8	5.1	<0.2	<0.5	269	0.3	0.84	0.02	<0.04	<0.05	<1	<0.3	<0.1	6.8	<0.1	<0.4	<0.6	<0.01
12629-0011	CB11	55	<1	8	6	4.7	<0.2	<0.5	197	0.3	0.68	<0.01	<0.04	<0.05	<1	<0.3	<0.1	6.0	<0.1	<0.4	<0.6	<0.01
12629-0012	CB12	53	<1	8	5	4.9	<0.2	<0.5	176	0.2	0.68	<0.01	<0.04	<0.05	<1	<0.3	<0.1	6.2	<0.1	<0.4	<0.6	<0.01
12629-0013	CB13	52	<1	19	4	4.7	<0.2	<0.5	143	0.2	0.64	0.02	<0.04	<0.05	<1	<0.3	<0.1	5.4	<0.1	<0.4	<0.6	0.01
12744-0013	CB16	37	<1	4	<3	4	<0.2	<0.7	151	<0.4	<0.9	<0.05	<0.2	<0.06	<0.4	<0.2	<0.9	3.8	<0.4	<0.7	<0.1	<0.05
12744-0014	CB17	<35	<1	6	<3	4	<0.2	<0.7	160	<0.4	<0.9	<0.05	<0.2	<0.06	<0.4	<0.2	<0.9	4.0	<0.4	<0.7	<0.1	<0.05
12744-0015	CB18	<35	<1	4	<3	2	<0.2	<0.7	118	<0.4	<0.9	<0.05	<0.2	<0.06	<0.4	<0.2	<0.9	3.6	<0.4	<0.7	<0.1	<0.05
12744-0016	CB21	57	<1	5	<3	3	<0.2	<0.7	121	<0.4	<0.9	<0.05	<0.2	<0.06	<0.4	<0.2	<0.9	2.4	0.4	<0.7	<0.1	0.27
12744-0017	CB22	37	<1	7	<3	3	<0.2	<0.7	103	<0.4	0.9	<0.05	<0.2	<0.06	<0.4	<0.2	<0.9	2.4	<0.4	0.8	<0.1	0.25
12744-0018	CB24	<35	<1	<2	<3	4	<0.2	<0.7	92	<0.4	<0.9	<0.05	<0.2	<0.06	<0.4	<0.2	<0.9	2.4	<0.4	<0.7	<0.1	0.13
12744-0019	CB27	<35	<1	4	<3	3	<0.2	<0.7	58	<0.4	<0.9	<0.05	<0.2	<0.06	<0.4	<0.2	<0.9	2.0	<0.4	<0.7	<0.1	0.09
12744-0020	CB28	<35	<1	3	<3	3	<0.2	0.9	56	<0.4	1.0	0.14	0.2	0.09	<0.4	<0.2	<0.9	2.2	<0.4	4.5	<0.1	0.59
12744-0021	CB30	<35	<1	5	<3	4	<0.2	<0.7	60	<0.4	<0.9	<0.05	<0.2	<0.06	<0.4	<0.2	<0.9	1.8	<0.4	<0.7	<0.1	0.13
12744-0022	CB33	<35	<1	6	<3	4	<0.2	<0.7	63	<0.4	<0.9	0.13	<0.2	<0.06	<0.4	<0.2	<0.9	1.5	<0.4	<0.7	<0.1	0.18
12744-0023	CB35	<35	<1	7	<3	4	<0.2	<0.7	62	<0.4	<0.9	<0.05	<0.2	<0.06	<0.4	<0.2	<0.9	1.5	<0.4	<0.7	<0.1	0.17
12744-0024	CB36	42	<1	<2	<3	9	<0.2	<0.7		<0.4	<0.9	<0.05	<0.2	<0.06	<0.4	<0.2	<0.9	<0.3	<0.4	<0.7	<0.1	<0.05
12744-0025	CB final from pump	<35	<1	5	<3	<1	<0.2	<0.7	26	<0.4	<0.9	<0.05	<0.2	<0.06	<0.4	<0.2	<0.9	<0.3	<0.4	<0.7	<0.1	<0.05

## Appendix 4 Fluid Chemistry Data (Biotic Core)

LIMS Code	Sample Code	Date/Time	Time from the start of the logging phase (hrs)	pH	Ca	Mg	Na	K	HCO <sub>3</sub> <sup>-</sup>	Cl <sup>-</sup>	SO <sub>4</sub> <sup>2-</sup>	NO <sub>3</sub> <sup>-</sup>	Cation Total	Anion Total	Balance	Br <sup>-</sup>	NO <sub>2</sub> <sup>-</sup>	HPO <sub>4</sub> <sup>2-</sup>	F <sup>-</sup>	NPOC
	BIOTIC				mg l <sup>-1</sup>	mg l <sup>-1</sup>	mg l <sup>-1</sup>	mg l <sup>-1</sup>	meq l <sup>-1</sup>	meq l <sup>-1</sup>	%	mg l <sup>-1</sup>	mg l <sup>-1</sup>	mg l <sup>-1</sup>	mg l <sup>-1</sup>	mg l <sup>-1</sup>				
12629-0014	CA1	08/10/2010 15:10		8.64	n/s	n/s	n/s	n/s	159	572	95	33.0	n/s	21.2	n/s	<4.00	<2.00	<20.0	<2.00	30.9
12629-0015	CA2	12/10/2010 14:10		9.34	n/s	n/s	n/s	n/s	153	19.9	<10	8.0	n/s	3.20	n/s	<4.00	<2.00	<20.0	<2.00	
12629-0016	CA3	18/10/2010 08:40		7.78	n/s	n/s	n/s	n/s	72.3	7089	<10	19.4	n/s	200.3	n/s	<4.00	<2.00	<20.0	<2.00	329
12629-0017	CA4	25/10/2010 10:00		7.87	n/s	n/s	n/s	n/s	86.4	9397	<10	11.3	n/s	265.6	n/s	<4.00	<2.00	<20.0	6.71	370
12629-0018	CA5	01/11/2010 10:15		7.82	22	5.02	5993	11.2	86.0	9272	<10	5.5	262.5	261.7	0.16	<4.00	<2.00	<20.0	<2.00	415
12629-0019	CA6	11/11/2010 09:05	140	7.73	23	4.84	6049	5.8	78.0	9223	22.4	47.7	264.8	261.4	0.65	<4.00	<2.00	<20.0	<2.00	423
12629-0020	CA7	18/11/2010 14:05	313	7.52	28	8.19	5971	5.6	115	9440	<10	7.1	262.0	267.0	-0.95	<4.00	<2.00	21	2.24	389
12629-0021	CA8	25/11/2010 10:15	477	8.19	31	10.1	5072	5.3	n/s	n/s	n/s	n/s	n/s	n/s	n/s	n/s	n/s	n/s	n/s	n/s
12629-0022	CA9	01/12/2010 10:00	620	8.18	26	8.37	2668	3.2	<5	327	<10	9.5	118.1	9.39	85.28	<5.00	<2.50	<25.0	<2.50	2403
12629-0023	CA10	08/12/2010 14:00	792	8.13	33	11.4	2642	3.1	<15	327	<10	9.3	117.6	9.37	85.24	<4.00	<2.00	<20.0	<2.00	2399
12629-0024	CA11	14/12/2010 15:45	938	8.19	29	10.0	2646	2.9	<15	327	<10	4.4	n/s	9.30	n/s	<4.00	<2.00	<20.0	<2.00	2412
12629-0025	CA12	28/12/2010 10:25	1269	n/s	28	11.0	2618	2.4	n/s	n/s	n/s	n/s	116.3	n/s	n/s	n/s	n/s	n/s	n/s	n/s
12629-0026	CA13	04/01/2011 10:30	1437	n/s	25	10.9	2646	2.2	n/s	n/s	n/s	n/s	117.3	n/s	n/s	n/s	n/s	n/s	n/s	n/s
12629-0027	CA14	11/01/2011 10:00	1604	7.99	23	9.97	2451	1.9	<5	331	<10	4.5	108.6	9.41	84.06	<4.00	<2.00	<20.0	<2.00	2375
12629-0028	CA15	18/01/2011 13:30	1776	7.91	21	9.85	2424	1.6	<5	335	<10	8.0	107.3	9.57	83.63	<4.00	<2.00	<20.0	<2.00	2369
12629-0029	CA16	25/01/2011 13:30	1944	8.01	22	10.5	2589	1.6	<15	325	<10	<4	n/s	9.18	n/s	<4.00	<2.00	<20.0	<2.00	2404
12629-0030	CA17	31/01/2011 15:30	2090	8.19	22	10.6	2583	1.6	<15	326	<10	8.0	n/s	9.34	n/s	<4.00	<2.00	<20.0	<2.00	2346
12629-0031	CA18	03/02/2011 11:20	2158	7.65	42	19.7	5910	2.5	<5	8158	<10	<4	n/s	230.1	n/s	<4.00	<2.00	<20.0	<2.00	628
12629-0032	CA19	10/02/2011 11:40	2326	7.94	19	5.37	6229	2.4	64.9	9864	<10	<4	272.4	278.3	-1.06	<4.00	<2.00	<20.0	<2.00	328
12744-0001	CA20	16/02/2011 14:00	2472	7.42	17	9.6	5941	1.7	<10	9587	5.2	3.4	260.1	272.1	-2.26	<2.00	<1.00	nd	28.8	151
12744-0002	CA21	23/02/2011 11:30	2638	7.49	17	8.9	5843	1.7	340	9625	<5	2.4	255.8	272.9	-3.23	<2.00	<1.00	<10.0	25.4	165
12744-0003	CA22	02/03/2011 15:00	2809	7.32	<14	7.9	5702	1.6	317	9543	<5	2.2	248.7	270.4	-4.18	<2.00	<1.00	<10.0	22.6	178
12744-0004	CA25	22/03/2011 14:00	3288	7.17	<14	5.8	5326	1.7	168	9179	<5	2.3	232.2	259.7	-5.60	<2.00	<1.00	<10.0	14.6	170
12744-0005	CA28	14/04/2011 14:00	3840	8.01	<14	6.2	5734	1.6	164	9039	<5	<2	250.0	255.5	-1.10	<2.00	<1.00	<10.0	10.6	237
12744-0006	CA31	05/05/2011 10:00	4340	7.10	<14	5.8	5399	1.5	164	8854	<5	3.5	235.4	250.4	-3.10	<2.00	<1.00	<10.0	11.3	215
12744-0007	CA32	11/05/2011 09:00	4483	7.29	<14	6.8	5685	2.0	182	9128	<5	9.2	247.9	258.4	-2.07	<2.00	<1.00	<10.0	13.6	206
12744-0008	CA34	26/05/2011 10:00	4844	7.14	<14	3.9	5575	1.4	121	9408	312	4.7	242.9	272.5	-5.75	<2.00	<1.00	<10.0	9.77	58.5
12744-0009	CA37	15/06/2011 10:00	5324	7.07	<14	4.6	5790	1.5	131	9216	6.4	<2	252.3	260.7	-1.64	<2.00	<1.00	<10.0	10.7	62.2
12744-0010	CA38	22/06/2011 09:15	5492	7.08	<14	4.8	5920	1.4	120	9302	5.8	<2	258.0	263.1	-0.99	<2.00	<1.00	<10.0	11.5	61.2
12744-0011	CA40	29/06/2011 10:00	5811	7.86	<14	4.4	5420	1.4	122	9362	<5	<2	236.2	264.7	-5.70	<2.00	<1.00	<10.0	12.1	68.0
12744-0012	CA final (pump)	29/06/2011 10:00	5811	7.11	<14	<0.1	5498	0.3	81.2	9395	<5	3.5	239.2	265.6	-5.24	<2.00	<1.00	<10.0	10.7	61.3

## Fluid Chemistry Data (Biotic Core) continued

LIMS Code	Sample Code	Total P	Total S	Si	SiO <sub>2</sub>	Ba	Sr	Mn	Total Fe	Reduced Fe	Oxidised Fe	Li	Be	B	Al	Ti	V	Cr	Co	Ni	Cu	
		mg l <sup>-1</sup>	mg l <sup>-1</sup>	mg l <sup>-1</sup>	mg l <sup>-1</sup>	µg l <sup>-1</sup>																
12629-0014	CA1	n/s	1179	n/s	n/s																	
12629-0015	CA2	n/s	336.3	n/s	n/s																	
12629-0016	CA3	n/s	<100	n/s	n/s																	
12629-0017	CA4	n/s	<100	n/s	n/s																	
12629-0018	CA5	<0.4	<30	2.5	5.4	212	44.1	13.9	16	<100	16	<12	<0.03	<550	31	0.5	7	8.4	3.38	28	5	
12629-0019	CA6	<0.4	<30	1.9	4.0	193	28.9	30.9	14	<100	14	<12	<0.03	<550	16	0.4	<3	4.1	5.81	62	3	
12629-0020	CA7	<0.4	<30	2.4	5.0	307	35.9	87.1	<4	<100	<4	<12	<0.03	<550	107	<0.3	<3	1.6	5.29	60	4	
12629-0021	CA8	<0.4	<30	3.5	7.6	352	43.0	472	<4	n/s	<4	<12	<0.03	<550	7	0.5	<3	4.2	97.0	327	3	
12629-0022	CA9	<0.4	<30	3.1	6.7	167	27.3	152	16	<100	16	<12	<0.03	<550	10	0.3	<3	4.1	79.4	112	3	
12629-0023	CA10	<0.4	<30	2.8	5.9	179	36.7	156	<4	<100	<4	<12	<0.03	<550	13	<0.3	<3	4.8	86.2	95	5	
12629-0024	CA11	<0.4	<30	2.2	4.6	149	26.5	98.3	<4	n/s	<4	<12	<0.03	<550	17	0.6	<3	2.1	66.1	58	7	
12629-0025	CA12	<0.4	<30	1.6	3.4	124	16.4	95.4	<4	<100	<4	<12	<0.03	<550	12	<0.3	<3	1.6	59.2	47	4	
12629-0026	CA13	<0.4	<30	1.4	3.0	109	12.7	113	5	<100	5	<12	<0.03	<550	23	<0.3	<3	5.7	68.9	66	8	
12629-0027	CA14	<0.4	<30	1.4	2.9	91.7	9.2	154	<4	<100	<4	<12	<0.03	<550	15	<0.3	<3	4.2	71.0	50	6	
12629-0028	CA15	<0.4	<30	1.3	2.8	75.0	7.7	228	<4	<100	<4	<12	<0.03	<550	14	0.3	<3	2.5	70.1	48	6	
12629-0029	CA16	<0.4	<30	1.2	2.6	64.6	7.3	325	<4	n/s	<4	<12	<0.03	<550	9	1.5	<3	2.5	67.2	48	7	
12629-0030	CA17	<0.4	<30	1.2	2.6	56.5	7.0	372	6	n/s	6	<12	<0.03	<550	26	<0.3	<3	3.6	65.3	48	8	
12629-0031	CA18	<0.4	<30	1.1	2.4	116	16.7	587	<4	n/s	<4	<12	<0.03	<550	7	0.4	<3	49.7	66.2	64	20	
12629-0032	CA19	<0.4	<30	1.5	3.1	92.7	15.3	13.5	18	<100	18	<12	<0.03	<550	19	0.6	4	0.4	0.29	7	<2	
12744-0001	CA20	<0.2	<50	<4.5	<10	61.0	<16	315	<14	<50	<14	<20	<0.5	<650	33	<2	<7	3.7	26.7	36	19	
12744-0002	CA21	<0.2	<50	<4.5	<10	61.0	<16	311	<14	<50	<14	<20	<0.5	<650	15	<2	<7	8.2	25.2	35	11	
12744-0003	CA22	<0.2	<50	<4.5	<10	39.0	<16	268	<14	<50	<14	<20	<0.5	<650	15	<2	<7	11.5	19.2	32	12	
12744-0004	CA25	<0.2	<50	<4.5	<10	138	<16	145	<14	<50	<14	<20	<0.5	<650	19	<2	<7	1.6	7.65	17	5	
12744-0005	CA28	<0.2	<50	<4.5	<10	23.0	<16	138	<14	<50	<14	<20	<0.5	<650	<12	<2	<7	2.8	6.76	17	4	
12744-0006	CA31	<0.2	<50	<4.5	<10	18.0	<16	116	<14	<50	<14	<20	<0.5	<650	28	<2	<7	1.6	4.93	13	5	
12744-0007	CA32	<0.2	<50	<4.5	<10	25.0	<16	320	<14	<50	<14	<20	<0.5	<650	17	<2	<7	11.3	26.5	508	7	
12744-0008	CA34	<0.2	<50	<4.5	<10	10.0	<16	61	<14	<50	<14	<20	<0.5	<650	13	<2	<7	1.2	1.72	103	6	
12744-0009	CA37	<0.2	<50	<4.5	<10	11.0	<16	65	<14	<50	<14	<20	<0.5	<650	41	<2	<7	7.0	0.94	41	5	
12744-0010	CA38	<0.2	<50	<4.5	<10	12.0	<16	68	<14	<50	<14	<20	<0.5	<650	66	<2	<7	3.2	1.20	36	<3	
12744-0011	CA40	<0.2	<50	<4.5	<10	10.0	<16	70	<14	<50	<14	<20	<0.5	<650	22	<2	<7	2.7	1.74	43	<3	
12744-0012	CA final from pump	<0.2	<50	<4.5	<10	<2	<16	10	21	588	n/a	<20	<0.5	<650	<12	<2	<7	2.4	0.22	26	10	

## Fluid Chemistry Data (Biotic Core) continued

LIMS Code	Sample Code	Zn	Ga	As	Se	Rb	Y	Zr	Mo	Cd	Cs	La	Ce	Pr	Nd	Hf	Ta	W	Tl	Pb	Th	U	
		µg l <sup>-1</sup>																					
12629-0014	CA1	n/s	n/s																				
12629-0015	CA2	n/s	n/s																				
12629-0016	CA3	n/s	n/s																				
12629-0017	CA4	n/s	n/s																				
12629-0018	CA5	45	<1	14	4	18.9	<0.2	<0.5	33	0.4	2.10	0.02	<0.04	<0.05	<1	<0.3	<0.1	20	<0.1	<0.4	<0.6	0.80	
12629-0019	CA6	37	<1	6	4	11.4	<0.2	<0.5	45	0.8	1.50	0.02	<0.04	<0.05	<1	<0.3	<0.1	8.3	0.2	<0.4	<0.6	0.79	
12629-0020	CA7	111	<1	9	3	11.3	<0.2	<0.5	32	0.8	1.40	0.01	<0.04	<0.05	<1	<0.3	<0.1	9.3	0.1	0.5	<0.6	1.40	
12629-0021	CA8	208	<1	5	3	9.8	<0.2	<0.5	144	3.4	1.09	0.02	<0.04	<0.05	<1	<0.3	<0.1	9.2	0.1	<0.4	<0.6	4.39	
12629-0022	CA9	237	<1	19	<2	5.7	<0.2	<0.5	341	0.7	0.58	0.01	<0.04	<0.05	<1	<0.3	<0.1	9.8	<0.1	<0.4	<0.6	4.22	
12629-0023	CA10	181	<1	20	<2	5.9	<0.2	<0.5	136	0.8	0.58	0.01	<0.04	<0.05	<1	<0.3	<0.1	8.3	<0.1	<0.4	<0.6	3.47	
12629-0024	CA11	186	<1	22	<2	6.7	<0.2	<0.5	96	0.7	0.74	0.01	<0.04	<0.05	<1	<0.3	<0.1	7.9	<0.1	<0.4	<0.6	2.61	
12629-0025	CA12	170	<1	21	<2	11.0	<0.2	<0.5	50	0.5	1.31	<0.01	<0.04	<0.05	<1	<0.3	<0.1	5.3	<0.1	<0.4	<0.6	2.05	
12629-0026	CA13	101	<1	21	<2	11.0	<0.2	<0.5	41	0.5	1.49	0.02	0.06	<0.05	<1	<0.3	<0.1	3.6	<0.1	<0.4	<0.6	1.64	
12629-0027	CA14	43	<1	18	<2	9.9	<0.2	<0.5	32	0.5	1.38	0.01	<0.04	<0.05	<1	<0.3	<0.1	2.7	<0.1	0.6	<0.6	1.20	
12629-0028	CA15	41	<1	18	<2	9.5	<0.2	<0.5	28	0.5	1.42	<0.01	<0.04	<0.05	<1	<0.3	<0.1	3.3	<0.1	0.8	<0.6	0.86	
12629-0029	CA16	44	<1	24	<2	10.0	<0.2	<0.5	28	0.4	1.52	<0.01	<0.04	<0.05	<1	<0.3	<0.1	4.1	<0.1	<0.4	<0.6	0.68	
12629-0030	CA17	51	<1	27	<2	9.7	<0.2	<0.5	27	0.4	1.57	0.01	<0.04	<0.05	<1	<0.3	<0.1	4.3	<0.1	<0.4	<0.6	0.57	
12629-0031	CA18	29	<1	13	<2	15.6	<0.2	<0.5	41	1.1	2.99	0.02	<0.04	<0.05	<1	<0.3	<0.1	4.7	0.2	<0.4	<0.6	1.33	
12629-0032	CA19	<25	<1	7	<2	4.4	<0.2	<0.5	126	0.2	0.64	0.05	0.12	<0.05	<1	<0.3	<0.1	4.6	<0.1	<0.4	<0.6	0.01	
12744-0001	CA20	<35	<1	10	<3	10	<0.2	0.8	26	0.4	2.0	0.08	<0.2	<0.06	<0.4	<0.2	<0.9	7.1	<0.4	<0.7	<0.1	0.50	
12744-0002	CA21	49	<1	9	<3	8	<0.2	0.9	25	<0.4	1.4	<0.05	<0.2	<0.06	<0.4	<0.2	<0.9	5.5	<0.4	<0.7	<0.1	0.31	
12744-0003	CA22	<35	<1	8	<3	7	<0.2	1.1	33	<0.4	1.2	<0.05	<0.2	<0.06	<0.4	<0.2	<0.9	5.4	<0.4	<0.7	<0.1	0.31	
12744-0004	CA25	46	<1	6	<3	5	<0.2	<0.7	21	<0.4	<0.9	0.06	<0.2	<0.06	<0.4	<0.2	<0.9	3.6	<0.4	<0.7	<0.1	0.10	
12744-0005	CA28	<35	<1	5	<3	5	<0.2	1.2	17	<0.4	<0.9	<0.05	<0.2	<0.06	<0.4	<0.2	<0.9	2.5	<0.4	<0.7	<0.1	0.21	
12744-0006	CA31	<35	<1	4	<3	4	<0.2	1.0	19	<0.4	<0.9	<0.05	<0.2	<0.06	<0.4	<0.2	<0.9	2.0	<0.4	<0.7	<0.1	0.16	
12744-0007	CA32	44	<1	3	<3	4	<0.2	1.2	51	<0.4	0.9	<0.05	<0.2	<0.06	<0.4	<0.2	<0.9	1.4	<0.4	<0.7	<0.1	0.13	
12744-0008	CA34	<35	<1	4	<3	3	<0.2	0.9	34	<0.4	<0.9	<0.05	<0.2	<0.06	<0.4	<0.2	<0.9	2.3	<0.4	0.9	<0.1	<0.05	
12744-0009	CA37	<35	<1	8	<3	3	<0.2	1.1	13	<0.4	<0.9	<0.05	<0.2	<0.06	<0.4	<0.2	<0.9	1.3	<0.4	<0.7	<0.1	0.13	
12744-0010	CA38	79	<1	7	<3	3	<0.2	0.8	15	<0.4	<0.9	<0.05	<0.2	<0.06	<0.4	<0.2	<0.9	1.2	<0.4	<0.7	<0.1	0.11	
12744-0011	CA40	65	<1	5	<3	4	<0.2	0.8	13	<0.4	<0.9	<0.05	<0.2	<0.06	<0.4	<0.2	<0.9	0.9	<0.4	<0.7	<0.1	0.08	
12744-0012	CA final from pump	<35	<1	<2	<3	<1	<0.2	0.9	5	<0.4	<0.9	<0.05	<0.2	<0.06	<0.4	<0.2	<0.9	0.3	<0.4	<0.7	<0.1	<0.05	

## References

British Geological Survey holds most of the references listed below, and copies may be obtained via the library service subject to copyright legislation (contact [libuser@bgs.ac.uk](mailto:libuser@bgs.ac.uk) for details). The library catalogue is available at: <http://geolib.bgs.ac.uk>.

ABELL, A. B., WILLIS, K.L. AND LANGE, D.A. 1999. Mercury Intrusion Porosimetry and Image Analysis of Cement-Based Materials. *Journal of Colloid and Interface Science*, 211, 39-44 .

GOLDSTEIN, J.I., NEWBURY, D.E., ECHLIN, P., JOY, D.C., FIORI, C. AND LIFSHIN, E. 1981. *Scanning Electron Microscopy and X-Ray Microanalysis*. Plenum Press, New York.

HALLSWORTH, C.R. AND KNOX, R.W.O'B. 1999. BGS Rock Classification Scheme. Volume 3: Classification of sediments and sedimentary rocks. *British Geological Survey Research Report, RR99-03*.

HARRISON, H., WEST, J.M., BATEMAN, K., CAVE, M., COOMBS, P., HARRINGTON, J., LACINSKA, A., MILODOWSKI, A.E., TURNER, G.H. AND WAGNER, D. 2009. Microbial effects on transport processes (BioTran) – Anaerobic flow-through Experiments using crushed Diorite and *Pseudomonas aeruginosa* (April 2008 – March 2009). *British Geological Survey Open Report OR/09/033*.

HARRISON, H., WAGNER, D., YOSHIKAWA, H., WEST, J. M., MILODOWSKI, A.E., SASAKI, Y., TURNER, G., LACINSKA, A., HOLYOAKE, S., HARRINGTON, J., NOY, D., COOMBS, P., BATEMAN, K. AND AOKI, K. 2011. Microbiological influences on fracture surfaces of intact mudstone and the implications for geological disposal of radioactive waste. *Mineralogical Magazine*, 75, pp 2449-2466. doi: 10.1180/minmag.2011.075.4.2449.

HILLIER, S., SUZUKI, K. AND COTTER-HOWELLS, J. 2001. Quantitative determination of Cerussite (Lead carbonate) by X-ray diffraction and inferences for lead speciation and transport in stream sediments from a former lead mining area of Scotland. *Applied Geochemistry*, 16, 597-608.

HOBBIE, J.E., DALEY, R.J. AND JASPER, S. 1977. Use of nucleopore filters for counting bacteria by fluorescent microscopy. *Applied and Environmental Microbiology*, 33, 1225-1228.

International Association for the Properties of Water and Steam formulation for Industrial Use, 1997.

JASS, J. AND LAPPIN-SCOTT, H.M. 1992. Practical course on biofilm formation using the modified Robbins Device. University of Exeter.

MILODOWSKI, A.E. AND RUSHTON, J.C. 2008. Mineralogical and porosity characterisation of potential aquifer and seal units for carbon capture and storage methodologies for the CASSEM Project. *British Geological Survey Research Report, CR/08/153*.

MILODOWSKI, A.E., STRONG, G.E., WILSON, K.S., HOLLOWAY, S. AND BATH, A.H. 1987. Diagenetic influences on the aquifer properties of the Permo-Triassic sandstones in the East Yorkshire and Lincolnshire Basin. Investigation of the Geothermal Potential of the UK. *British Geological Survey*.

MOORE, D.M. AND REYNOLDS, R.C. 1997. *X-RAY Diffraction and identification and the analysis of clay minerals (2nd edition)* Oxford University Press, New York.

PETTIBOHN, F.J., POTTER, O.E. AND SEIVER, R. 1987. *Sand and Sandstone*. New York: Springer.

SCHMIDT V. AND McDONALD, D.A.. 1979B. Texture recognition of secondary porosity in sandstones. In: SCHOLLE, P.A. AND SCHUGLER, P.R. (editors). Aspects of Diagenesis. *Society of Economic Paleontologists and Mineralogists Special Publication*, 26, 209-225.

SNYDER, R.L. AND BISH D.L. 1989. *Quantitative Analysis* (Chapter 5)., In: Bish, D.L., Post, J.E. (Eds), Modern powder diffraction. *Mineralogical Society of America Reviews in Mineralogy*, 20, 101-144.

TURNER, G.H., AND RUSHTON, J.C. 2012. Assessment of Biofilm Development on Potential Radioactive Waste Host Rocks under Controlled Conditions. *British Geological Survey Internal Report OR/12/057*.

VAUGHAN, D.J., WOGELIUS, R., BOULT S. AND MERRIFIELD, C. 2001. Quantifying the effects of biofilm growth on hydraulic properties and on sorption equilibrium microscopic to macroscopic measurements. *Progress summary 02/01 – 11/01 Williamson Research Centre, University of Manchester*.

WAGNER, W., SAUL, A. AND PRUSS, A., 1994 International Equations for the Pressure along the Melting and along the Sublimation Curve for Ordinary Water Substance, *J. Phys. Chem. Ref. Data*, 23, No 3.